8-10-2005

Power System Fault Detection Using Conductor Dynamics

Jeff Dicharry
University of New Orleans

POWER SYSTEM FAULT DETECTION USING CONDUCTOR DYNAMICS

A Thesis

Submitted to the Graduate Faculty of the
University of New Orleans
in partial fulfillment of the
requirements for the degree of

Master of Science
in
The Department of Electrical Engineering

by

Jeff Dicharry

B.S.E.E. Louisiana State University, 2000

August 2005

Acknowledgement

The research presented in this paper could not have been possible without the hard work and patience of the professors at the University of New Orleans. The quality of education provided for my degree is a reflection of the knowledge and willingness of the instructors. I would especially like to thank the members of my thesis committee, Henri A. Alciatore, M.S., Edit J. Bourgeois, Ph.D., and Vesselin Jilkov, Ph.D.

I would also like to recognize my co-workers at Entergy Services, Inc. for their willingness to teach me about substation design and the power industry. I would like to thank Tammy Lapeyrouse for giving me the opportunity to be employed as a substation designer at Entergy and involved with the IEEE substations committee. The experiences I gained from employment and the IEEE have proved beneficial in my educational degree and professional career.

I would like to thank my parents, Joseph M. Dicharry and Maureen C. Dicharry, whose encouragement and belief in me are responsible for my successes in life.

Finally, I would like to thank Rebecca D. Schneider for her support and patience throughout my graduate education.

Table of Contents

List of Figures

List of Tables

Abstract

Power system fault detection is conventionally achieved using current and potential measurements. An alternate and unconventional form of protective relaying is feasible using rigid bus conductor motion as the means of detection. The research presented focuses on the detection of power system faults using visual displacement of conductor spans. Substation rigid bus conductor motion is modeled using dual spring-mass systems for accurate representation of conductor response to electromagnetic forces generated during system faults. Bundled rigid conductors have advantages including detection independent of system load currents and improved ability to detect polyphase and single phase faults. The dynamic motion of the conductors during the fault is optically monitored with a laser detection system. Time-overcurrent characteristics are derived for the application of fault detection. The response time of the conductor detector system is slower than conventional relays due to the natural frequencies of the conductor span limiting the speed of its displacement. This response time makes the fault detection system using conductor displacement an ideal candidate for a backup relay in power system protection schemes.

1.0 Introduction

Protective relaying in power systems is crucial to safety and reliability. From the simple household fuse to high voltage transmission line breakers, the purpose of the protective devices is to interrupt flow effectively. This interruption results from a three step process: detect, decide, and act.

Typical power system protective relays utilize electromechanical or microprocessor technology to perform the three step process. Based on relay settings, the relay can detect the fault and make a decision to trip a protective device. If the decision is made to trip, the action is performed using a trip signal output from the relay and the circuit is opened. The critical inputs to the protective relay are current and potential transformers connected to the monitored power system element.

A properly protected power system has several relays with overlapping zones of protection. The primary purpose of this is to provide adequate backup protection in the event of improper operation. Relay settings including time and overcurrent relationships ensure proper coordination with overlapping zones. Backup relays within the same zone provide additional security, but often rely on the same source of electrical power and current or potential transformers. This does, however, provide a margin of security for improperly set relays. Figure 1.1 depicts an example of l time-overcurrent curves for relay coordination.

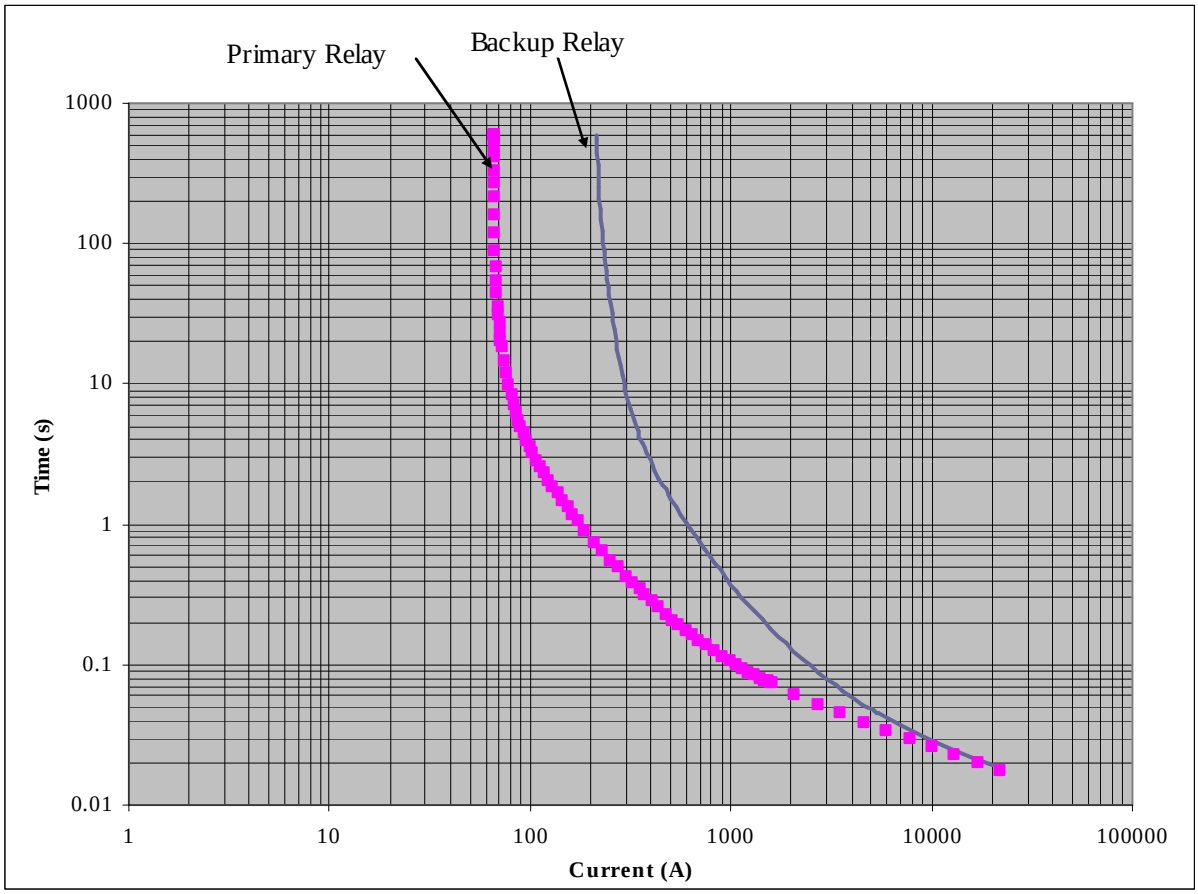

Figure 1.1: Typical Relay Time-Overcurrent Curves

Inspection of figure 1.1 indicates primary relays are designed to trip before backup relays. This is based on higher current for a shorter period of time. Typically, these values are only attained during system faults. In the event that the primary relay does not operate as planned, the backup relay will trip with some time delay. Overlapping zones of protection also have similar time-overcurrent coordination curves.

Figure 1.2 includes the location of a typical power system device damage curve. It is imperative that protective devices act prior to the damage curve or the relays will provide inadequate protection. If the magnitude and duration of fault currents violate the damage curve, the device needs to be repaired or replaced. Power system equipment replacement costs

increases stress upon utility budgets with influence on customer rate bases. Replacement or repair of such equipment is difficult due to the physical size and availability. Any way to avoid equipment damage should be utilized to minimize these negative effects.

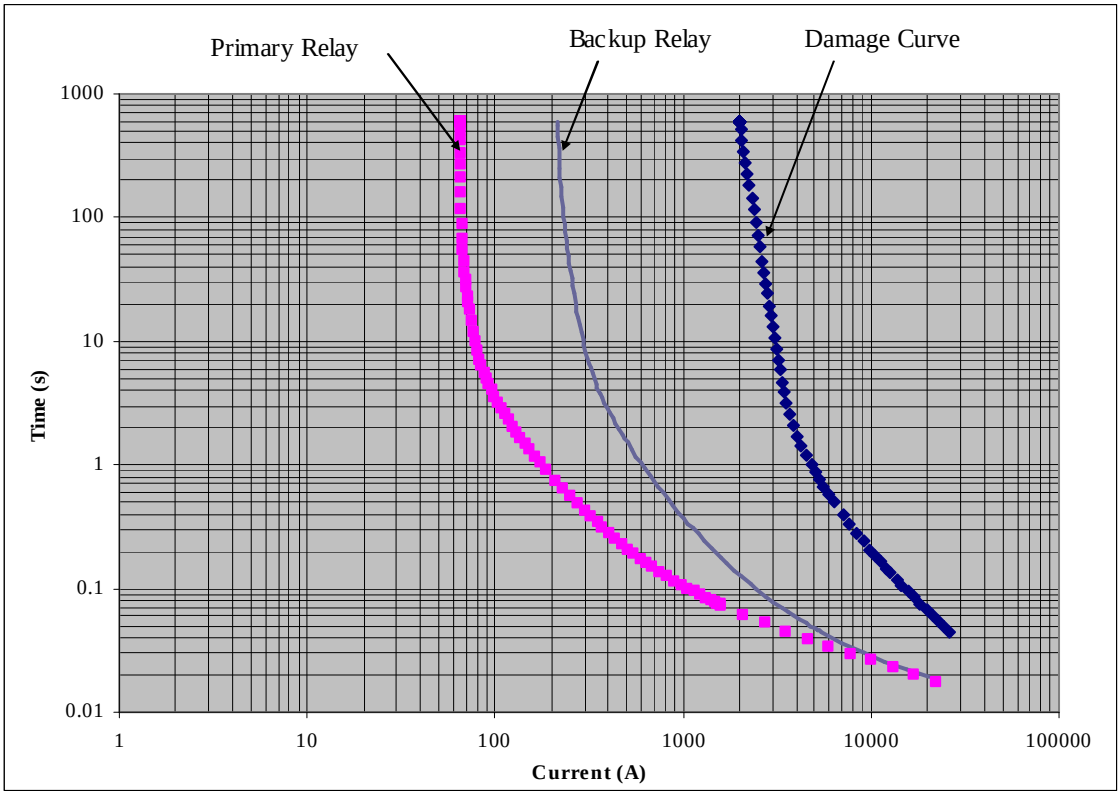

Figure 1.2: Typical Relay and Damage Time-Overcurrent Curves

Figure 1.3 depicts a second backup relay. This type of protection acts similar to an overcurrent relay with time delay or a differential relay with time delay. When the current reaches the set level, sends an instantaneous trip signal. The location of the line is determined based on relay coordination with proper settings. The redundant backups serve as an extra layer of protection to the power system.

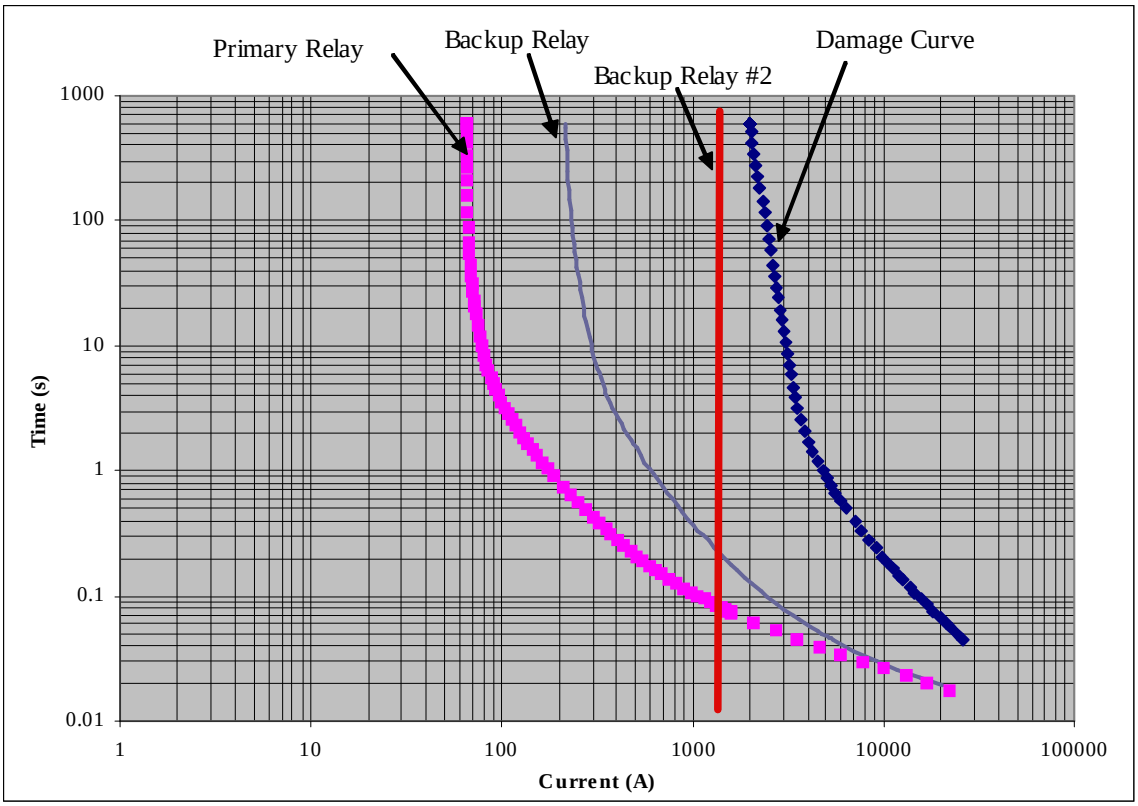

Figure 1.3: Typical Relay and Damage Time-Overcurrent Curve with Backup Relays

The intention of the research presented in this document is to present a method of backup relay protection similar to the backup relay #2 depicted in figure 1.3. Through detailed analysis, the novel application of conductor dynamics will be used for the purpose of fault detection. This will be accomplished without the use of conventional equipment including electromechanical relays, microprocessor relays, potential transformers, and current transformers. Through deflection calculations and varied design parameters, the motion of rigid bus conductors can provide visual indication of a power system fault and is capable of being integrated on the time-overcurrent curves.

1.1 Motivation for Research

The use of a new method of power system fault detection serves as backup protection device with relatively low construction and maintenance costs. While the emphasis of the research presented in this thesis is focused upon the application to power systems inside medium to high voltage substations, the information presented can be applied in a variety of electrical applications at various voltage levels.

1.2 Objectives of Study

The primary objective of the research presented in this paper is to provide design details and analysis methodology for a substation design engineer to design a section of substation rigid bus for the purpose of fault detection through visual indication.

A secondary objective to the research presented is to reveal the advantages of bundled rigid bus in the application of fault detection using conductor dynamics.

While the design and dynamic response of substation rigid bus inside substations has been widely studied, the research focuses on the use of dynamic analysis for bus spans [2]. Static analysis was not chosen for this research due to its limitations for the application of the transient dynamic response.

1.3 Outline of Topics Covered

Section 2 includes the details and derivations of the transient nature of several types of power system faults. The information presented will be used to provide an accurate dynamic response model.

Section 3 describes the dynamic motion of the bus based on deflection characteristics and its application to rigid bus. This section also presents limitations to conventional three phase bus configurations for its use in fault detection and lists advantages for bundled conductors.

Section 4 focuses on the dynamic analysis of bundled substation rigid bus and its analogy to the dual spring-mass mechanical system. Emphasis is placed on natural frequencies and variations of span components.

Section 5 describes the calibration and determination of relay settings in relay coordination. The method chosen to detect faults uses an optical system configuration for visual deflection indication.

Appendix A provides a detailed example of the use of conductor dynamics for the purpose of fault detection.

Appendix B contains a flowchart to be utilized for the design of conductor bus spans to effectively detect fault currents based on displacement. It is a practical guide for the substation designer to effectively apply the principles presented in this research.

2.0 Power System Fault Currents

Power system fault current analysis is an extensive portion of power engineering. Entire textbooks have been written describing methodology for the detailed analysis of power system faults. This section briefly summarizes the transient and steady state portion of fault currents. Both of these components are necessary for the proper dynamic analysis of the substation bus during fault conditions.

2.1 Derivation of Fault Current Components

A detailed derivation of fault current components is given in [3]. The components derived are the steady state and transient portions of fault currents and should not be confused with the method of symmetrical components for fault current analysis in unbalanced systems [1]. The information derived in [3] is summarized in this section.

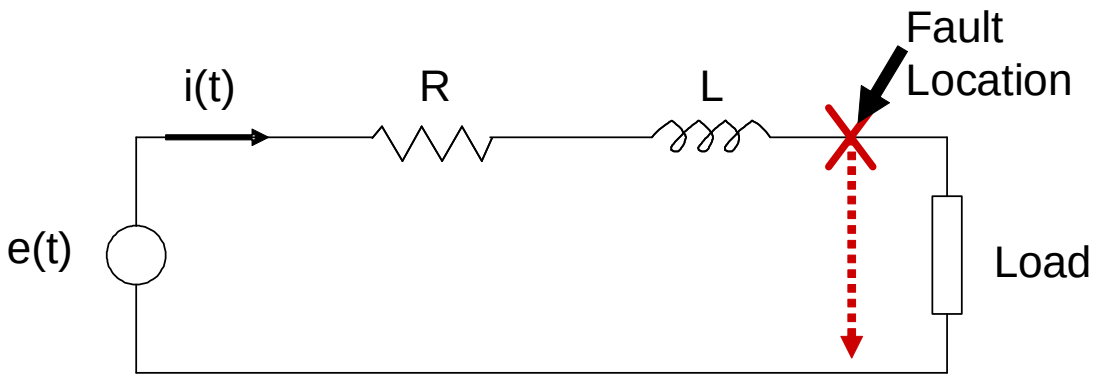

Figure 2.1: Circuit Model for Power System Fault Analysis

The voltage source in figure 2.1 is defined in equation 2.1. The source is sinusoidal with system frequency (ω), RMS voltage magnitude (V), and phase angle (ϕ).

$$e(t) = \sqrt{2}\ V \cos(\omega t + \phi) \tag{2.1}$$

Analysis of the circuit in figure 2.1 with shorted load during a fault using Kirchhoff's voltage law yields equation 2.2.

$$e(t) = R\ i(t) + L\frac{di(t)}{dt} \tag{2.2}$$

The use of the Laplace transform and solving for i(t) assuming initial current i(0)=c in equation 2.2 is shown in equation 2.3. N(s) is defined as the Laplace transform of cos(wt+ø).

$$i(s) = \frac{\sqrt{2}\ V}{R + sL} N(s) + \frac{L}{R + sL} c \tag{2.3}$$

The inverse Laplace transform of equation 2.3 yields:

$$i(t) = c\, e^{-\frac{R}{L}t} + \int_0^t \sqrt{2}\frac{V}{L} e^{-\frac{R}{L}(t-\tau)} \cos(\omega\tau + \phi) d\tau \tag{2.4}$$

This is further evaluated by expansion of the integral to equation 2.5:

$$i(t) = \frac{\sqrt{2}\,V}{R^2 + w^2L^2}(R\cos(\omega t + \phi) + \omega L\sin(\omega t + \phi)) \tag{2.5}$$

$$-\frac{\sqrt{2}\,V}{R^2 + w^2L^2}e^{-\frac{R}{L}t}(R\cos(\omega t + \phi) + \omega L\sin(\phi)) + ce^{-\frac{R}{L}t}$$

For ease of evaluation, variables ζ and I are identified in equations 2.6 and 2.7.

$$\tan(\xi) = -\frac{\omega L}{R} \tag{2.6}$$

$$I = \frac{V}{R^2 + \omega^2L^2} \tag{2.7}$$

Substitution of equations 2.6 and 2.7 into 2.5 is shown in equation 2.8.

$$i(t) = \sqrt{2}\,I\cos(\omega t + \phi + \xi) + [c - \sqrt{2}\,I\cos(\phi + \xi)]e^{-\frac{R}{L}t} \tag{2.8}$$

Inspection of equation 2.8 reveals both the steady state (equation 2.9) and transient (equation 2.10) components of the fault current.

$$i(t)_{steadystate} = \sqrt{2}\,I\cos(wt + \phi + \xi) \tag{2.9}$$

$$i(t)_{transient} = [c - \sqrt{2}\,I\cos(\phi + \xi))\,e^{-\frac{R}{L}t}] \tag{2.10}$$

2.2 Analysis of Fault Current Components

The steady state fault current in equation 2.9 is commonly referred to in the power industry as the fault current at a particular location. The introduction of the transient portion of fault current in equation 2.10 shows the first several cycles of the fault current can be much higher than the value of steady state current. This neglects initial current and assumes $\phi = -\zeta$. Figure 2.2 depicts this scenario using a 60Hz frequency.

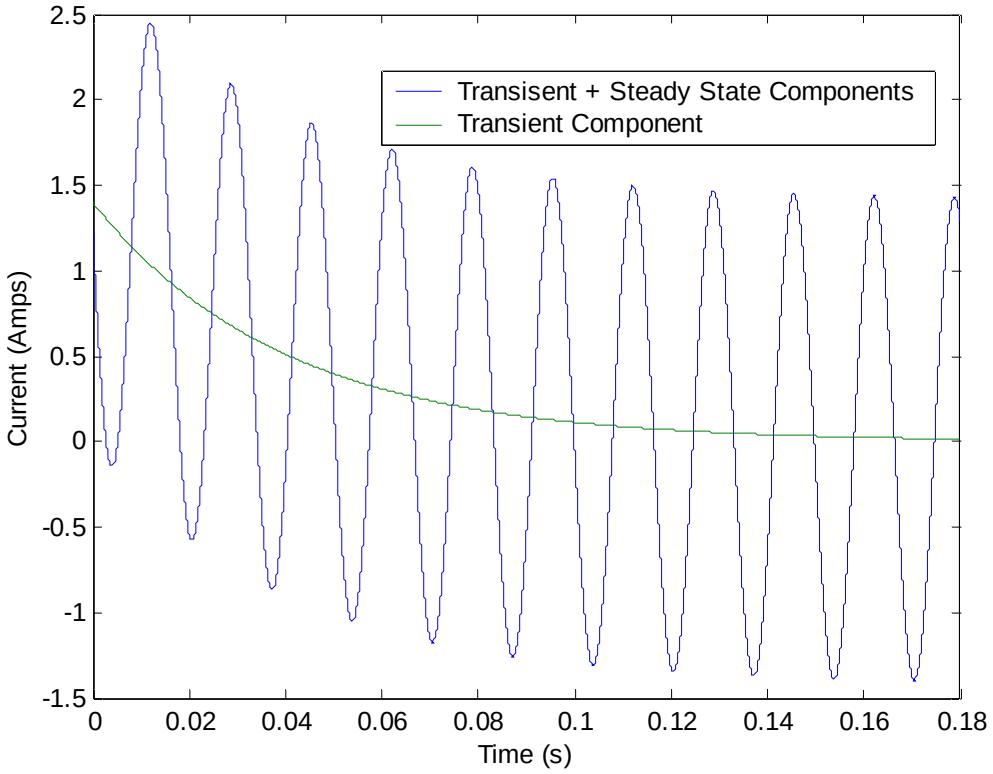

Figure 2.2: Fault Current Including Transient Component

The transient fault current is a function of the system resistance and reactance. The ratio of this reactance and resistance is commonly referred to as the X/R ratio of the power system. Figure 2.3 depicts the exponential characteristics of the transient component of fault current with several X/R ratios using 1 amp of current.

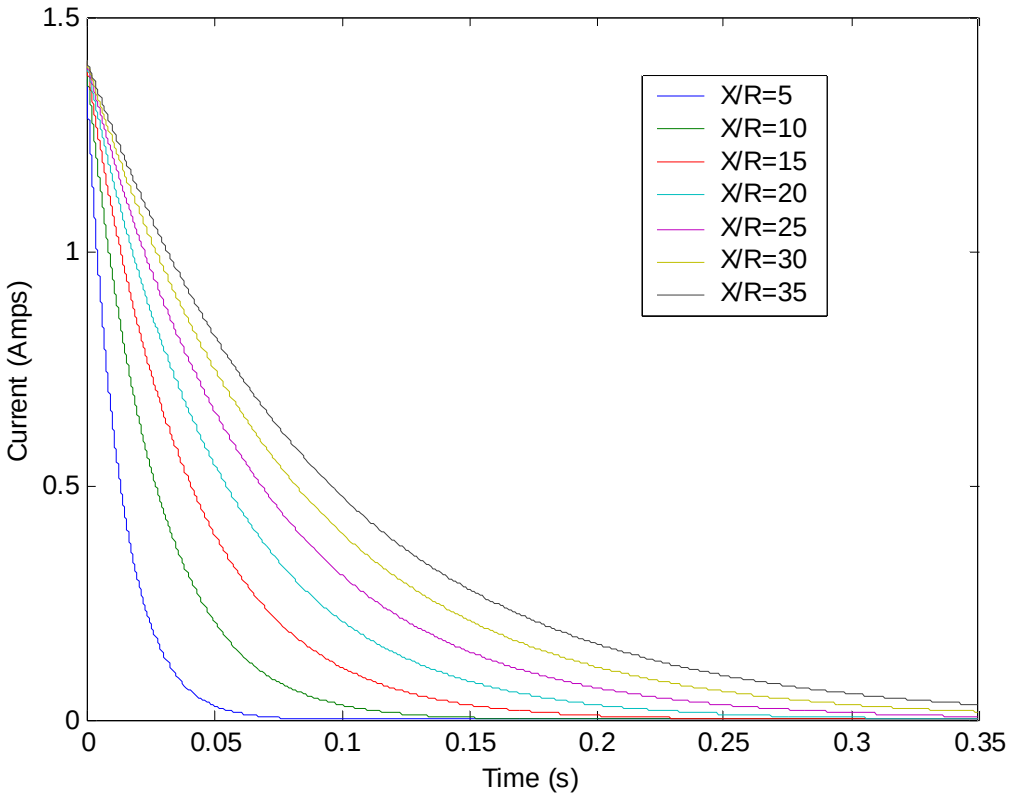

Figure 2.3: Transient Fault Component Based on System X/R Ratio

Inspection of figure 2.3 and equation 2.10 indicates that the magnitude of the fault current transient component is the same at the initiation of the fault for any X/R ratio. It decays slower with a higher X/R ratio than a low one. The response of the bus to the system fault current and its generated forces is a function of this X/R ratio.

The X/R ratio is a function of fault location. A fault near a transformer generally has a high X/R ratio due to the windings of the transformer and its impact in increasing the reactance at the fault location. This increased reactance will slow the transient decay time in comparison with a low voltage distribution feeder with a smaller X/R ratio and shorter decay time. Any use of protective relaying should consider this X/R ratio for the instantaneous and transient fault current considerations.

The frequency components of fault currents including transient components can be attained using Fourier analysis. The primary frequencies are 60Hz with a DC component. Figure 2.4 depicts the components for the first 11 msec of the time domain signal in figure 2.2. The Fourier transform of the waveform of this time domain signal is defined as:

$$\left|G(w)\right| = \sqrt{2}I\left(\frac{\omega_o}{\omega^2 + {\omega_o}^2} + \frac{\cos(\phi + \xi)}{\omega + \frac{R}{L}}\right).$$

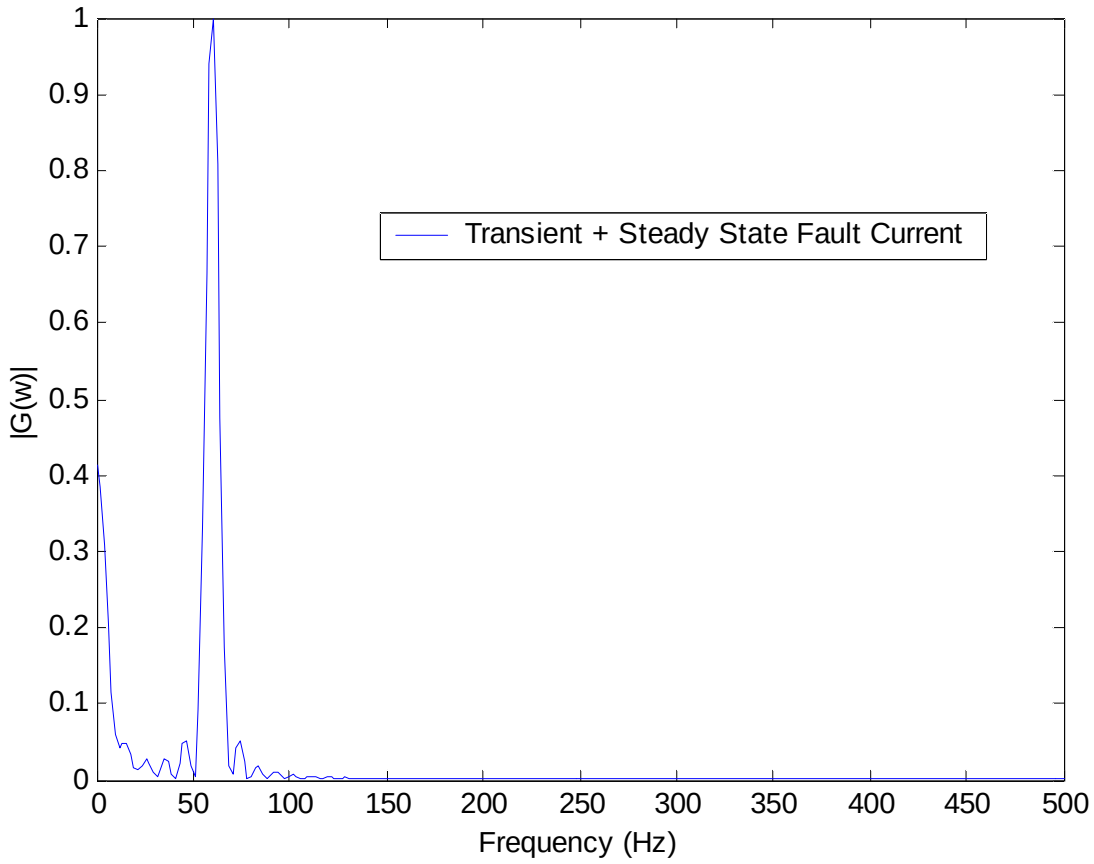

Figure 2.4: Frequency Components of Fault Current

2.3 Types of Power System Faults

The four primary types of faults are detailed in [1]. These include phase to ground, phase to phase, phase to phase to ground, and three phase. The use of symmetrical component analysis described in [1] proves beneficial for calculation of each type of fault.

It is critical that the protection designed for the power system respond to each possible fault condition. While the power system designer can account for several different types of faults, the protective equipment may not be able to distinguish between the various types of faults. An accurate system model for studying power system faults including correct system impedance parameters will minimize calculated fault current errors.

An example of the B phase to ground fault is depicted in figure 2.5 using an X/R ratio of 15, fault current magnitude of 20kA RMS, and load current of 2kA RMS. Symmetry of approximately 120 degrees between phases is maintained through the fault duration.

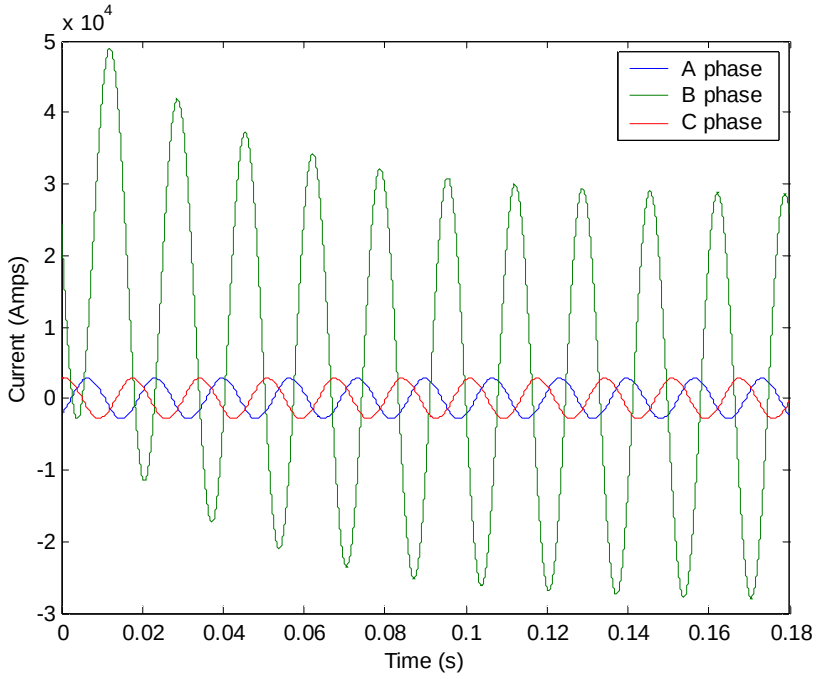

Figure 2.5: Example of B-Phase to Ground Fault Current

An example of a phase to phase fault is shown in figure 2.6. The same assumptions used in figure 2.5 have been used for depiction of the fault. Because the fault current does not include a ground path, the two faulted phases are symmetric in steady state magnitude as indicated in [6]. While the transient component is shown as identical for both phases, the transient portion of each phase may not actually be identical as indicated in [2]. The phase angle of the C phase current relative to A phase is a function of system topology and varies with system locations.

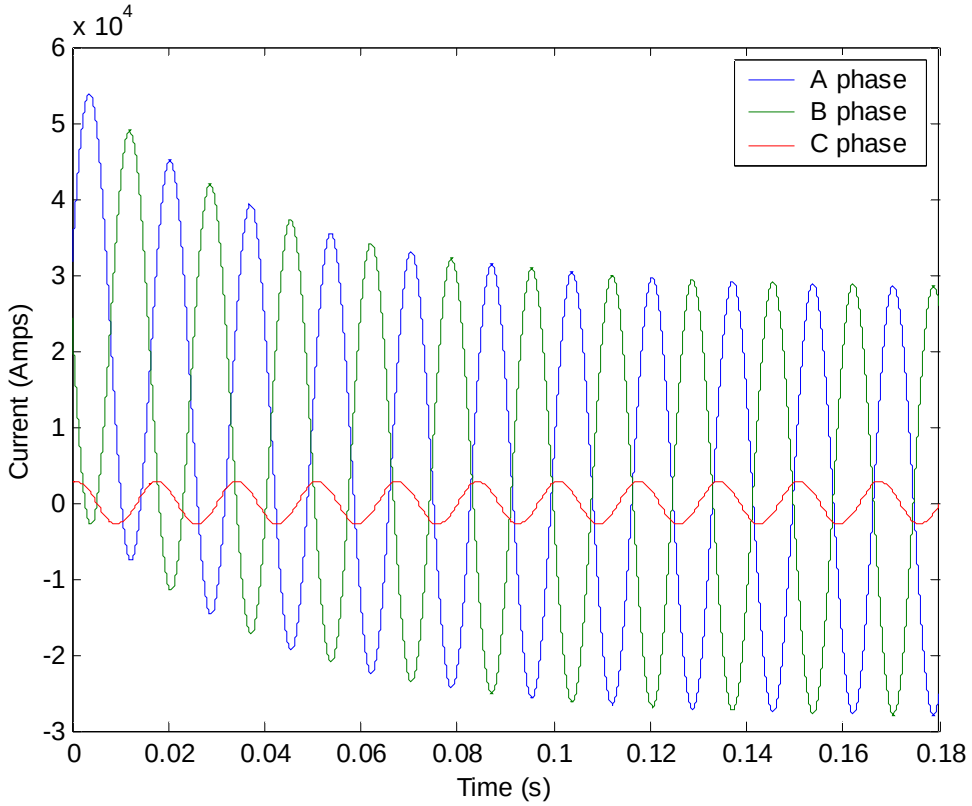

Figure 2.6: Example of A to B Phase Fault Current

The introduction of the ground path in the phase to phase fault depicted in figure 2.6 removes the symmetry of the faulted phases as indicated in figure 2.7 using the same assumptions. Actual phase angles and transient component contributions will vary according to system topology as previously described.

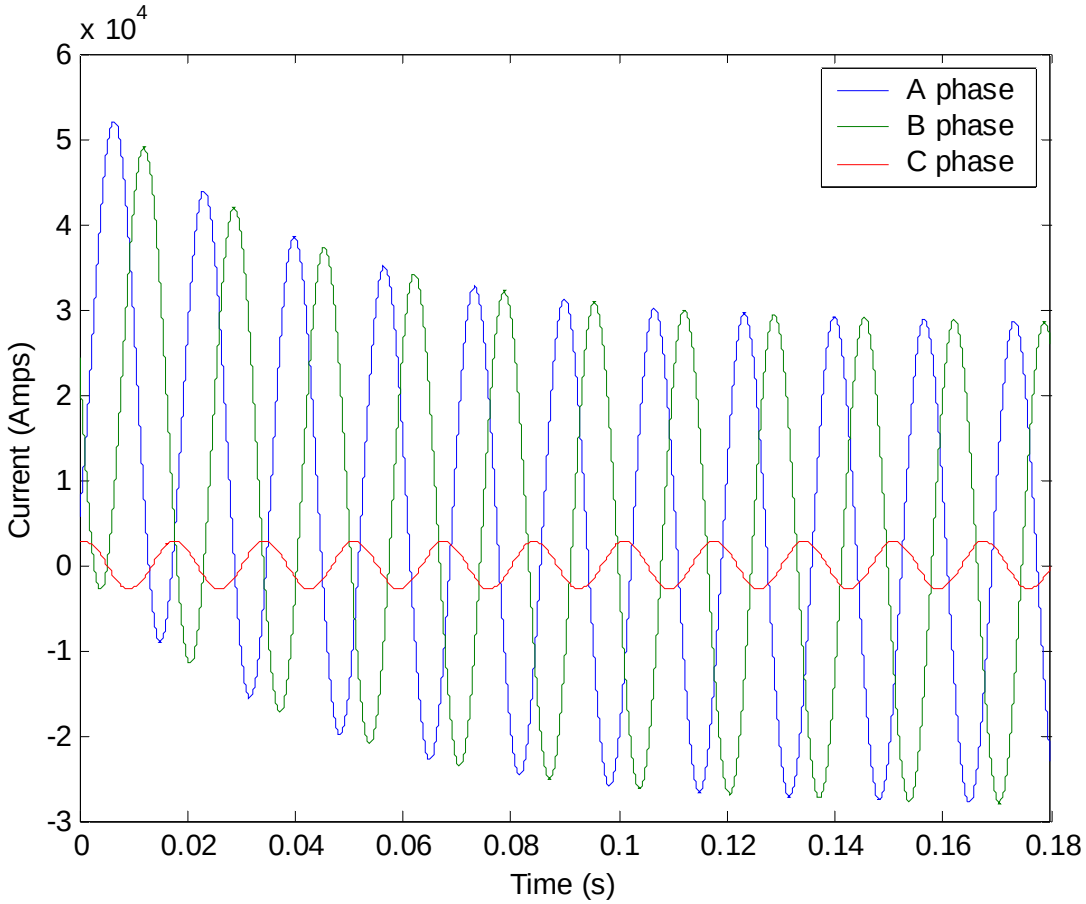

Figure 2.7: Example of A to B Phase to Ground Fault Current

Three phase faults provide phase angles of approximately 120 degrees as indicated in figure 2.8. Similar to phase to phase and phase to phase to ground faults, actual transient components for faulted phases vary with system topology. The magnitudes of the faulted phase currents are equal assuming a balanced three phase system. The introduction of the ground path in three phase faults does not alter the fault currents.

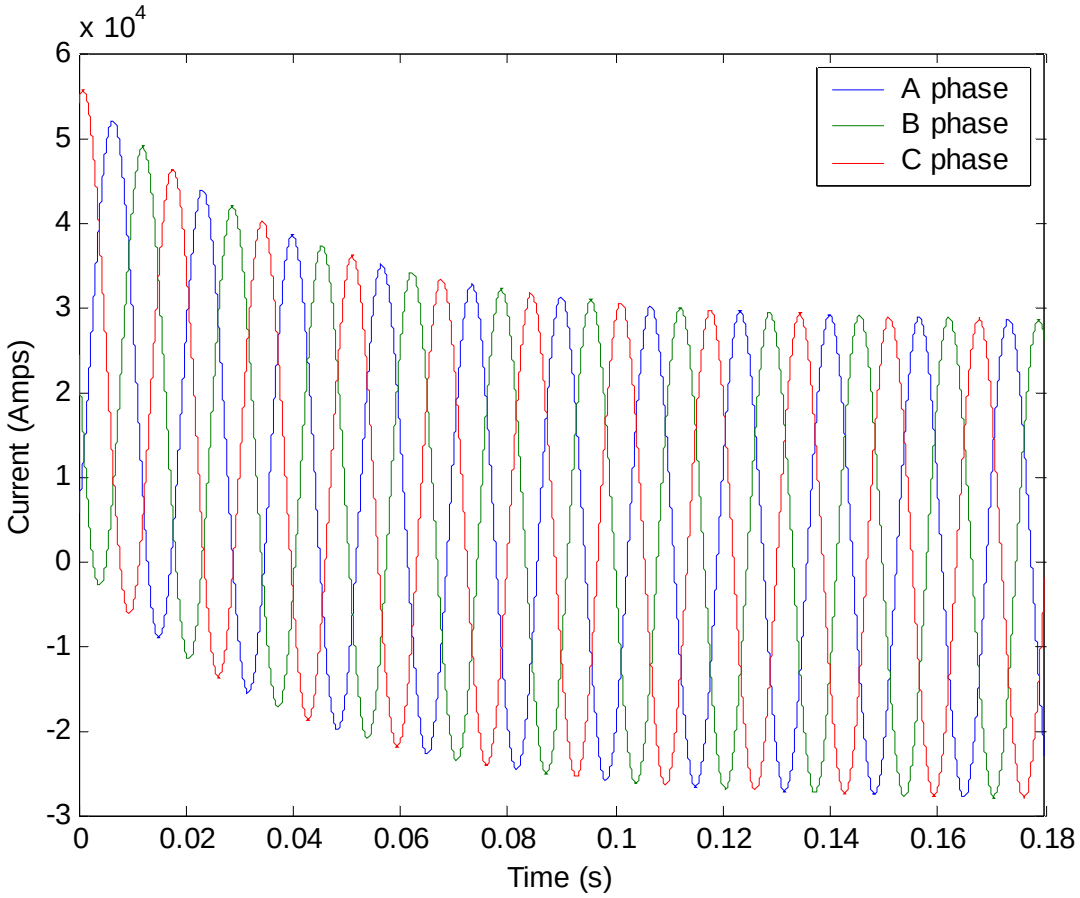

Figure 2.8: Example of Three Phase Fault Current

The purpose of identifying the various types of system faults is to ensure the proposed methods of relaying encompass all types of faults. The simple flow of too much current on an electrical device can cause heat, flames, equipment damage, and lethal ground potential rise. A protection scheme not encompassing every fault scenario provides additional risk to equipment, personnel, and the general public.

3.0 Fault Current Forces

Extensive studies have been performed on substation rigid bus using various static and dynamic models. This section describes methodology for both static and dynamic analysis of fault current forces between rigid bus conductors. The conclusion is made that the dynamic modeling of electromechanical forces provides a more accurate representation of actual forces generated than static forces.

3.1 Electromagnetic Conductor Forces

The magnetic force on a current carrying wire is detailed in [7]. The equations used in this section are primarily obtained from [7] with application to the motion of bus relevant to fault current response.

The force vector due to electromagnetism on a conductor is defined in equation 3.1. The force is dependent upon the conductor length, magnetic field generated, and applied current.

$$F = iL \otimes B \tag{3.1}$$

Equation 3.1 applied to the scenario of two parallel conductors depicted in figure 3.1 yields a cross product which can be reduced to equation 3.2, based on the parallel nature of the design.

$$\left|F_{ab}\right| = i_b \, L \, B_a \cos(0) \tag{3.2}$$

The magnetic field contribution from conductor A, B_a at wire B is defined in equation 3.3 where the permeability constant of air is $\mu_o = 4\pi \times 10^{-7}$ and d is the distance between conductors.

$$\left|B_a\right| = \frac{\mu_o \, i_a}{2 \, \pi \, d} \tag{3.3}$$

Substitution of equation 3.3 into equation 3.2 with time varying input currents yields equation 3.4. The output force vector is a function of time based on time and direction of the input currents.

$$\vec{F}_{ab}(t) = \frac{\mu_o \, L \, i_a(t) \, i_b(t)}{2 \, \pi \, d} \tag{3.4}$$

Two parallel conductors are depicted in figure 3.1. Currents are injected into the two conductors with magnitudes $I_a(t)$ and $I_b(t)$. The direction convention of equation 3.4 is noted in figure 3.1. The force on each conductor is identical in magnitude such that $|F_{ab}| = |F_{ba}|$. Direction is dependent upon the direction of current as described in [7].

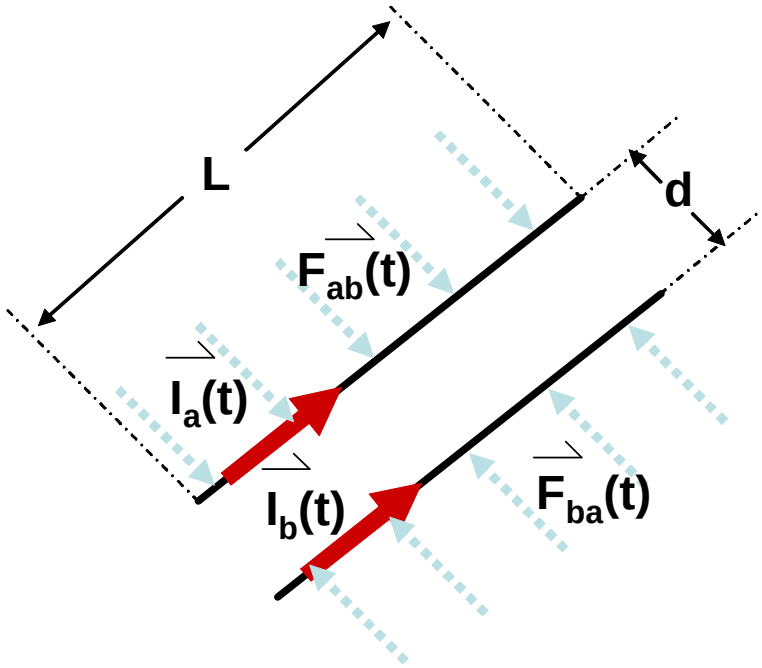

Figure 3.1: Parallel Conductor Forces

If the currents $I_a(t)$ and $I_b(t)$ are in the same direction, the resulting force vector $F_{ab}(t)$ produces a pinch effect where the two conductors are pulled together. On the contrary, currents in opposite directions produce repelling forces. The use of DC current produces static

forces on conductors where AC currents produce dynamic forces with points of zero force at the zero crossing of either input, $I_a(t)$ or $I_b(t)$.

In the electric utility, the use of static (DC) forces are not as common due to a primarily AC dominated power grid. [1] explains the use of voltage vectors with their 120 degree phase separation in the electric grid. Consider, for example, figure 3.1 with input currents separated with a phase angle of 120 degrees as indicated in figure 3.2. This configuration is similar to two phases of a distribution line without the presence of the third. The application of equation 3.4 with separation distance d = 1 ft and current magnitude of 1kA produces the dynamic force (#/inch) as indicated in figure 3.3.

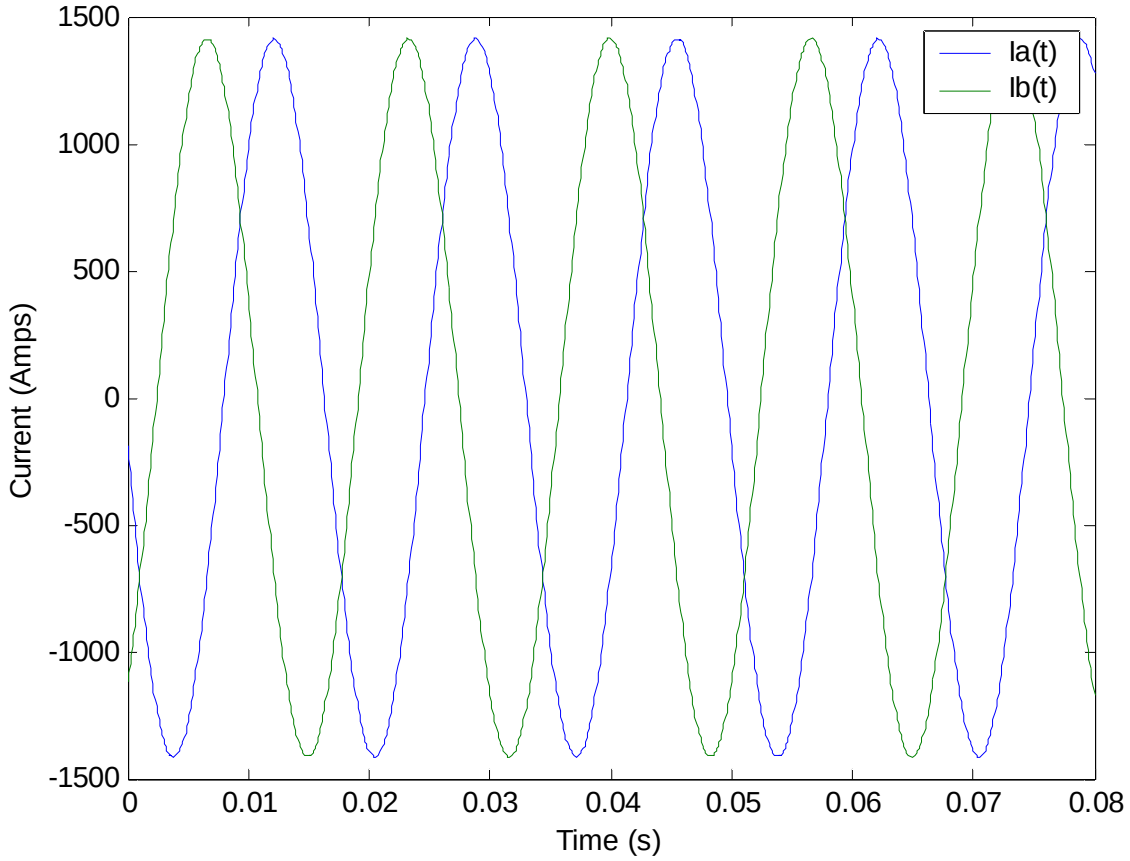

Figure 3.2: Input Currents 120 Degrees Out of Phase

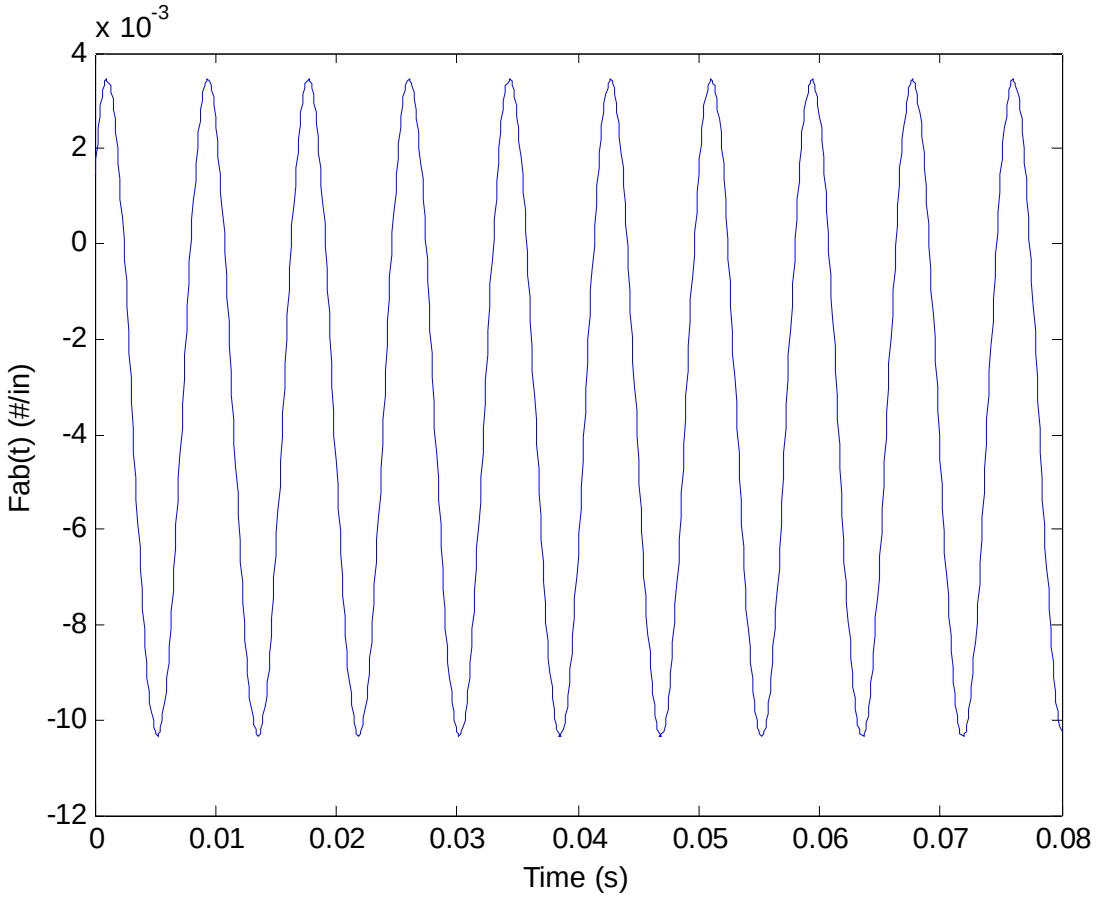

Figure 3.3: Electromagnetic Force $F_{ab}(t)$

Figure 3.3 shows a sinusoidal force with positive and negative portions at its force frequency. This force frequency is twice that of the power frequency. A Fourier analysis of the frequency content is shown in figure 3.4. For the case of the 60 Hz power frequency, the frequency of force is 120Hz with a DC component. The Fourier transform is defined as:

$$\left|G(w)\right| = \frac{\mu_o L I^2}{2 \pi d}\left(\frac{\omega}{\omega^2 + 4\omega_o{}^2} + \frac{1}{\omega}\right).$$

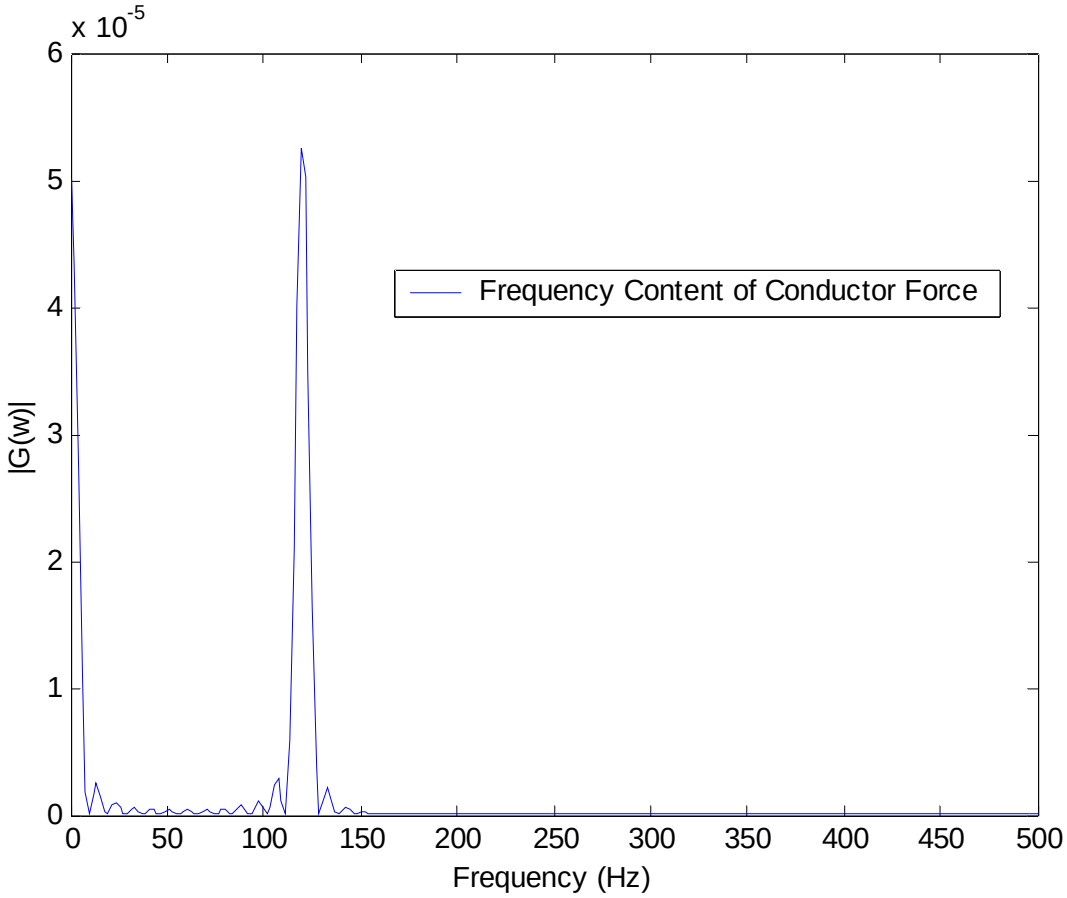

Figure 3.4: Frequency Content of Force $F_{ab}(t)$

For comparative purposes, the use of equation 3.4 using the maximum magnitudes of the input waveforms only (not the time varying portion) indicates a static force of approximately 4 times the dynamic force. This example shows the conservativeness nature of static analysis. Dynamic analysis is more appropriate for situations which require accurate force calculations. A conservative static value is industry accepted in [2] for calculations of bus structures designs. For the application of fault detection using dynamics, this static analysis does not account for the actual forces generated.

The presence of a transient component in fault current forces produces non-sinusoidal force waveforms until the transient components decay. Figure 3.5 depicts the input current waveforms of figure 3.2 including a transient portion with X/R = 15.

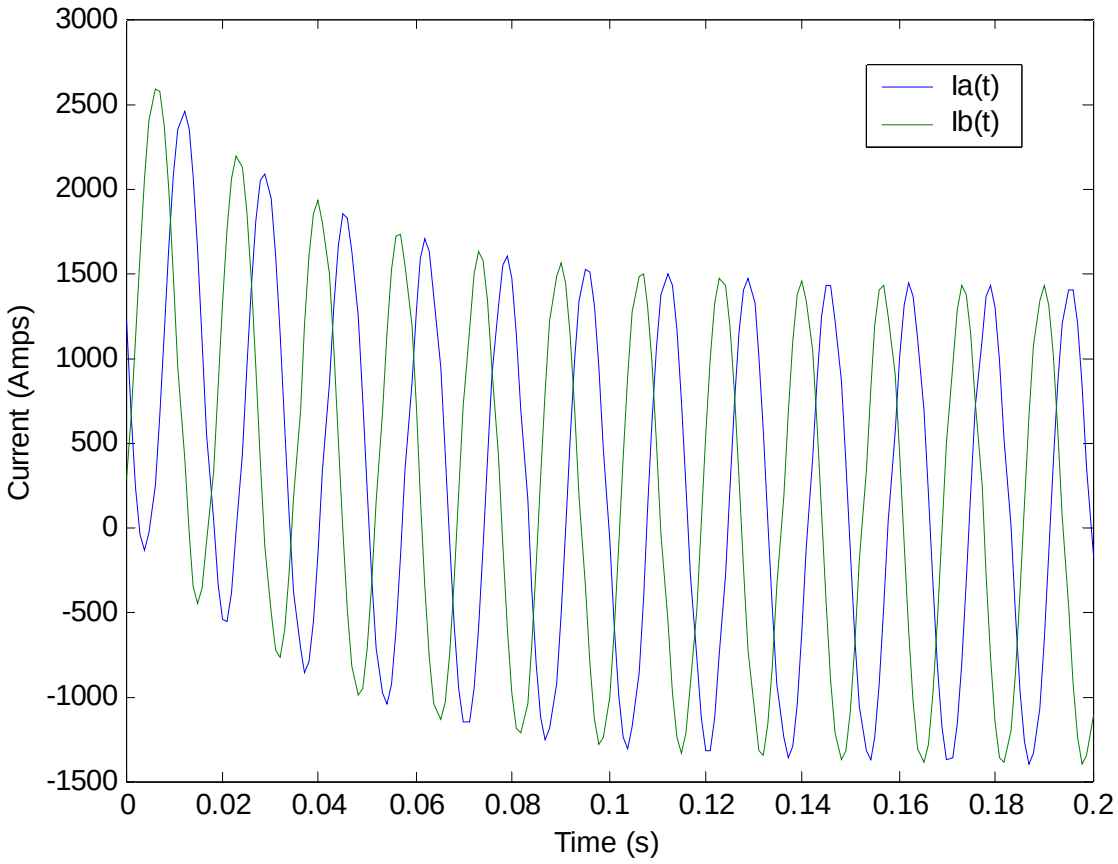

Figure 3.5: Input Currents 120 Degrees Out of Phase with Transients

Figure 3.6 shows the electromagnetic force waveform for the two currents presented in figure 3.5. After the transient forces decay, the steady state waveform is identical to figure 3.3. Its associated frequency spectrum for the first 11msec is shown in figure 3.7. The Fourier transform is defined as:

$$\left|G(w)\right| = \frac{\mu_o \, L \, I^2}{\pi \, d}\left(\frac{1}{2}\left(\frac{\omega}{\omega^2 + 4{\omega_o}^2} + \frac{1}{\omega}\right) + \frac{\cos(\phi + \xi)}{\omega + \frac{R}{L}}\right).$$

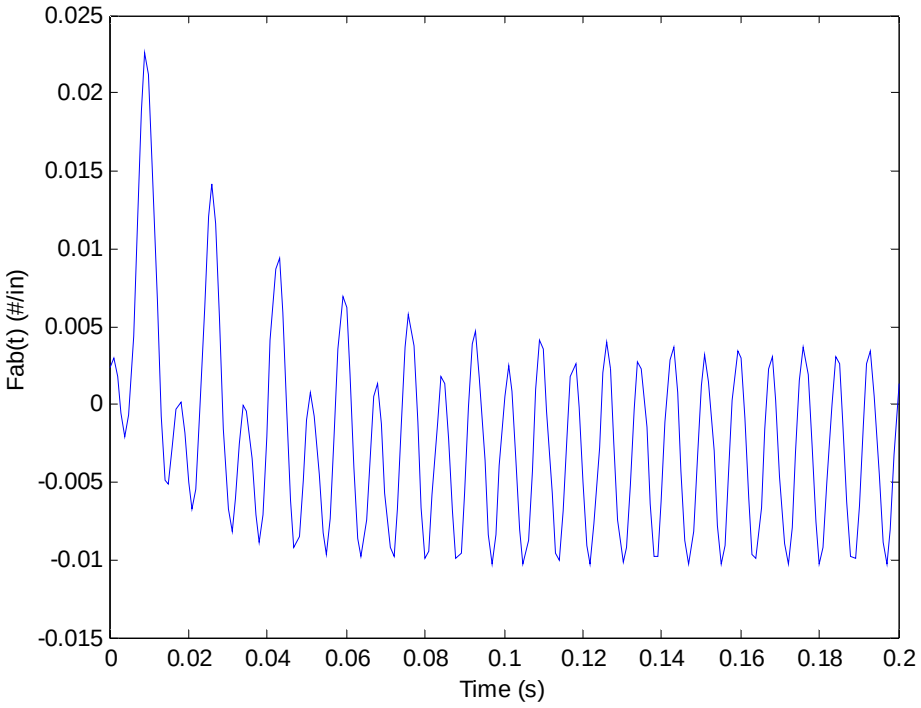

Figure 3.6: Electromagnetic Force $F_{ab}(t)$ with Transients

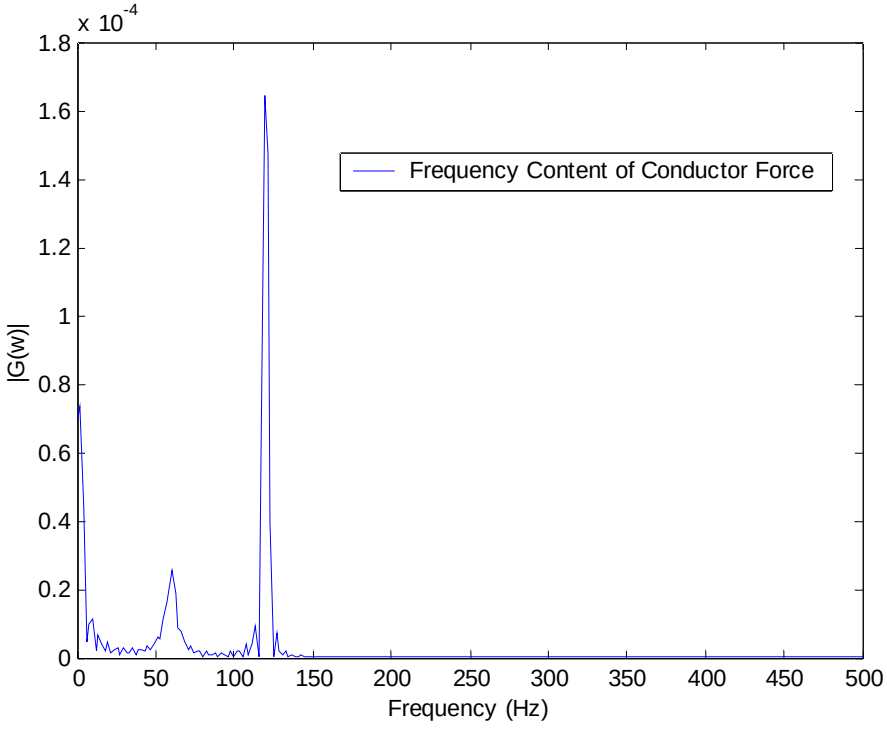

Figure 3.7: Frequency Content of Force $F_{ab}(t)$ with Transients

During the decay, a 60Hz force contribution is present. A similar peak 120Hz force is most apparent with contributions from a DC portion. Inspection of figure 3.6 indicate the first several cycles more closely resemble a 60Hz waveform than a 120Hz one. The necessity for the use of the transient 60Hz and DC component will become apparent on the discussion of bus response in section 4.

3.2 Three Phase Electromagnetic Conductor Forces

The use of three phase electric systems is common throughout the power industry. The infrastructure for the power grid particularly in substations and transmission lines, revolves around construction of sets of three identical phases. Figure 3.8 depicts a typical substation bus with insulator supports[1].

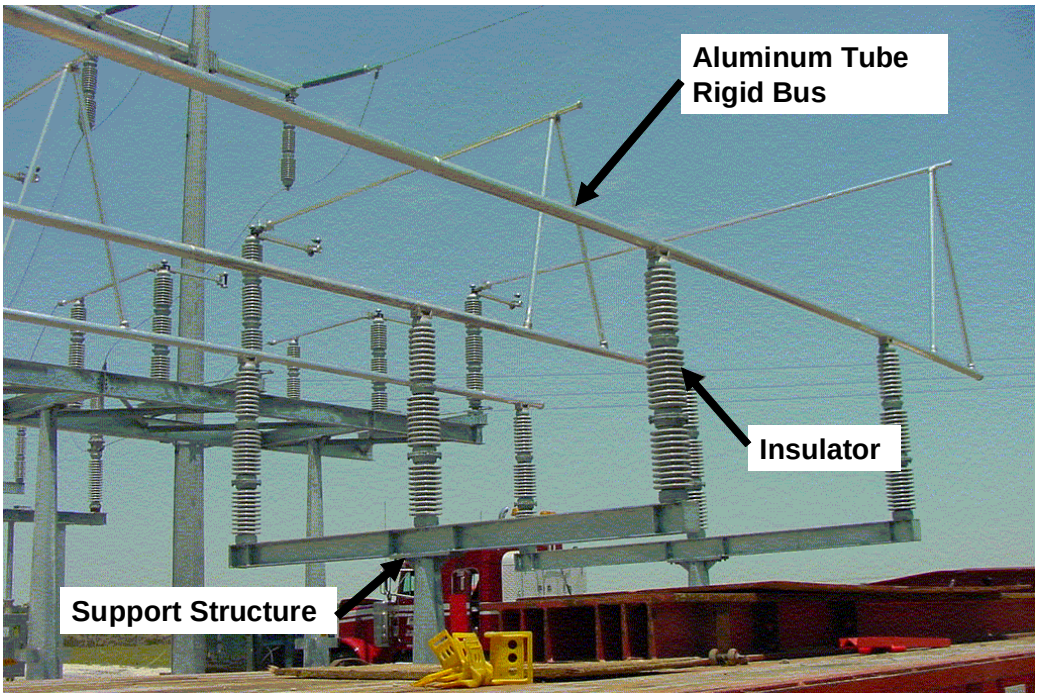

Figure 3.8: Example of Substation Three Phase Rigid Bus

[1] Photo courtesy of Entergy Services, Inc.

Figure 3.8 depicts a single support structure to which three station post insulators are attached. The insulators are in line to support rigid bus tubing using a bus clamp. Multiple spans of bus are used to carry current to electrical devices inside the substation. The substation designer has the flexibility to utilize multiple structures, insulators, and busbar according to electrical and physical constraints for the construction of substation bus. Figure 3.8 is one possible configuration which should be analyzed in detail by the substation designer. Design forces characterized for substation rigid bus in [2] include ampacity, corona, vibration, gravitational, wind, fault current, expansion, insulator, and conductor.

The various forces acting on substation bus spans add as vectors. Figure 3.9 depicts the net fault current forces for a plan view of a typical three phase span of bus. The forces are depicted at different points along the conductor for clarity purposes; however, the forces actually are evenly distributed on the bus as described in section 3.1.

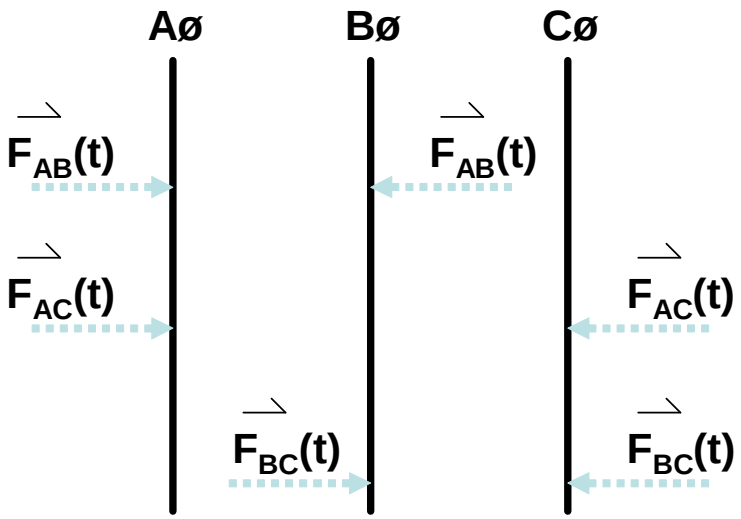

Figure 3.9: Three Phase Fault Current Force Vectors

Assuming the positive X direction is from the A phase towards the C phase, the net force for the three phases are defined in equations 3.5 through 3.7.

$$F_A(t) = F_{AB}(t) + F_{AC}(t) \tag{3.5}$$

$$F_B(t) = F_{AB}(t) - F_{BC}(t) \tag{3.6}$$

$$F_C(t) = -F_{AC}(t) - F_{BC}(t) \tag{3.7}$$

3.3 Single Conductor Three Phase Rigid Bus

Due to the unpredictable nature of faults and their seemingly random phase selection, any protection system should be able to detect any type of fault at any moment in time. This holds true for optical detection based conductor deflection. The conductor must deflect noticeably for any type of fault possible. Contributions from other phases have significant influence on this deflection. This section discusses the electromagnetic force influences from each conductor during the fault.

Inspection of equation 3.4 reveals a dependence upon the dynamic parameters of $I_a(t)$ and $I_b(t)$. For load current magnitudes much smaller than fault current magnitudes, the force between phases is extremely small and can generally be neglected. Since these fault current magnitudes are much higher than load currents, it is the scenario of a fault for which forces become significant enough to move the bus and allow for visual fault detection.

The ratio of the static force produced in a phase to phase fault using equation 3.4 versus a phase to ground fault is the ratio of fault current to load current of the unfaulted phase. Using dynamic analysis, the ratio can be calculated as indicated in the example below. Due to the unpredictable nature of faults, it is possible for a conductor to see significantly less force for a phase to ground fault than a phase to phase one. The ability to visually distinguish a fault using conductor dynamics becomes challenging from a design perspective. The dependence of A and

B phase currents in equation 3.4 produces a large swing of possible fault current forces dependent upon type of fault. This swing is significant enough to violate the stress limits on a conductor or barely move a conductor during deflection.

For example, assume an A phase to ground fault and a A to B phase fault in a three phase bus. The fault current is assumed to be 40kA RMS (steady state) and load current of 2kA RMS in the unfaulted phases. Using equations 3.4 and 3.5 with 3 ft phase spacing and load current of 2000 amps on unfaulted phases, the time varying amplitude of the electromagnetic force on phase A from phase B is depicted in figure 3.10. The influence of the C phase load current is apparent on the magnitude of each peak of the waveform offset from the previous peak.

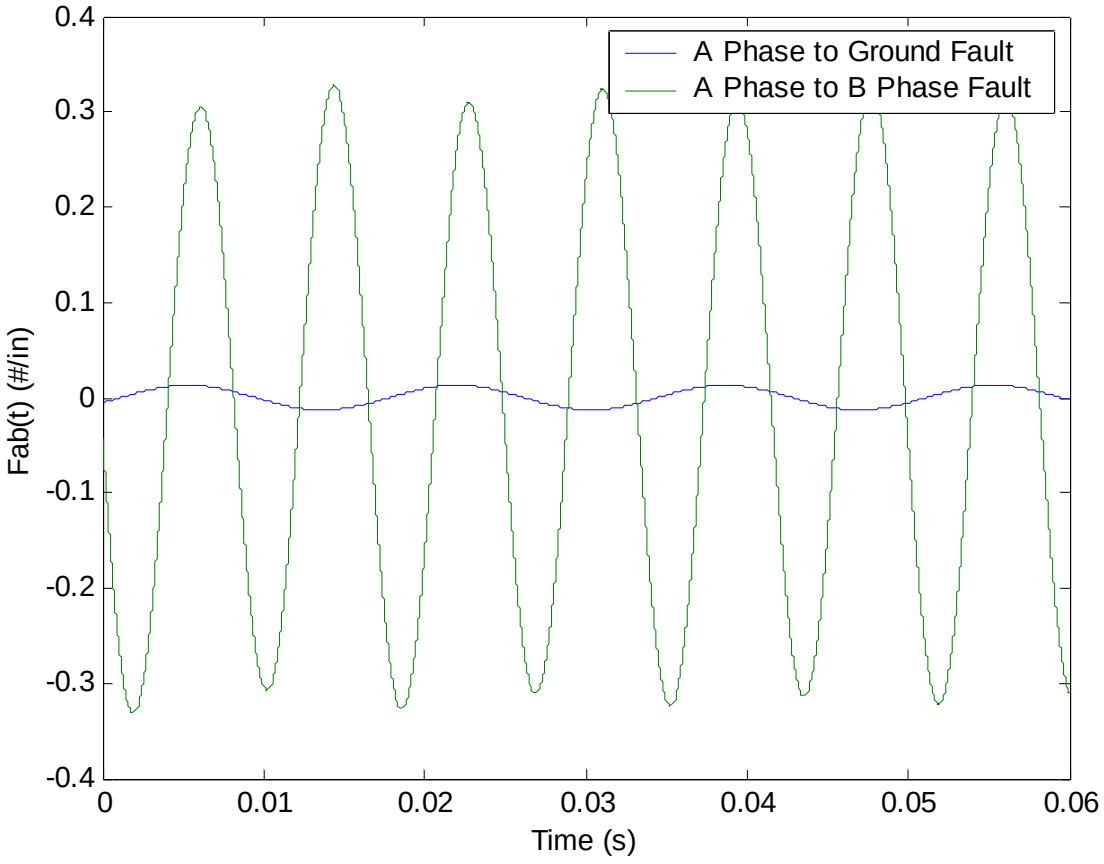

Figure 3.10: Example of Forces Generated for Two Fault Types

The static ratio of fault current force is 20. Dynamically at an instant in time, however, the ratio is approximately 22. Inclusion of the ground path in the fault or a three phase fault produces similar ratios. In either the static or dynamic analysis, it is clear in figure 3.10 that the ratio of force generated can be large depending upon which type of fault occurs for a system.

3.4 Bundled Conductor Three Phase Rigid Bus

The use of bundled rigid conductors is generally not common in substations. Typically, bundled conductors are used on transmission lines or jumper conductors which require additional ampacity or to reduce the effects of audible corona on EHV substations. Conductor sizing is generally based on heat rate for each installation (ampacity) and available hardware for the conductors chosen. The rigid bus ampacity values from single conductors are usually sufficient for heating due to load currents. The additional hardware and construction time are generally unnecessary. Overall, the concept has not been utilized much inside the substation.

The use of bundled rigid conductors has a distinct advantage for fault detection purposes which will be analyzed in this section and in section 4. These include conductor deflection independent of unfaulted phase load current values or type of fault. Symmetry of the bundle requires deflection of both phases to prevent false trips due to natural phenomenon such as animal interference with the detection device.

As depicted in figure 3.10, the electromagnetic force differences from phase to phase and phase to ground faults can be high. The deflection differences of each type of fault are substantial enough to limit the detection of the fault depending upon conditions. Section 4 will discuss this in detail.

Equation 3.4 shows the dependence on load current in unfaulted phases to produce electromagnetic forces. Thus, low load faults versus high load faults will produce different forces on the conductors. Deflection of the bus is affected by this load current. A fault detection system should be able to properly detect faults for any load level. This reality limits the use of conventional three phase, single conductor bus designs.

Figure 3.11 depicts a plan view of the electromagnetic forces using a six conductor, three phase bundled bus. As in figure 3.9, the forces are depicted at different points along the conductor for clarity purposes; however, the forces actually are evenly distributed on the conductors. It should be noted that phases A and D, B and E, C and F are equipotential and bundled.

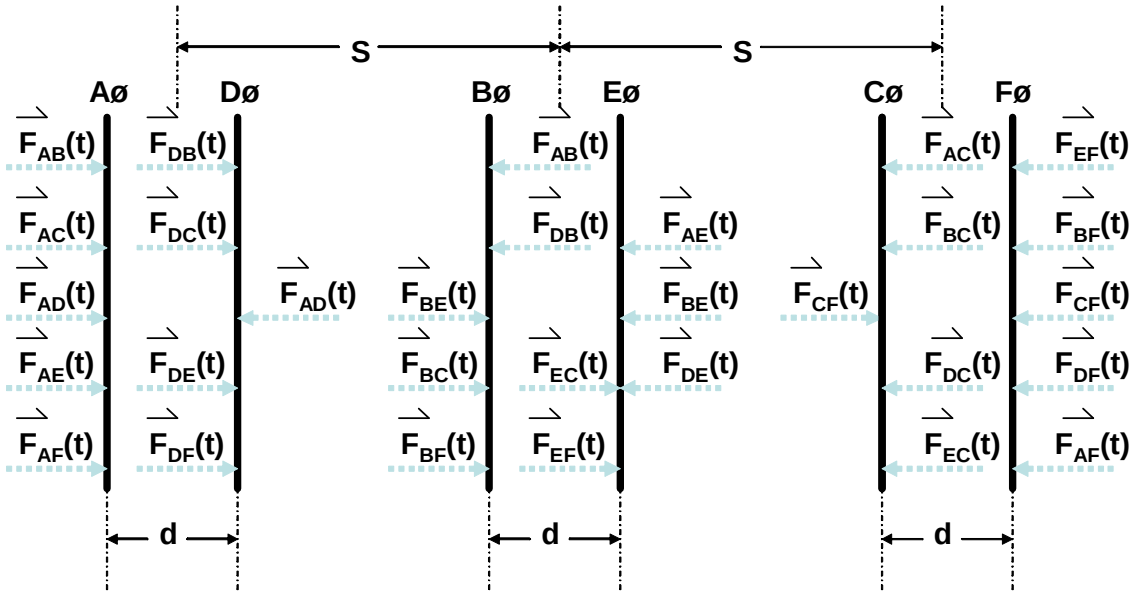

Figure 3.11: Bundled Fault Current Force Vectors

Each bundled conductor depicted in figure 3.11 is separated by a distance d. Each bundle is separated by distance S. Assuming the bundles are equipotential with equal current distribution, the force seen on each conductor bundle is symmetric and independent of which

type of fault is present in the system, neglecting the contributions from other phases. The net force on the bundles including outside phases is listed in equations 3.8 through 3.13.

Assuming the positive X direction is from the A phase towards the C phase, the net force for the three phases are defined as:

$$F_A(t) = F_{AB}(t) + F_{AC}(t) + F_{AD}(t) + F_{AE}(t) + F_{AF}(t) \tag{3.8}$$

$$F_D(t) = F_{DB}(t) + F_{DC}(t) + F_{DE}(t) + F_{DF}(t) - F_{AD}(t) \tag{3.9}$$

$$F_B(t) = F_{BE}(t) + F_{BC}(t) + F_{BF}(t) - F_{AB}(t) - F_{DB}(t) \tag{3.10}$$

$$F_E(t) = F_{EC}(t) + F_{EF}(t) - F_{AE}(t) - F_{BE}(t) - F_{DE}(t) \tag{3.11}$$

$$F_C(t) = F_{CF}(t) - F_{AC}(t) - F_{BC}(t) - F_{DC}(t) - F_{EC}(t) \tag{3.12}$$

$$F_F(t) = -F_{AF}(t) - F_{BF}(t) - F_{CF}(t) - F_{DF}(t) - F_{EF}(t) \tag{3.13}$$

Application of equation 3.4 to the bundled conductors in figure 3.11 indicates that the closer two conductors are, the stronger their electromagnetic force generated. Thus, the force on phase A from phase F will be significantly less than that of phase A on phase D. In order to utilize the bundled configuration to accurately detect faults based on deflection due to bus dynamics, the design should try to keep d<<S as depicted in figure 3.11. This will increase the bundle isolation and create a response with negligible effects from load currents on unfaulted phases.

Electromagnetic forces due to the pinch effect can be extreme and must be analyzed for any possible violation of conductor stress limits. Equation 3.14 shows the maximum span length for a conductor with two pinned ends as given in [2]. C is 3.46 for English units, L_s is the maximum allowable span length (inches), F_A is the maximum allowable stress (lb/in), S is the

total section modulus (in^3), and F_T is the total force (lb/ft). The maximum stress is typically the elastic limit of the material.

$$L_s = C\sqrt{\frac{12\,F_A\,S}{F_T}} \tag{3.14}$$

In addition to stress limits determining the maximum separation distance of a conductor bundle, the deflection of the conductor under stress due to the electromagnetic forces must be considered. Clearly, the two conductors should not be close enough to collide into each other as the deflection occurs. Such a scenario could damage the conductor or structure. Section four discusses time varying bus deflection in detail.

4.0 Substation Bus Response

In order to accurately detect system faults using conductor dynamics, the response of the conductor to the electromagnetic forces must be accurately analyzed.

Like the static and dynamic analyses of the electromagnetic forces in section 3, the mechanical response will be analyzed in this section. The use of both static and dynamic responses of the substation rigid bus will be discussed.

4.1 Static Analysis of Rigid Bus Mechanical Response

Static mechanical analysis for a dynamic natured system will produce conservative results independent of time. In reality, this approach is commonly used for the selection of bus materials. The information provided in [2] is based mostly from this static analysis. The conservative results are used to provide for a margin of safety in the selection of substation materials.

These conservative results also neglect the time variable. As described in sections 2 and 3, the time variable is critical in the use of fault detection.

In the simple case of a single span of bus, the following example describes the simplicity yet inaccuracy of strict static analysis when accurate, time dependent results are necessary.

The deflection of a single span of rigid bus with tightly clamped bus on insulators can be modeled as a beam with a constant load applied as seen in figure 4.1 per [8].

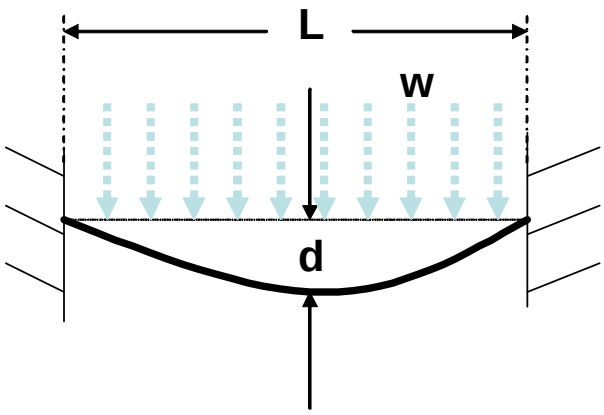

Figure 4.1: Beam Deflection Due to an Evenly Distributed Load

The uniform load, w (#/in), shown in figure 4.1, produces a beam deflection at the midspan of the beam of length L (in) given in equation 4.1 where E is the modulus of elasticity (#/in^2) and I is the moment of inertia (in^4).

$$d = \frac{w L^4}{384 E I} \tag{4.1}$$

If a static load, w, is applied to this simple beam, the beam moves from its at rest position to its newly deflected position and remain until the load is removed. This approach of static analysis does not account for any time delay required for the beam to get from its at rest position to its deflected one. If accurate time based fault detection is required, this method is inadequate. Dynamic analysis is selected to improve this accuracy.

This is merely one example of a single span of bus deflection. The substation designer has the flexibility to vary the number of spans and conductor types according to substation requirements. The methods for analysis of these are given in [2]. The use of the single conductor span with two support insulators will be commonly used throughout this paper (figure 4.2). Implementation of the methodology used in this paper allows for the flexibility of mounting structure dimension and spans using the single span as a starting point for the design.

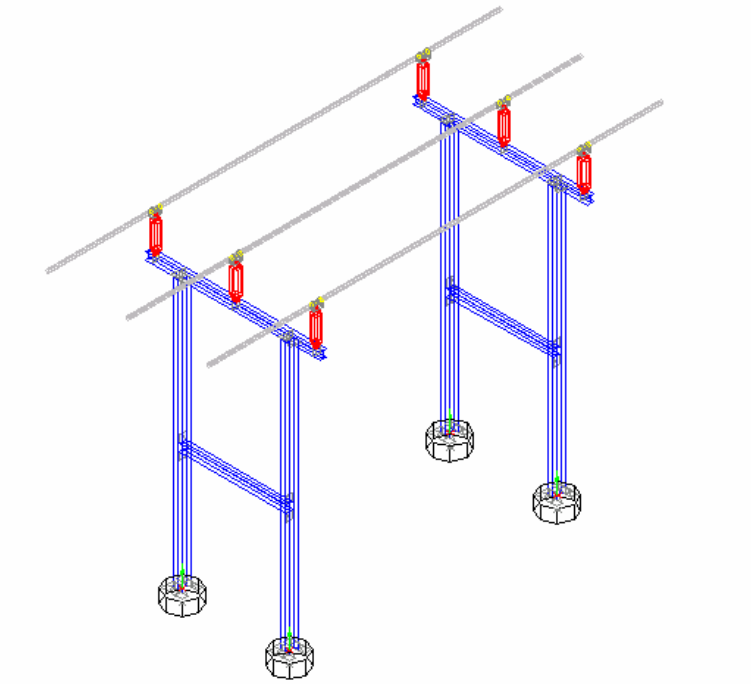

Figure 4.2: Example of a Single Bus Span with Two Structures

Utilization of the bundled rigid bus configuration as discussed in section 3.4 is depicted in figure 4.3.

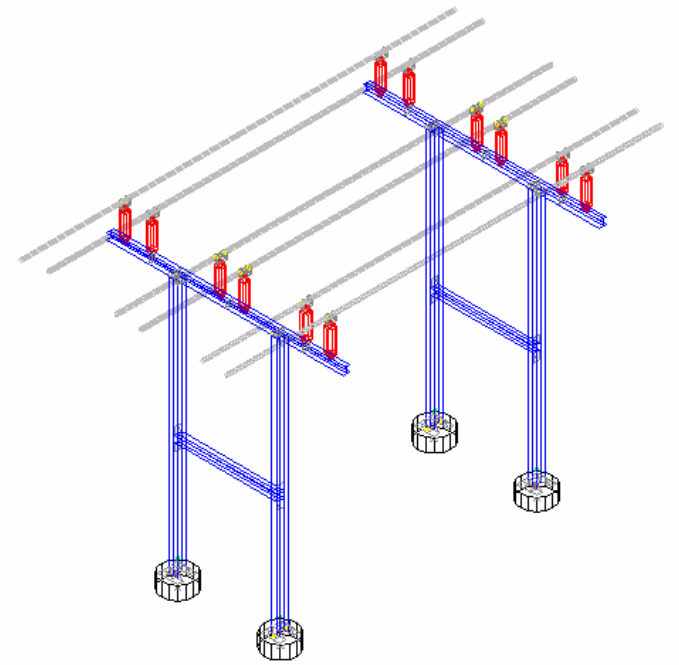

Figure 4.3: Example of a Single Bus Span with Bundled Rigid Conductors

4.2 Dynamic Analysis of Rigid Bus Mechanical Response

The dynamic analysis of substation rigid bus is best accomplished using the analogy of a spring-mass system. The deflection shown in figure 4.1 has a time component dependent upon the natural frequency of the span. Figure 4.4 depicts a simple spring model of a conductor span where k is the spring constant, m is the system mass, P(t) is the applied force, and x(t) is the displacement.

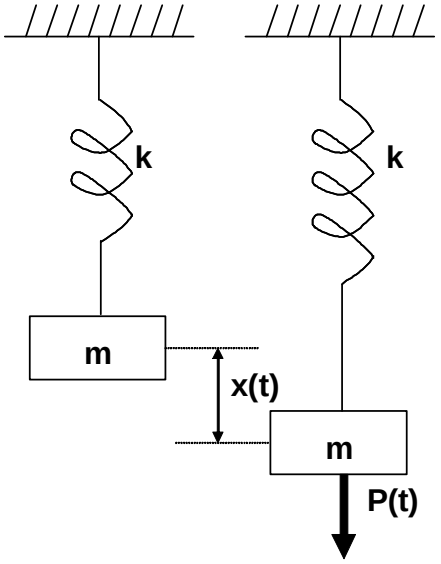

Figure 4.4: Spring-Mass System Representation of Rigid Bus Span

The dynamic analysis of the simple spring mass system is detailed in [9] and modeled by the differential equation 4.2.

$$m\frac{d^2x}{dt^2} + kx = P\sin(\omega_f t) \tag{4.2}$$

Because it has one degree of freedom, the X direction will be used to indicate motion of the mass. On the rigid conductor spans depicted in figures 4.2 and 4.3, the direction of force is perpendicular to the ground plane. The driving force, P(t) is defined as a sinusoidal waveform

with forced frequency, ω_f . In the case of a power system fault, the driving forces are the electromagnetic forces described in section 3.2.

Solving equation 4.2 for displacement, x(t), results in equation 4.3 where P is the amplitude of the driving force and ω_n is the system natural frequency.

$$x(t) = \frac{P/k}{1-\left(\omega_f/\omega_n\right)^2} \tag{4.3}$$

The natural or circular system frequency is defined in equation 4.4. It is independent of any outside forces and is the time required for steady state deflection to occur.

$$\omega_n = \sqrt{\frac{k}{m}} \tag{4.4}$$

The driving frequency should not be confused with the system natural frequency. The system can be excited using any value of P(t) with distinct driving frequencies. In the case of the span of rigid bus on the 60 Hz power grid as described in previous sections, these are primarily 120 Hz with a DC offset with some 60 Hz components dependent upon the system X/R ratio.

[10] discusses the concept of a magnification factor. The ratio of the displacement, x(t), to the static displacement, -kx, is a magnification factor, ς (sigma), described in equation 4.5.

$$\varsigma = \frac{|x(t)|}{P/k} = \frac{1}{1-\left(\omega_f/\omega_n\right)^2} \tag{4.5}$$

Further analysis of equation 4.5 reveals an asymptote when the forced frequency is equal to the natural frequency. Figure 4.5 depicts this asymptote and the magnification factor.

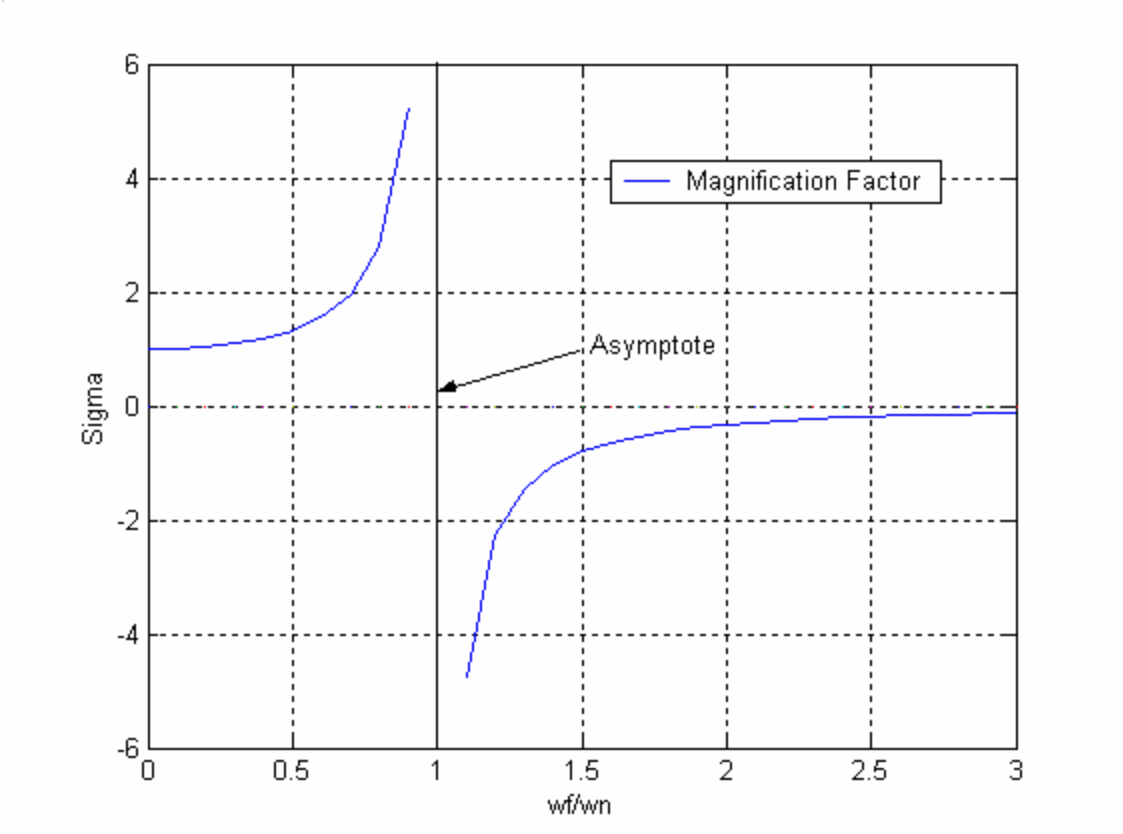

Figure 4.5: Magnification Factor of a Spring-Mass System

The asymptote of figure 4.5 represents an interesting and common natural phenomenon. Any system excited at its natural frequency appears to have infinite gain and maximum output per given input. A simple example of this is a child in a swing. As the "pusher" of the swing, it is often desirable to swing the child high with minimal effort. If the pusher adapts the frequency of the pushes to match that of the rhythm of the swing, the mathematical representation is depicted as the asymptote in figure 4.5. In reality, the swing would not have infinite gain to any input due to wind resistance, imperfections in the hardware, and motion of the child. If the swing is pushed at a rhythm not equal to the natural frequency, the "pusher" will have a difficult time getting the swing to move higher (and would also have a disappointed child).

These same natural frequency characteristics apply to that of substation bus deflection. If the bus is excited at a frequency equal to its natural frequency, the bus could stress to its elastic

limits and create permanent damage. The major means of excitement for rigid bus are seismic, wind, and electromagnetic. In general, it is desirable to design substation equipment such that the natural frequencies of conductor spans do not have a chance of becoming excited with a large magnification factor by any of these forces. For electromagnetic force excitement, the IEEE recommends the use of dampers if the natural frequency of the conductor span is greater than the power frequency [2]. Additionally, if twice the natural frequency of a span is greater than the force driving frequency due to wind, damping is recommended. Damping commonly involves the installation of flexible conductor inside a tubular conductor.

On the other hand, the natural frequency presents unique design characteristics. For example, [11] presents the novel application of removal of ice from flexible bundled conductors by exciting the span with frequencies near its fundamental frequency. This oscillatory excitement causes conductor bundles to literally collide with each other and remove ice by these collisions.

In the application of fault detection, the natural frequency of the bus span plays a key role. In accordance with the magnification factor described in this section, the ratio of the driving frequency to the rigid bus span's natural frequency will be greater than unity. As in the analogy of a child on a swing, the theoretical value of infinite gain cannot be reached by the conductor driven at its natural frequency. This is mostly due to the resistance of the bus supports and insulator supports and the damping it provides. Although this infinite gain characteristic cannot be attained, it still represents the frequencies producing the most stress on the span.

Figure 4.6 depicts a typical frequency response output for the spring mass system depicted in figure 4.4. The peak gain is not infinite for the reasons described in this section. The natural frequency of the system is approximately 4.5 Hz.

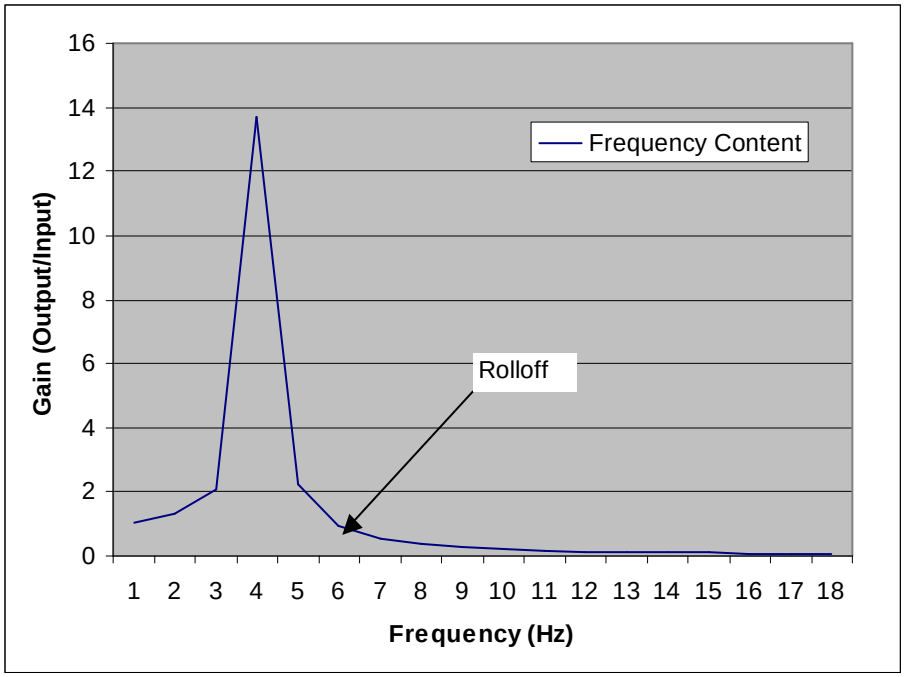

Figure 4.6: Frequency Response of a Spring-Mass System

The components of rigid bus spans must be translated to parameters of the spring-mass models for the purpose of dynamic analysis.

The natural frequency of a single bus span with fixed ends is defined in equation 4.6 as described in [2].

$$f_n = \frac{\pi K^2}{C L^2}\sqrt{\frac{EI}{m}} \tag{4.6}$$

where f_n = natural frequency of conductor span

K = 1.51 for fixed ends on the conductor span

C = 24 for English units

L = conductor length (ft)

E = modulus of elasticity (lb/in^2)

I = moment of inertia (in^4)

m = mass per unit length (lb/ft)

The conductor spring constant, k_{bus}, is determined by combining equations 4.4 and 4.6 into equation 4.7.

$$k_{bus} = \frac{4\pi^4 K^4}{C^2 L^4} E I \tag{4.7}$$

Figure 4.7 is an application of equation 4.6 to show several conductor's natural frequency versus length. The figure provides information that shows a correlation between the stiffness of the conductor verses its natural frequency. Smaller natural frequencies correspond to larger and stiffer conductors. Additionally, higher natural frequencies correspond to shorter conductor spans These characteristics are useful in conductor selection in addition to ampacity/heat requirements in [2].

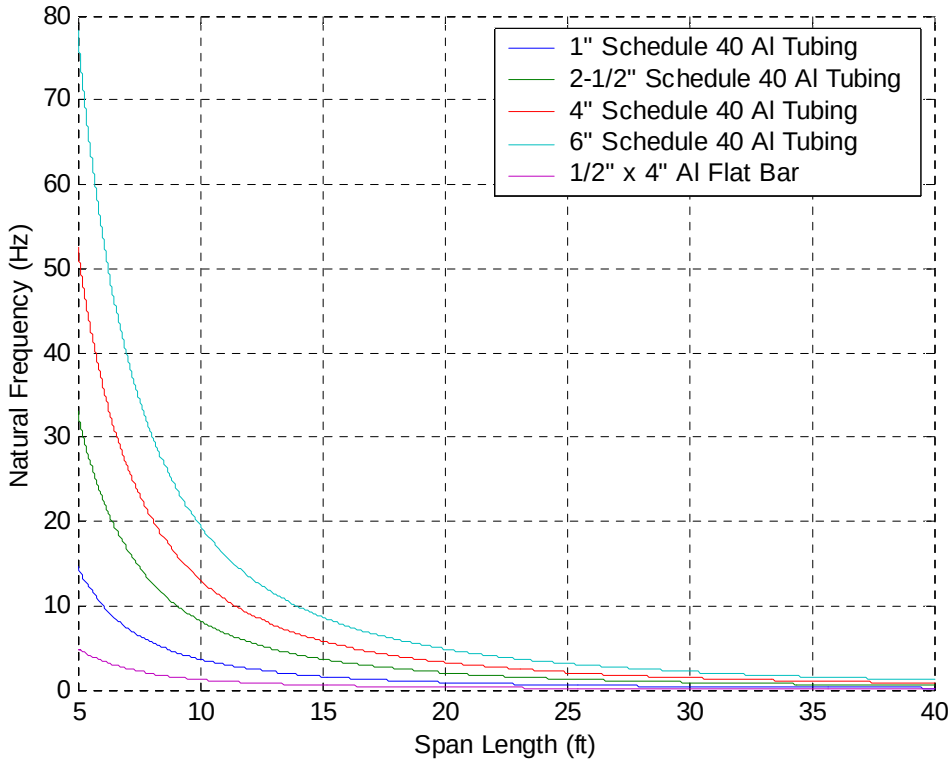

Figure 4.7: Natural Frequencies for Several Conductor Types

The analogy of the spring-mass system should include the support insulators. Tips of the insulators will move at their natural frequencies when driving forces are applied. [12] describes the concept of a spring constant for insulator supports. This insulator spring constant is defined in equation 4.8 where E is the section modulus, I is the moment of inertia, and H is the height of the insulator.

$$k_{ins} = \frac{3\,E\,I}{H} \tag{4.8}$$

Equation 4.9 gives the natural frequency for insulators. In reality, this natural frequency is the basis for determining tip displacement versus applied load to a span of conductor. Both the natural frequencies for the bus span and insulator have been verified using the chirp response method via adaptive filtering in [12].

$$f_{ins} = \frac{1}{2\pi}\sqrt{\frac{k_{ins}\,g}{.226\,F_i + F_b}} \tag{4.9}$$

where f_{ins} = insulator natural frequency

g = gravitational constant (386.4 in/s^2)

F_i = insulator weight (lb)

F_b = effective weight of conductor transmitted to support fitting (lb)

The dynamic model for a single span of bus including the response of the insulators is depicted in figure 4.8.

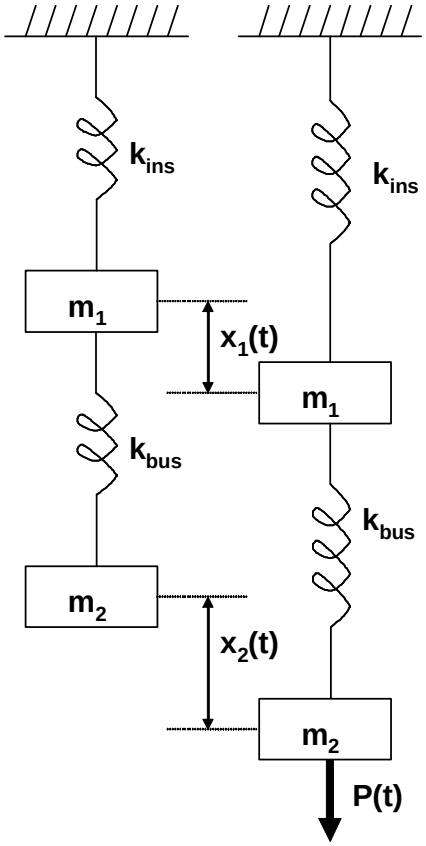

Figure 4.8: Spring-Mass System Representation of Rigid Bus Span with Insulators

The dual spring-mass system of figure 4.8 can be electrically analyzed using the model in figure 4.9.

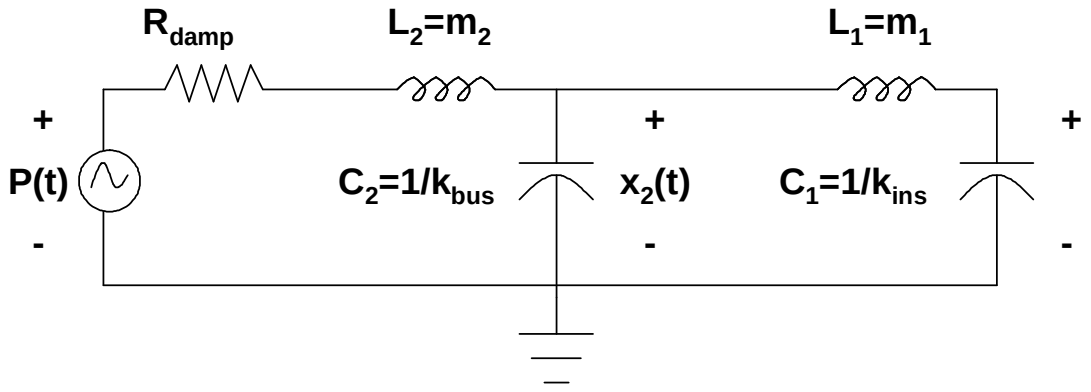

Figure 4.9: Electrical Equivalent Model of a Mechanical Spring-Mass System

The damping resistor, R_{damp} has been included in the electrical model to dampen the response of the linear system. Without such a resistor, the energy due to friction of supports and

wind resistance would not dissipate any of the energy from the input source. This produces a ringing effect which would never settle to any DC value.

The differential equations governing the electrical equivalent circuit are shown in equations 4.10 and 4.11 (neglecting the resistance contribution). The mechanical system equivalents are shown in equations 4.12 and 4.13.

$$L_1 \frac{d^2 q_1}{dt^2} + \frac{q_1}{C_1} + \frac{q_1 - q_2}{C_2} = 0 \tag{4.10}$$

$$L_2 \frac{d^2 q_2}{dt^2} + \frac{q_2 - q_1}{C_2} = P(t) \tag{4.11}$$

$$m_1 \frac{d^2 x_1}{dt^2} + k_1 x_1 + k_2 (x_1 - x_2) = 0 \tag{4.12}$$

$$m_2 \frac{d^2 x_2}{dt^2} + k_2 (x_2 - x_1) = P(t) \tag{4.13}$$

The frequency response of the dual spring-mass system, figure 4.10, shows the presence of two distinct natural frequencies. The smaller natural frequency is the conductor span's frequency and the larger is the insulator natural frequency. This is consistent with the conclusions in [12].

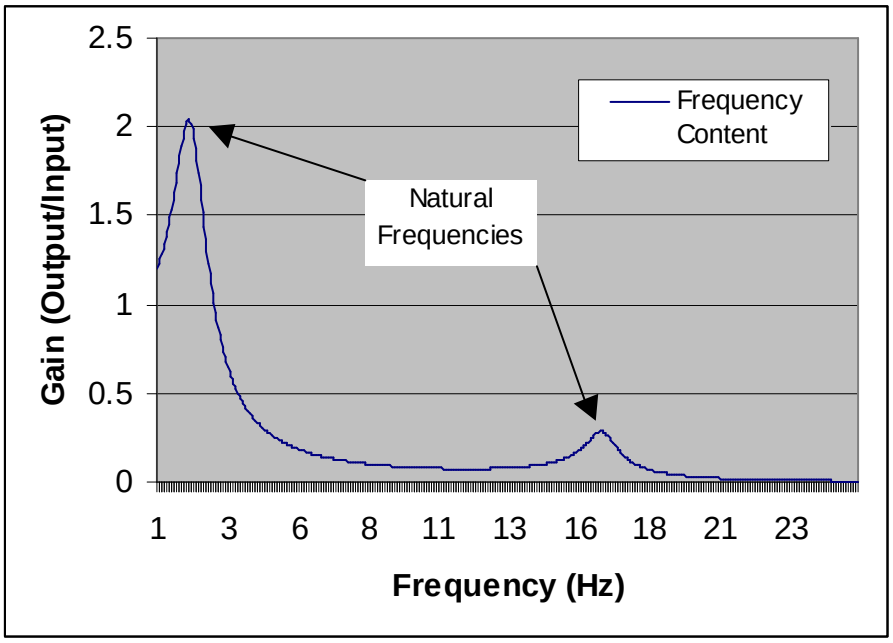

Figure 4.10: Natural Frequencies of a Dual Spring-Mass System

The transient step response for the system of figure 4.8 is depicted in figure 4.11. The motion of the conductor is shown to have a swinging effect with damping contributions from R_{damp}. The period of oscillation for the response is the reciprocal of the fundamental (lowest and most dominant natural) frequency of the conductor. The second natural frequency of the system contributes its oscillating characteristics showing insulator tip displacement at the conductor midspan. Since the driving frequencies are either 120 or 60 Hz, the motion of the spring-mass system mostly moves due to DC components. This displacement is seen as the step response as indicated in figure 4.11.

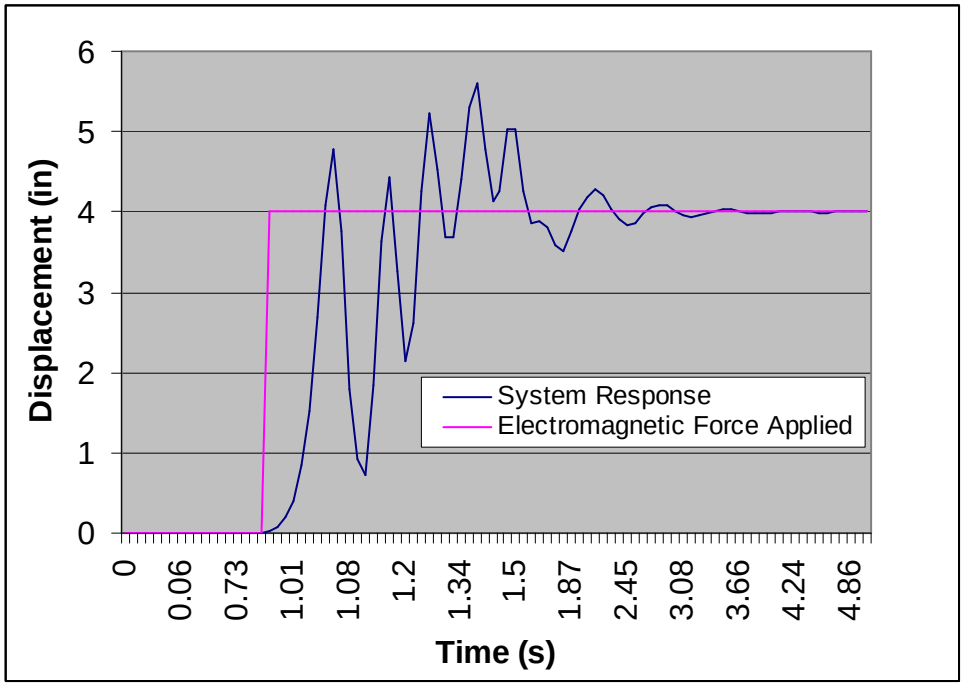

Figure 4.11: Transient Step Response of a Dual Spring-Mass System

Determination of the system natural frequencies is accomplished using matrices for the mechanical spring system in figure 4.8. The equations can be put into matrix form as written in equations 4.14 and 4.15.

$$\begin{pmatrix} m_1 & 0 \\ 0 & m_2 \end{pmatrix} \begin{pmatrix} \frac{d^2x_1}{dt^2} \\ \frac{d^2x_2}{dt^2} \end{pmatrix} + \begin{pmatrix} k_1 + k_2 & -k_2 \\ -k_2 & k_2 \end{pmatrix} \begin{pmatrix} x_1 \\ x_2 \end{pmatrix} = \begin{pmatrix} 0 \\ 0 \end{pmatrix} \tag{4.14}$$

$$\overline{M}\ddot{x} + \overline{K}x = 0 \tag{4.15}$$

The matrix $\overline{K}$ is defined as the stiffness matrix for the system. Manipulation of the differential equation matrices yields the determination of the natural frequencies for the system [9] in equation 4.16.

$$\det(\overline{M}^{-1}\overline{K} - \omega^2\bar{I}) = 0 \tag{4.16}$$

where $\overline{\overline{M}}$ =system mass matrix

$\overline{\overline{K}}$ = system stiffness matrix

$\bar{\bar{I}}$ = identity matrix

ω = system natural frequencies (rad/s)

The eigenvalues of $\overline{\overline{M}}^{-1}\overline{\overline{K}}$ results in the determination the natural frequencies, ω_1^2 and ω_2^2. The square root of the eigenvalues will result in the two natural frequencies of the system.

The mode shapes of the oscillatory spring-mass system are the eigenvectors of $\overline{\overline{M}}^{-1}\overline{\overline{K}}$. The system will have as many distinct mode shapes as the order of the matrices. Thus, the system of the busbar with insulator supports contains two modes of oscillation. The actual free motion of the system is determined using superposition of the various modal shapes of the linear system. Because the first mode of oscillation is most dominant and the higher order modes are less dominant, a system can be approximated using this superposition technique over the first few modes.

By including the insulators in the model for displacement, a more accurate response can be determined for the system than the busbar. To further improve the modeling, the natural frequencies of the bus support structure should be included in the model. The IEEE indicates further analysis is possible using the structure/insulator combination [2]. The use of single phase lolly column support structures tends to absorb energy which reduces the displacement of the bus. Because the analysis in this paper utilizes three phase bus supports with little self-deflection due to canceling effects of faulted phases, the analysis of the influence of single phase bus supports will not be covered. For the modeling in the application of figure 4.3, the effect of the support structure is assumed to be minimal [2].

4.3 Dynamic Response of Bundled Conductor Faults

The displacement of bundled conductors during a fault should be equal and opposite as depicted in figure 4.12 assuming minimal influence from outside phases. This is a characteristic of the pinch effect discussed in section 3.

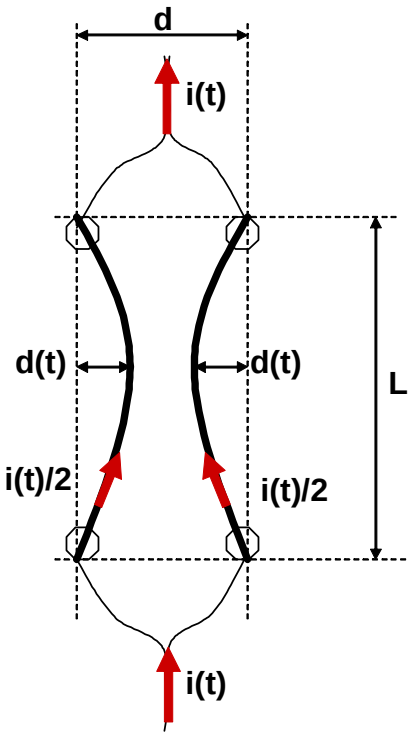

Figure 4.12: Bundled Conductor Displacement Due to Fault Forces

Equation 4.17 is an application of equation 3.4 with input current $i(t) = i\sin(\omega t)$ split equally between both conductors.

$$F_{ab} = \frac{\mu_o L (i/2)^2 \sin^2(\omega t)}{2\pi d} \tag{4.17}$$

Figure 4.13 is a plot of equation 4.17 with magnitude of input current equal to 10 kA RMS, separation distance of 2 ft, and no transient fault current (X/R = 0).

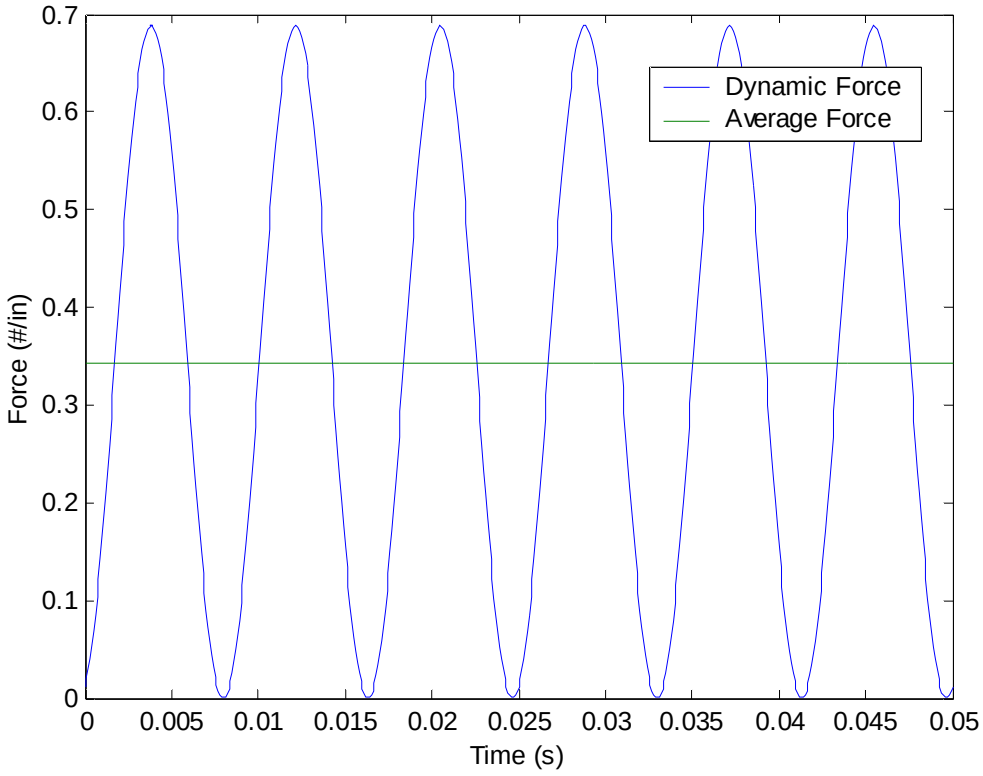

Figure 4.13:Bundled Conductor Short Circuit Forces

The function is primarily driven by $\sin^2(\omega t)$. The sinusoidal function as an input signal can be broken down into components and its outputs added together via superposition to attain the system output. The sinusoidal half angle formula [13] can be applied to bundled conductors to show the components of the linear system.

$$\sin^2(\omega t) = \frac{1 - \cos(2\omega t)}{2} = \frac{1}{2} - \frac{\cos(2wt)}{2} \tag{4.18}$$

Equation 4.18 indicates a DC component equal to half the peak time varying signal. The AC component is equal to a sinusoidal component with frequency of twice the power frequency.

As discussed throughout section 4, system inputs with frequencies near the system natural frequencies have the most influence on the output of the system. Equation 4.18 shows there are two components for the bundled conductor arrangement which can be included as

inputs to the system. The AC component in a 60 Hz electric system will show up as purely 120 Hz if the X/R ratio is considered negligible. The same holds true after the transient fault current portions have subsided.

Figure 4.14 shows the influence from the transient portion of fault currents due to the X/R ratios discussed in section 2. During the presence of the transient component, there is significant influence from the 60 Hz and DC portions of fault current. The green and red arrows indicate the development of a 120 Hz sinusoidal function, $\sin^2(\omega t)$, in the steady state. The 0, 60, and 120 Hz components are displayed in figure 3.7 via Fourier analysis.

The DC component in the steady state is present for the duration of the fault. The initial DC component is also present, but varies according to the transient duration. Deflection of the bus does not vary significantly with varying X/R ratios because the additional DC components will decay faster than the bus can displace. The amount of DC component in the force signal is influenced directly by the X/R ratio, as discussed in section 3.

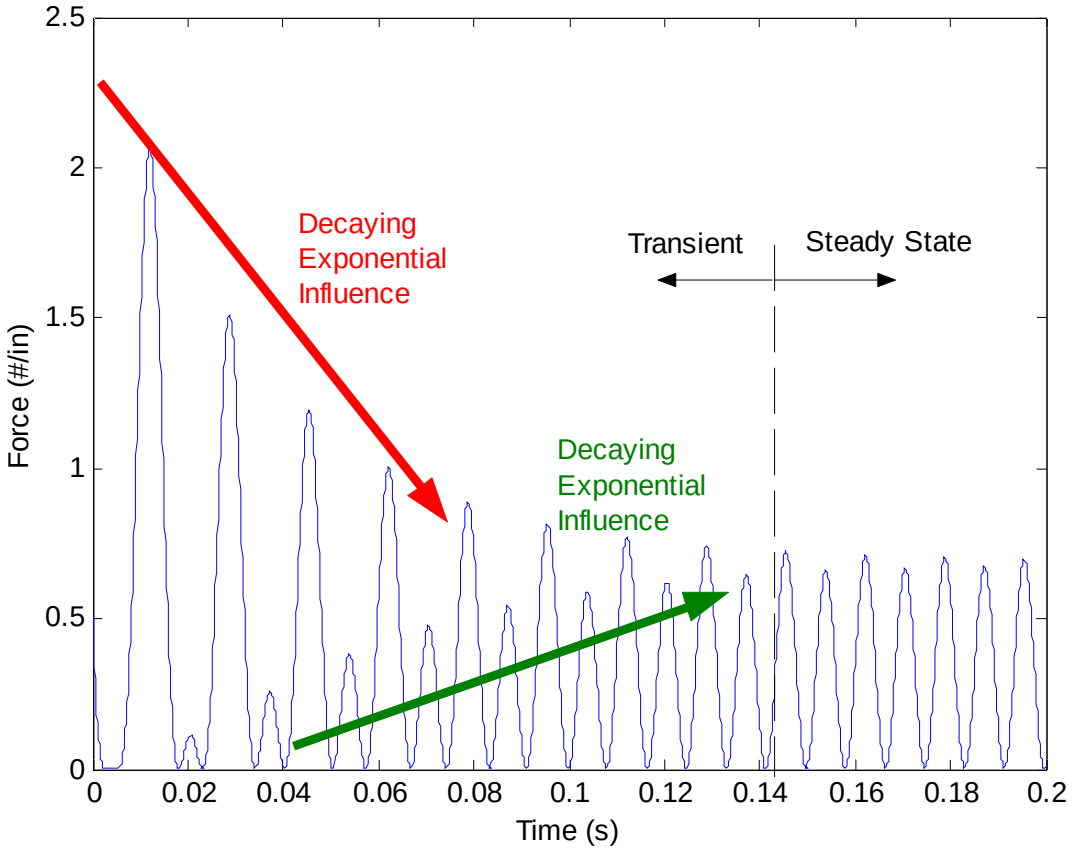

Figure 4.14: Transient Bundled Conductor Short Circuit Forces

The deflection on a bus span to an input signal must be evaluated during design to ensure the bus is not excited electrically near the natural frequencies of the bus span. Based on the research of this paper and [2], it can be concluded that the higher order frequencies of the input waveform have little influence on the bus span. The approach of using the DC component of the fault current as the primary and most influential component of the conductor motion can be utilized effectively, regardless of typical X/R ratios. For the purpose of this paper in its recommendations for fault detection, the bus span's natural frequencies should have negligible influence from the AC component of the fault current forces. It is the DC component which will

have the most significant impact. The DC component input is the average of the electromagnetic force generated. An example of this is depicted in figure 4.15.

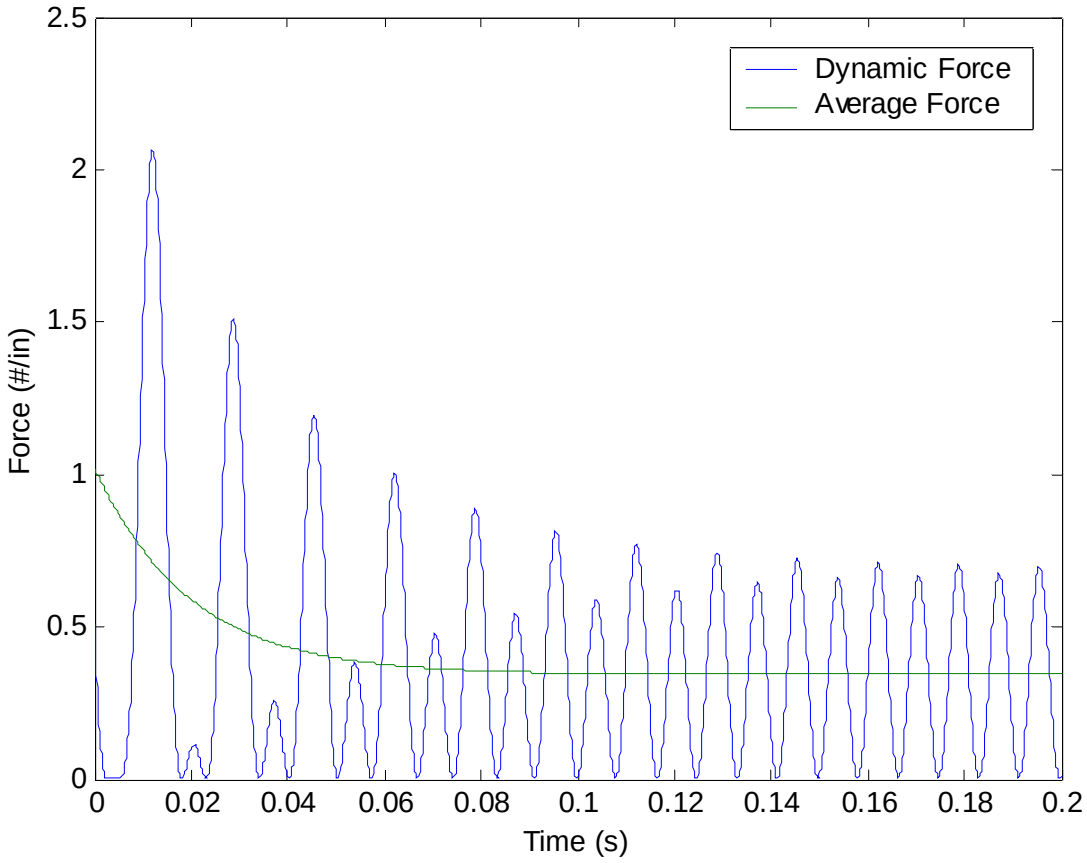

Figure 4.15: Average Bundled Conductor Short Circuit Forces

Using the average input force as the input function to the dual spring-mass system, the displacement of the conductor midspan can be accurately modeled. The fundamental frequency becomes the most important setting for the conductor response to this input function. It primarily drives conductor deflection generally slower than the transient component of fault current can influence deflection. This simplifies analysis of bundled conductor deflection by using the input function of the average input force.

5.0 Optical Method of Fault Detection

Electromechanical forces generated during power system faults affect all power system equipment in series with the fault. This includes insulators, conductors, support structures, breakers, transformers, and generators. Theoretically, any of these power system components could be measured for the effects of fault current detection. For example, stresses on insulators or structures could be measured using strain gauges. This paper focuses on the optical method of detection in which the motion of the conductor span is measured at its midpoint. The span can then be designed to provide accurate detection which can be integrated into a relay time-overcurrent curve.

5.1 Physical Configuration

Conventional relay selection and settings require the use of set points to trigger action upon detection of faults. The conductor dynamics approach to fault detection also requires set points. The method for choosing a single set point will be discussed in this section. This set point is the determined using the physical analysis of conductor deflection and integrating to the electrical domain of relay settings.

Crucial to understanding the operation of the optical fault detection system is the proposed physical configuration of figure 5.1. Each conductor is equipped with a reflective mirror which reflects normal to the ground plane. Its purpose is to reflect a transmitted laser source back to its detector located beneath each mirror.

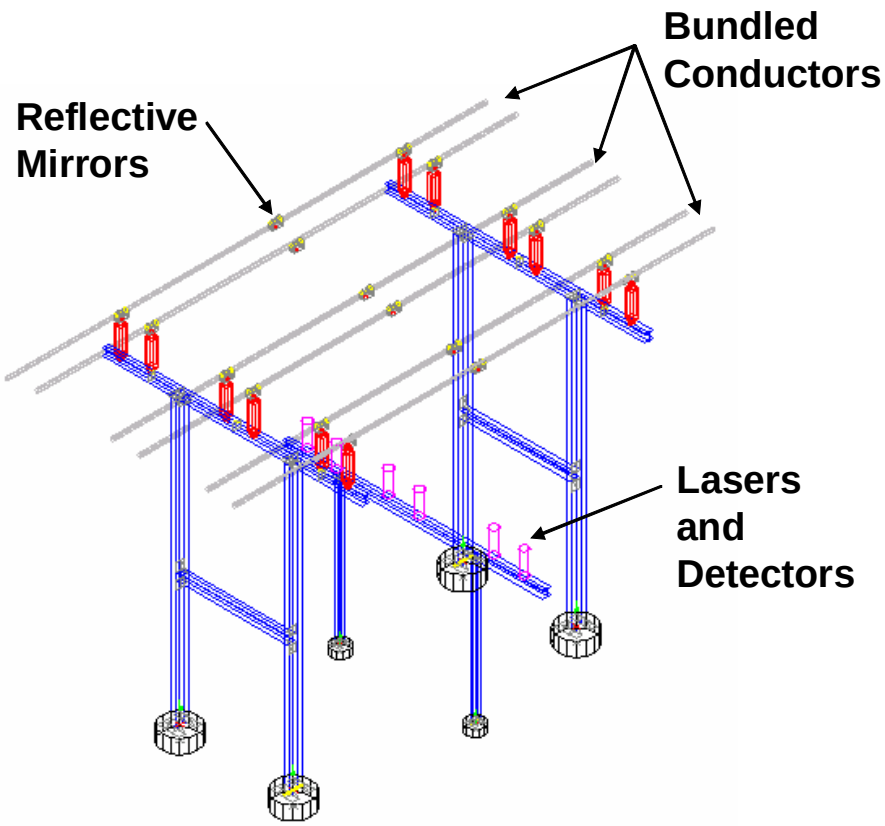

Figure 5.1: Physical Fault Detection Configuration

The presence of a fault is detected using a binary signal of two laser beams per bundle. Since the displacement of each bundle is theoretically identical assuming minimal influence from outside phases, the displacement of the bundle is detected and registered if both conductors of the bundle are displaced. The primary reason for detecting displacement of both conductors in a bundle is to mitigate potential false trips. For example, a bird could fly in the path of one conductor's laser beam and the device will not detect a fault condition. Stationary animals landing or climbing on the laser/detector combination would not cause false trips. Because the odds of both beams blocked simultaneously are smaller than one beam blocked, nuisance trips can be avoided. Failed laser detectors or those that did not receive signals could provide indication for required maintenance using XOR logic.

The entire fault detection span should be housed inside an electrical substation. The equipment used requires power, control, and signal cables. It should ideally be near its interrupting device for quick response. Additionally, such a bus span can easily be integrated into line and transformer bays if consideration is given for the required span distance. Finally, interference from the public should be minimized inside the gates of the substation. For these reasons, installation of such a bus span is ideal inside a substation.

5.2 Time-Current Coordination

A fault occurring anywhere in series with a protective device should be detected provided sufficient fault current flows to displace the bus past its at rest reflective mirror location. As is the nature of fault currents, the further away from the source, the more line impedance limits the magnitude of fault current. Consideration should be given based on system topology and possible fault locations to determine set points. The same logic applies for conventional transmission line relaying settings.

In the event of a fault, all three phases are generally tripped. The type of fault and phases involved are irrelevant if the logic is designed to trip all three phases. Thus, the detection and settings must hold to the weakest and least detectable fault scenario. The system topology must be accurately modeled and analyzed to determine if it will trip for all types of fault scenarios. Figure 5.2 depicts an electrical representation of the trip logic using AND and OR gates with the phasing convention of figure 3.11.

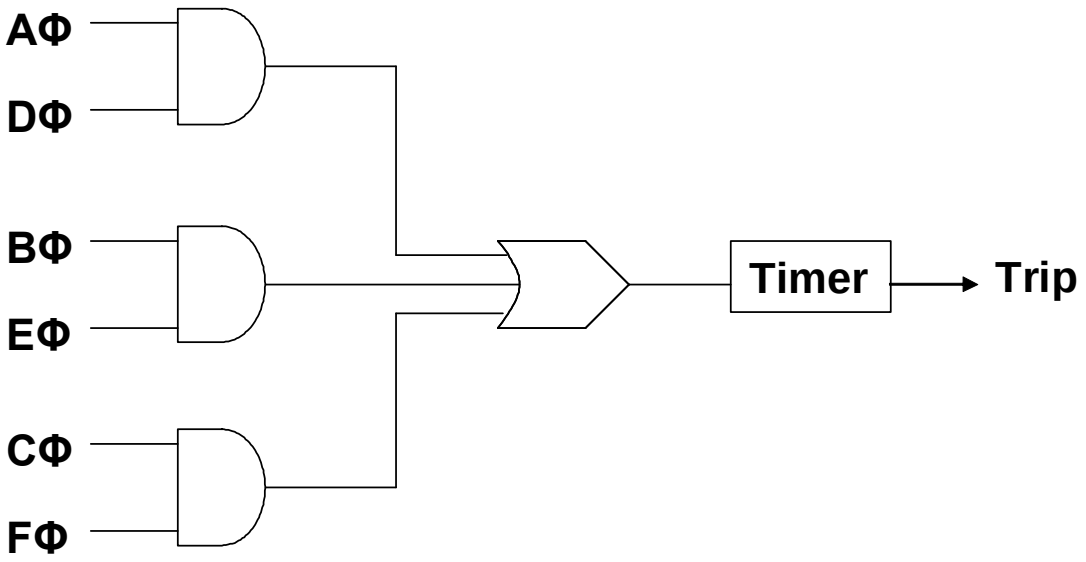

Figure 5.2: Electrical Diagram of Detection Logic

The inverted phase detector signal is used as inputs to the logic diagram. If the mirror reflects from the source to the detector, the input signal used is represented as a 0 in the diagram. If the bus is displaced beyond the mirror such that it does not reflect back, the input of a 1 is used in the logic diagram.

The OR gate is used to send an instantaneous displacement signal on any set of bundled conductors to the timer. The timer should be set according to system topology. It is the set point for the system and is based on the amount of time the bus has been displaced from its natural form of a straight physical beam.

The size of the reflective mirror is important in determining the timer setting. Any bus deflection which is smaller than the mirror size does not trigger a displacement signal. This allows for some flexibility in alignment tolerances as well as vibrations due to mild seismic or low wind conditions. Static influence of wind on the bus response is briefly discussed in [2] and can be analyzed in the design process if required. Alternately, the system could be disabled if gusts are detected. Unfortunately, this may work against the purpose of the system. Line faults

are often triggered by trees brushing in the wind against conductors. Disabling the system for such a gust could prove disastrous for power system equipment in series with the faulted line.

Figure 5.3 illustrates a profile view of figure 5.1. The importance of the mirror size is emphasized. Ideally, the system should focus the beam at the center of the mirror. During deflection, the beam should clear the mirror without reflecting. Such is the basis for the binary operation if the bus has deflected due to fault current forces.

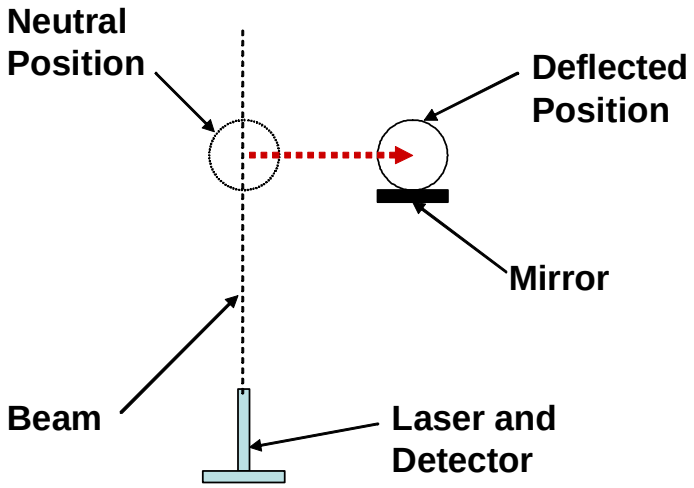

Figure 5.3: Profile View of Physical Fault Detection Configuration

Figure 5.4 shows an example of conductor displacement due to fault current forces. The red line is determined by the size of the reflective mirror. If the displacement is greater than ½ of the mirror length, the reflection does not occur and bus displacement is recognized (figure 5.5) as a binary signal.

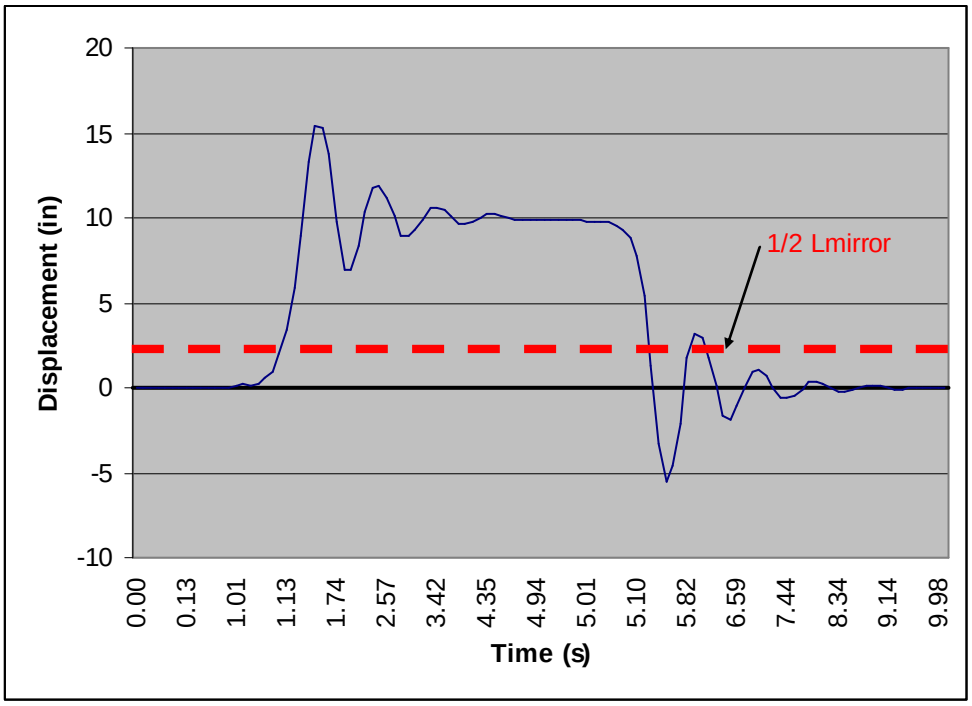

Figure 5.4: Conductor Displacement with Reflecting Mirror Position

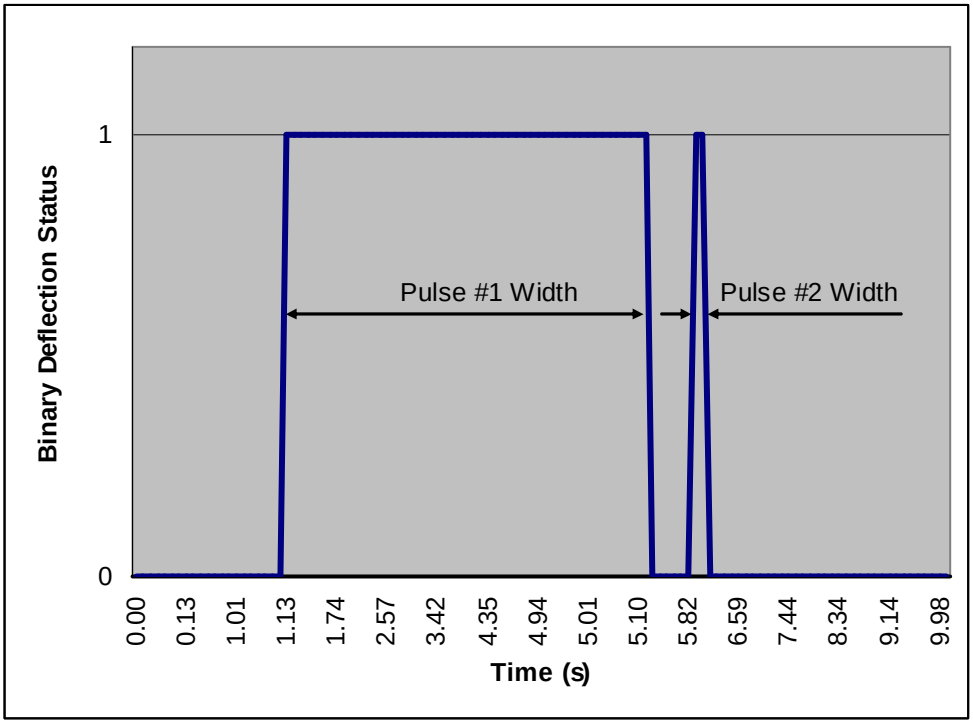

Figure 5.5: Deflection Displacement Detection Pulses

The two pulses shown in figure 5.5 are a result of displacement beyond that of the reflecting mirror width. Proper setting of a delay timer causes the logic diagram of figure 5.2 to ignore pulse #2. The trip signal should not be initiated based on the oscillation of the bus after the fault is cleared. Pulse #1 is a large amount of time and the setting of the delay timer should trigger a trip signal for such a length of time.

Inspection of figure 5.4 shows that the size of the mirror does have considerable impact on the detection pulses of figure 5.5. If the mirror size was chosen to be larger than 5, the second pulse would not exist in the detection plot of figure 5.5. If the mirror was chosen to be less than 5", more secondary pulses would be present in the detection plots. The delay timer would need to be adjusted not to trip on these additional pulses.

When the fault current forces are relieved due to interrupting devices, the bus returns to its at rest position. The amount of time required for this to occur is a function of the fundamental frequency of the conductor span.

Figure 5.6 shows this dependence upon the natural frequency. T1 is the time in which the fault current is cleared. T2 is the time at which the pulse signal is detected.

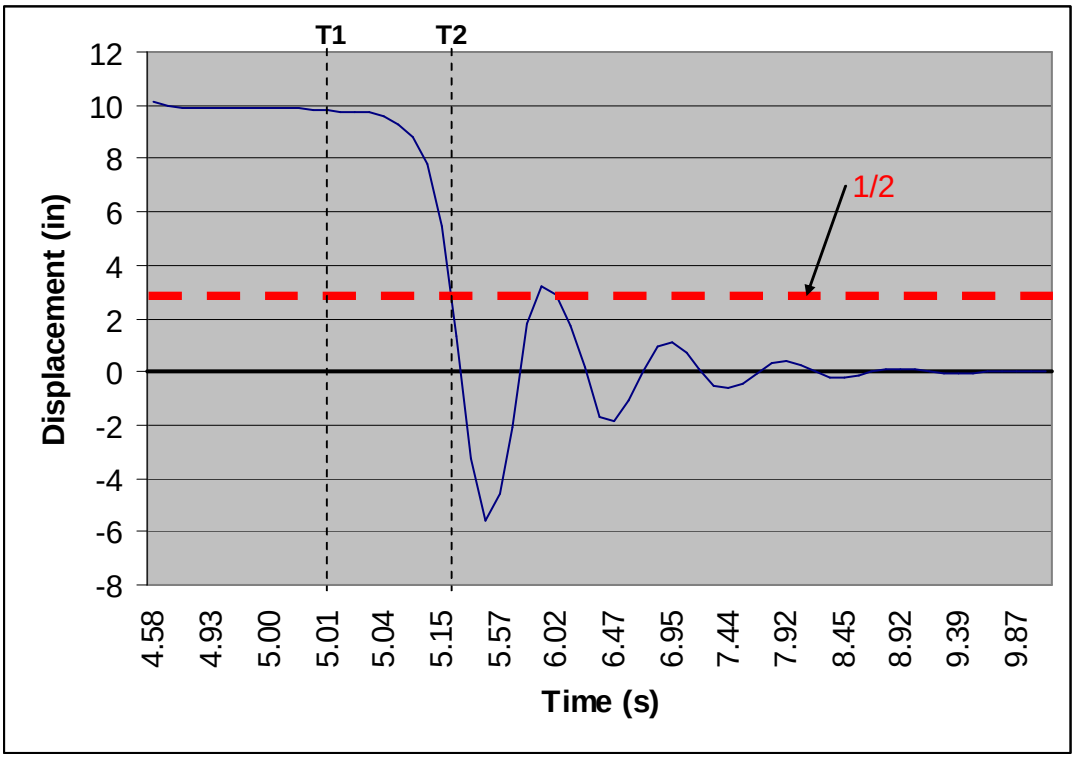

Figure 5.6: Conductor Displacement Following Fault Clearing

The time period of conductor motion from its deflected position to the at rest position follows that of equation 5.1.

$$T2 - T1 = \cos(\omega_n t) \tag{5.1}$$

The fall time indicated as T2-T1 should be considered in selection of conductor natural frequency and time delay settings. Timer settings and mirror sizing should be determined based on this fall time. To minimize unnecessary outages, the amount of time required for the bus to return to its at rest position should be reflected in the timer setting and mirror size.

The pulse width is the primary means of fault detection. The time delay setting of the relay should be set as the threshold for the trip signal. The setting should be designed to not send a trip signal until any primary relaying has a chance to operate. This also applies to relaying

associated with circuit breakers closer to the faulted segment. Deflection of the bus for these occurrences must be calculated to ensure proper relay settings.

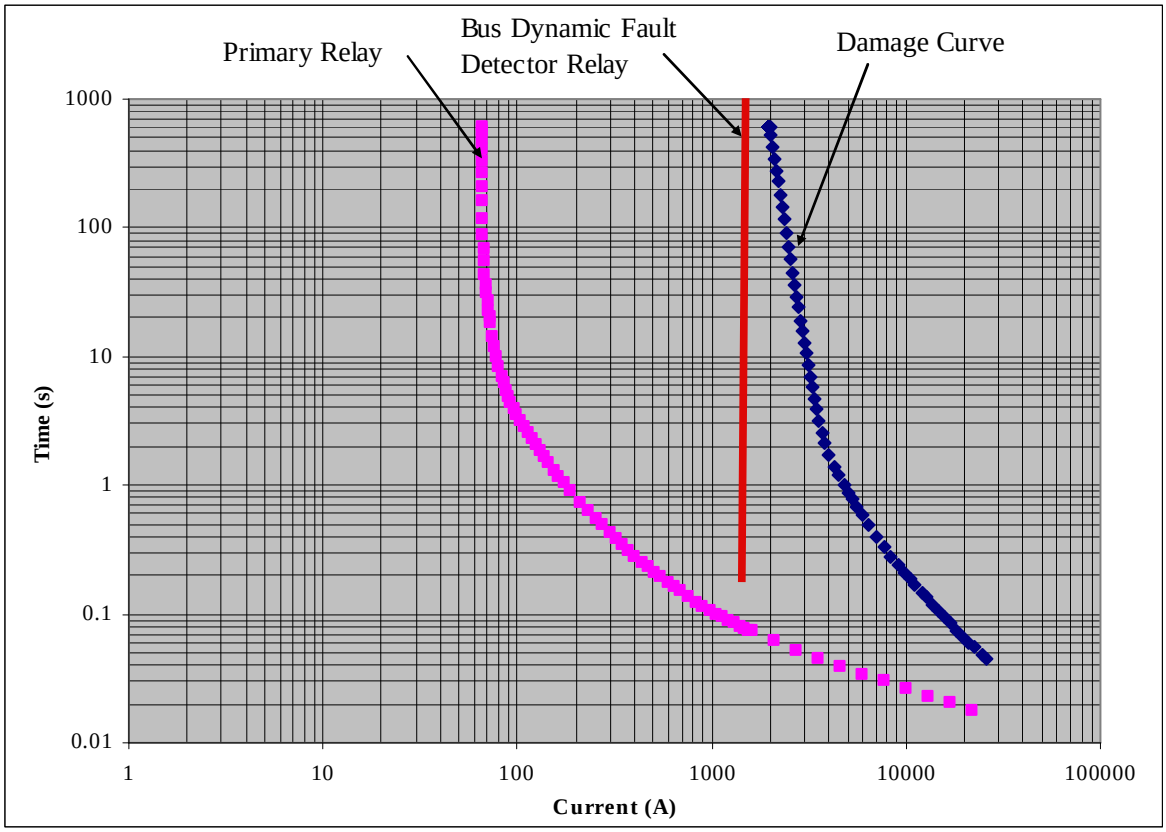

Figure 5.7: Typical Bus Dynamic Fault Detector Setting

The fault detector based on conductor dynamics cannot retrieve fault current data directly. The use of the pulse width is the only means of detecting the fault. This is plotted as a single line on the time-overcurrent curve. The red line of figure 5.7 does not reach the X axis because it has a delay of approximately 0.2 seconds before detection is possible. This is based on the fundamental frequency of the bus span. It is important for the setting to be before the equipment damage curve, but not act before the primary relay has acted.

The logic described in figure 5.2 must produce a trip signal for any type of conductor fault. The relay timer setting to be calibrated using the smallest type of fault current desired. For faults near the detector, this could be slightly less than the maximum calculated fault current;

however, this approach is not recommended since it is reflective of a bolted fault. If any impedance is inserted in a fault or if a fault occurs down a segment of line, the delay setting may not detect due to a limited deflection. Thus, the fault would be undetected.

The fault current for different types of faults will vary. As discussed in section 2, these differ according to system topology. The settings used for the fault detector should reflect the smallest of the types of fault currents. The use of bundled conductors with proper spacing will minimize the displacement due to outside phases, so the smallest value of fault current for the various types of faults should be considered for this reason. The span response must also be analyzed for larger fault currents to ensure conductor stresses are not violated or collisions inside bundles do not occur.

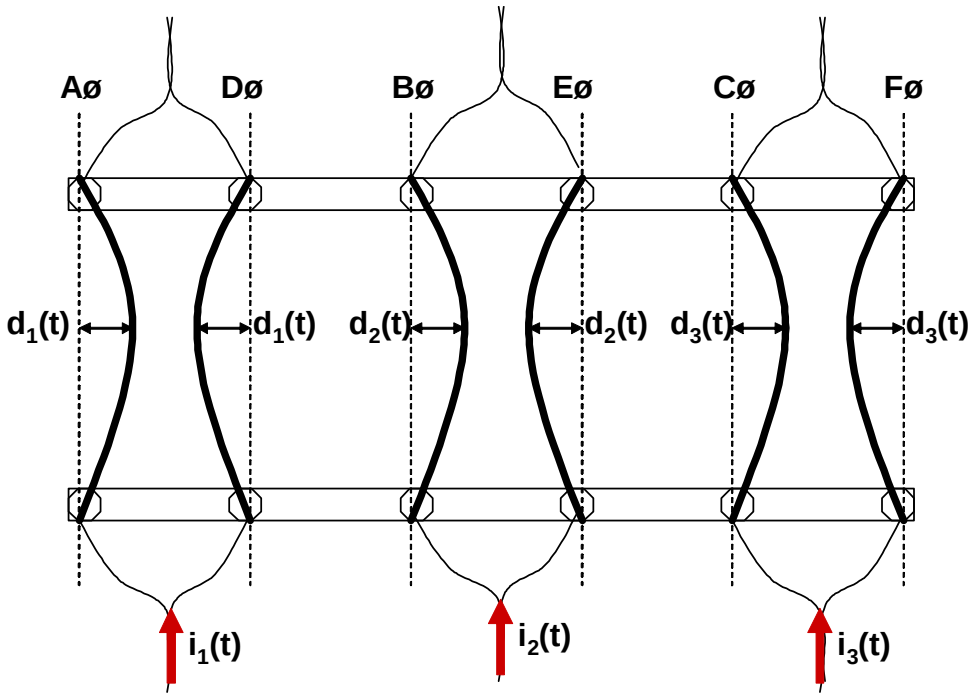

Figure 5.8: Displacement of Conductor Bundles

Figure 5.8 shows the deflection resulting from different fault currents to the power system. Realization that the deflection from bundle to bundle will differ according to type of fault is crucial in the design phase.

5.3 Multiple Circuit Detection Coordination

Coordination of fault detection using multiple circuits inside a substation can be accomplished by setting the relays for the appropriate amount of fault current for each circuit. Each fault scenario should be analyzed to determine what the minimum time delay setting or mirror size should be for each fault detector. The value of fault current through a circuit will vary according to contribution based on faulted circuit location and selection. This variance should be analyzed to determine maximum and minimum fault current levels for a particular circuit. This information is necessary to properly set the timer of the protection device.

Figure 5.9 shows a 4 circuit substation bus with a fault on circuit 1. Fault current contributions from circuits 2, 3, and 4 are indicated as 5kA, 10kA, and 12kA respectively.

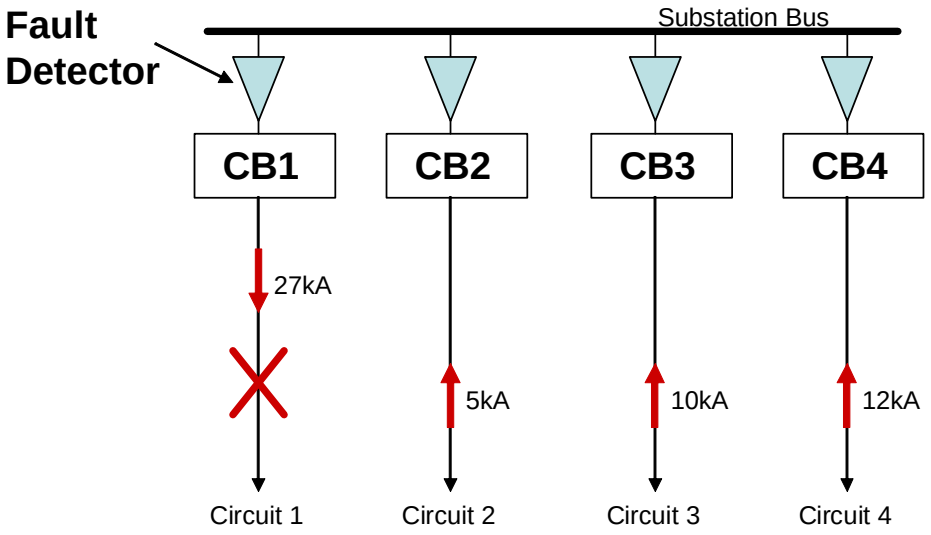

Figure 5.9: Fault Current Contributions for Fault on Circuit 1

Figures 5.10 through 5.12 show the scenarios of faults on circuits 2, 3, and 4 for the same substation bus as figure 5.9.

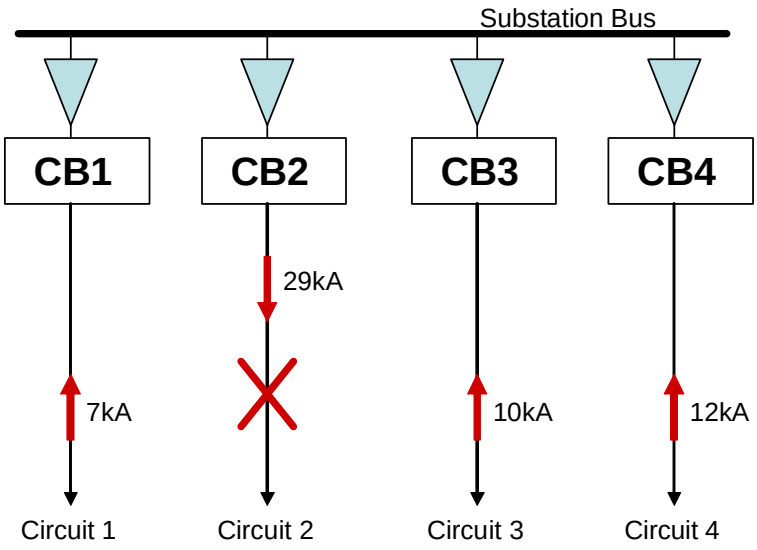

Figure 5.10: Fault Current Contributions for Fault on Circuit 2

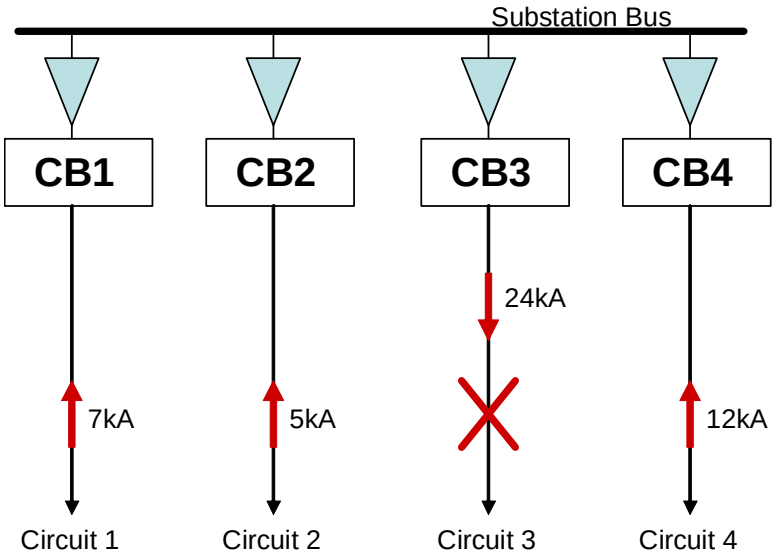

Figure 5.11: Fault Current Contributions for Fault on Circuit 3

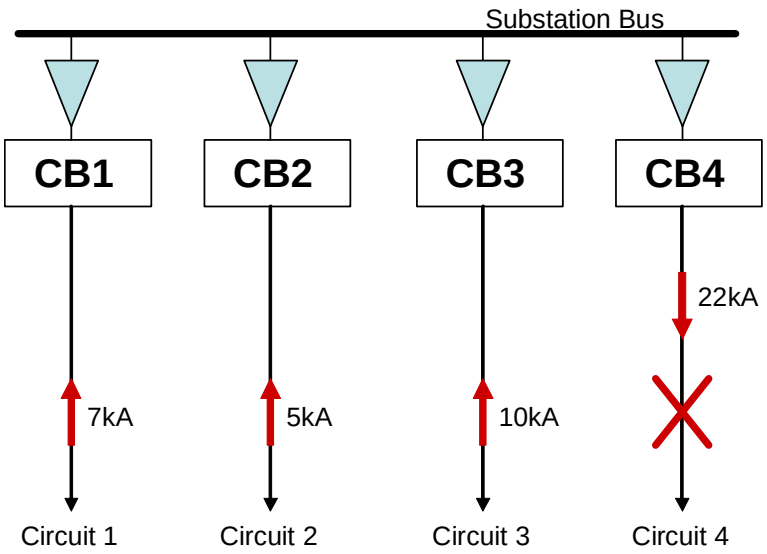

Figure 5.12: Fault Current Contributions for Fault on Circuit 4

Table 5.1 shows a summary of figures 5.9 through 5.12. Inspection of this table shows circuit 1 should not provide a trip signal for 7kA, but should for 27kA. The timer setting should be adjusted to compensate for this. Appropriate timer delay settings can be calculated using the methodology presented in section 5.2. The values for circuits 2, 3, and 4 can be determined from the table as well.

Table 5.1: Fault Current Contributions for Various Faulted Circuits

Faulted Circuit	Circuit 1 Current	Circuit 2 Current	Circuit 3 Current	Circuit 4 Current
1	27kA	5kA	10kA	12kA
2	7kA	29kA	10kA	12kA
3	7kA	5kA	24kA	12kA
4	7kA	5kA	10kA	22kA

It is recommended that every fault situation be analyzed in a table similar to table 5.1. This allows for recognition of fault current levels for determination of relay settings. While such analysis is not necessary for every application, its need should be evaluated in the design of the conductor dynamic fault detection system.

6.0 Conclusions and Further Research

The use of conductor dynamics in detecting faults is not a common practice in the electric grid. Modern protection practices commonly utilize current and potential transformers to measure currents and voltages. Detection based on conductor deflection adds a different form of protection which could prove valuable in the event of relay, current transformer, and potential transformer failures. Conductor response to electromagnetic forces during fault conditions is a physical phenomenon which can be monitored for fault detection.

The focus of the research presented is on the optical means of fault detection for the large power system inside substations. The use of bundled rigid conductors has several distinct advantages over single conductor applications. These include conductor displacement for single phase faults equal in magnitude to polyphase faults. False trips due to beam blockage can be minimized by triggering on symmetric motion inside a bundle. Additionally, triggering of conductor motion regardless of load current on unfaulted phases is attainable.

Fortunately, the electromagnetic forces generated during fault conditions extend to a variety of applications. The tools presented in the paper should allow a power system designer to effectively analyze and design substation conductor spans for the purpose of fault detection.

The concept of fault detection using conductor dynamics is not impractical. Through detailed analysis of substation rigid bus, this paper demonstrates the feasibility of this application.

6.1 Suggestions for Further Research

While the mathematical approach to fault detection is discussed in detail throughout this paper, it is beneficial to verify the actual conductor motion for a span using test equipment. The use of a power laboratory for the purpose of verification and calibration was unavailable during the time of this research. One suggestion for further research is conductor displacement verification for a variety of conductor spans and fault durations using bundled conductors in a laboratory setting.

The analysis of the substation bus spans was accomplished using dynamic analysis similar to a dual spring-mass system. This gives a true representation of forces and response as a function of time. Because bundled rigid conductors are not commonly used or analyzed in substation bus designs, a second suggestion for further research is the application of finite element analysis techniques [4, 5]. Comparisons of finite element analysis to measured results for single conductor arrangements have proved to be more accurate than dynamic analysis [4].

Appendix A

Design Application of Fault Detection using Conductor Dynamics

The objective of appendix A is to design and provide settings for a backup relay for the transmission line of the power system in the electrical oneline of figure A.1. The detector should operate in 60 cycles (1 second) if the primary relaying fails.

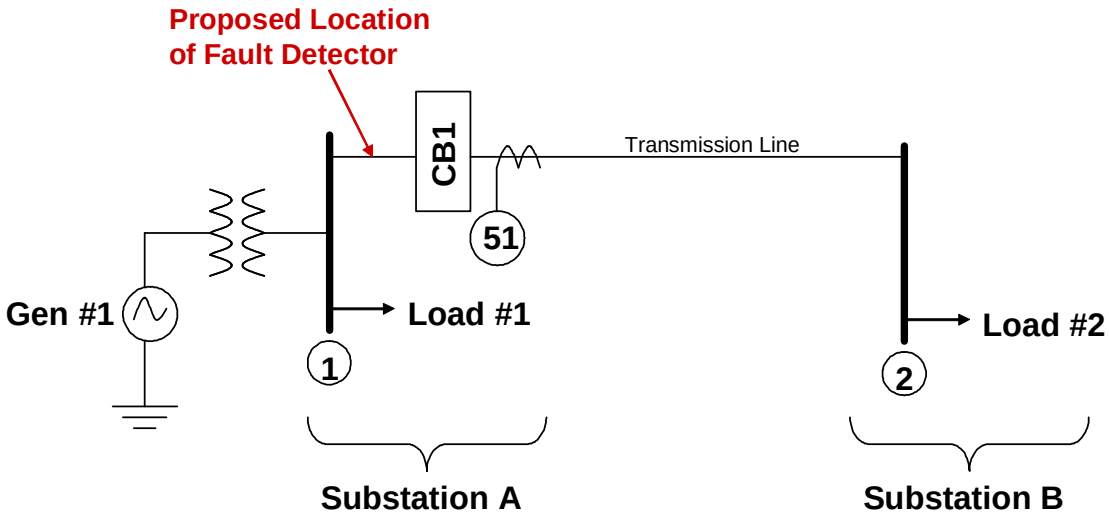

Figure A.1.: Appendix A Power System Electrical Oneline

Buses 1 and 2 are energized at 230kV with circuit breaker CB1 rated at 1200 amps RMS and interrupting capability of 40kA RMS. One overcurrent relay (type 51) with current transformers is used to trip for faults on the transmission line connecting buses 1 and 2.

The proposed location of the fault detector using bus dynamics is shown in red. It is in series with the transmission line to be protected. It is placed ahead of the circuit breaker; however, electrically it could be placed behind it. In order to properly coordinate with the overcurrent relay, it should monitor the same line and thus be in series.

Table A.1 shows the calculated fault current values at buses 1 and 2 with and without a 40 ohm fault impedance. The X/R ratios at each bus are also given. This data was calculated using system topology and is considered a required input for design of the fault detector.

Table A.1.Appendix A RMS Fault Current Values

	Bus 1	**Bus 2**
Bolted Fault		
Phase - Ground	38.5kA	36.5kA
Phase – Phase	39kA	37kA
Phase - Phase - Ground	39kA	37kA
Three Phase	40kA	40kA
40 Ohm Impedance Fault		
Phase - Ground	32kA	30kA
Phase – Phase	32.5kA	30.5kA
Phase - Phase - Ground	32.5kA	30.5kA
Three Phase	33 kA	31kA
X/R Ratio	15	15.67

The detector using bus dynamics will be constructed as shown in figure 5.1. Bundled rigid bus will be utilized for the advantages discussed previously. Several design parameters need to be established including conductor type, separation distances, span length, and conductor settings.

The first parameter to establish is the minimum conductor size according to ampacity. If the bus span is chosen to match the ampacity of the breaker size, each phase of the conductor bundle should be rated 600 amps assuming maximum load current splitting equally in the bundle. According to [2], any schedule 40 tubular aluminum 6061-T6 bus greater than 1" diameter will suffice for ampacity purposes. A 2-1/2" tubular bus has been chosen for this application to raise the natural frequency of the span and thus increase the response time.

Figures A.2 and A.3 show the phase to ground fault current including transient components from the system X/R ratio. The plots were developed from the given system fault

information and the use of equations 2.9 and 2.10. The 40 ohm fault impedance values were chosen because they represent a relatively low fault value compared to a less common and higher bolted fault. Assuming the fault detector can operate for the fault with impedance, the bolted fault detector should also work for a bolted fault. The load current of 1200 amps RMS on the unfaulted phases is also shown for comparative purposes.

According to the given fault data in table A.1, the smallest value of fault current is at bus #2 with an X/R ratio of 15 and a 40 ohm impedance fault. This will be analyzed for setting configuration.

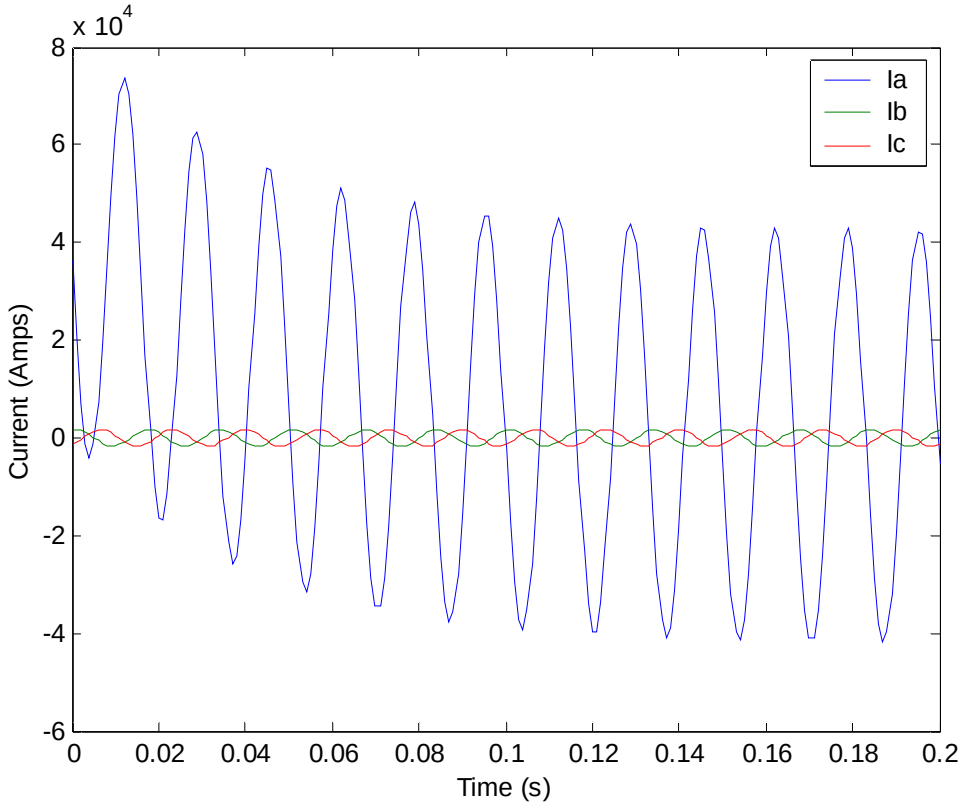

Figure A.2.: Phase to Ground Fault Current

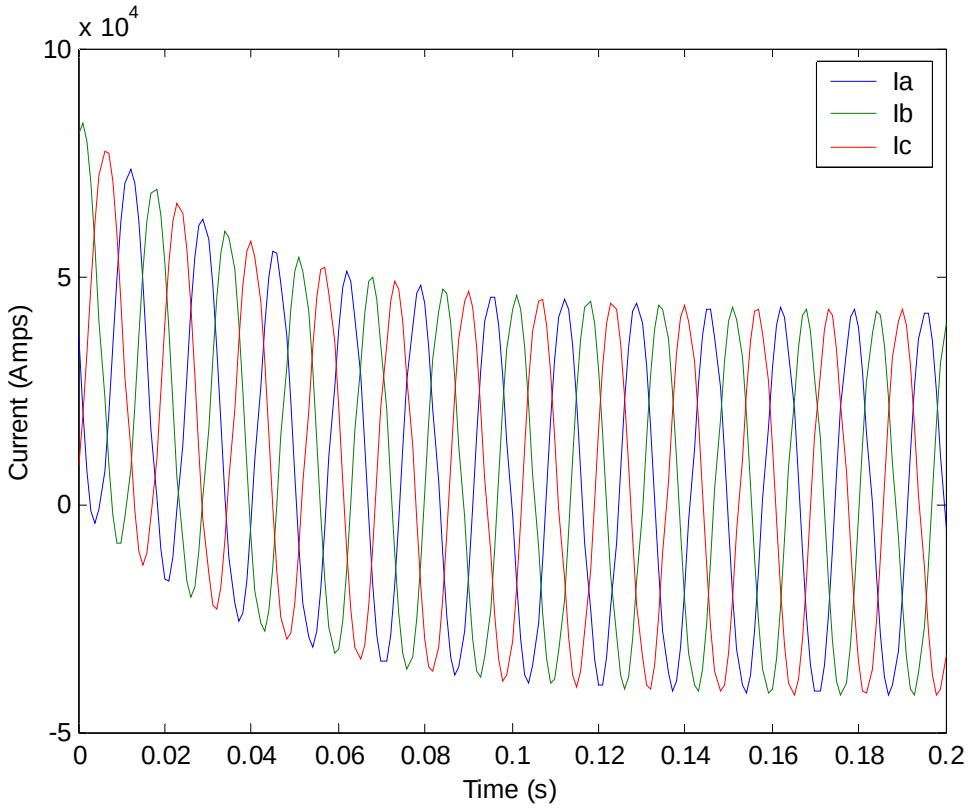

Figure A.3.: Three Phase Fault Current

The selection of conductor bundle and phase spacing can be narrowed down according to available space inside the substation and typical conductor arrangements. In this example, the arrangement of figure 3.11 will be used with d = 2 ft and S = 12 ft. The length of the span and conductor type will be chosen after the forces have been calculated.

The electromagnetic forces can be calculated for each conductor using equation 3.4. These forces are vectorially added according to equations 3.8 through 3.13. The results are presented in figures A.4 through A.9. The direction of force is seen as symmetric about the X axis. This physically is seen as the pinching of the conductors in a bundle towards each other.

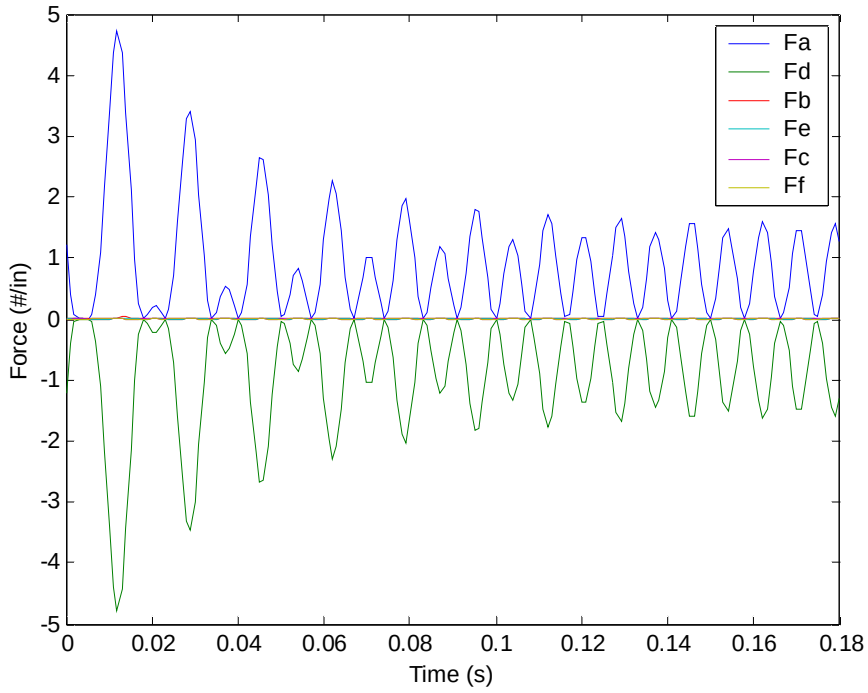

Figure A.4: A Phase to Ground Fault Conductor Forces

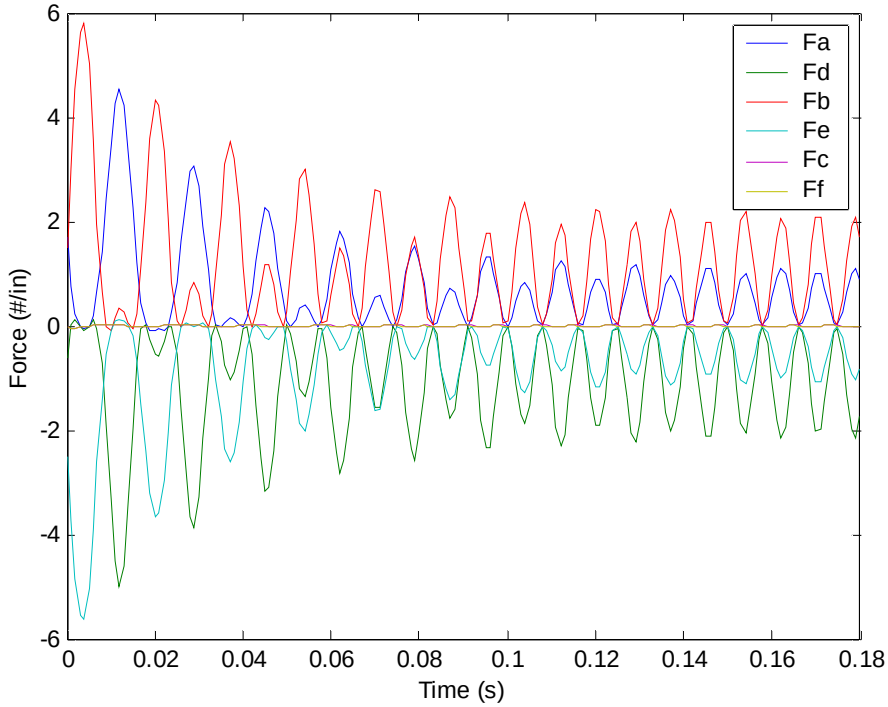

Figure A.5: A to B Phase Fault Conductor Forces

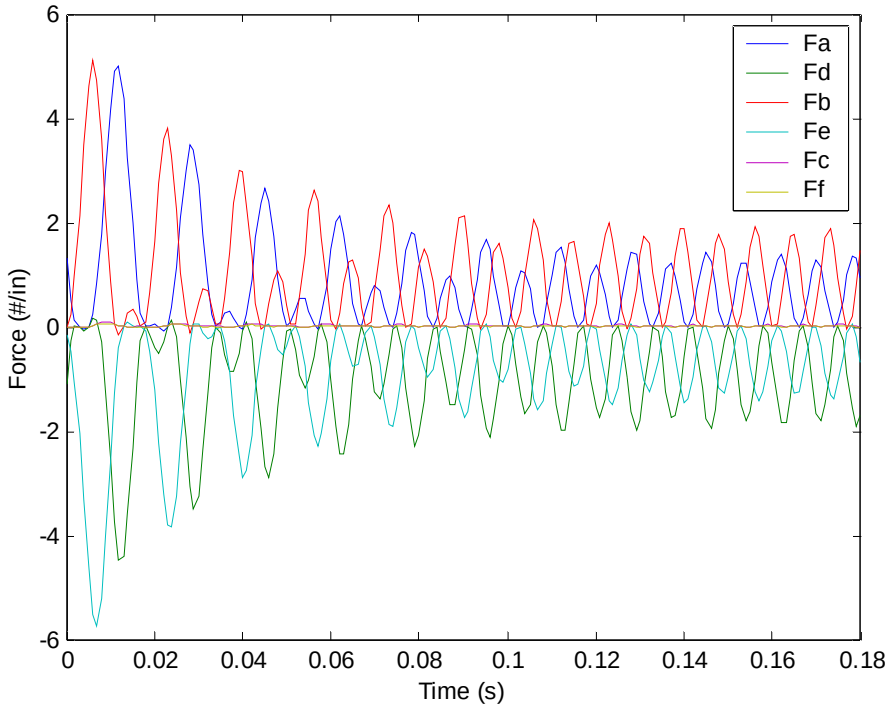

Figure A.6: A to B Phase to Ground Fault Conductor Forces

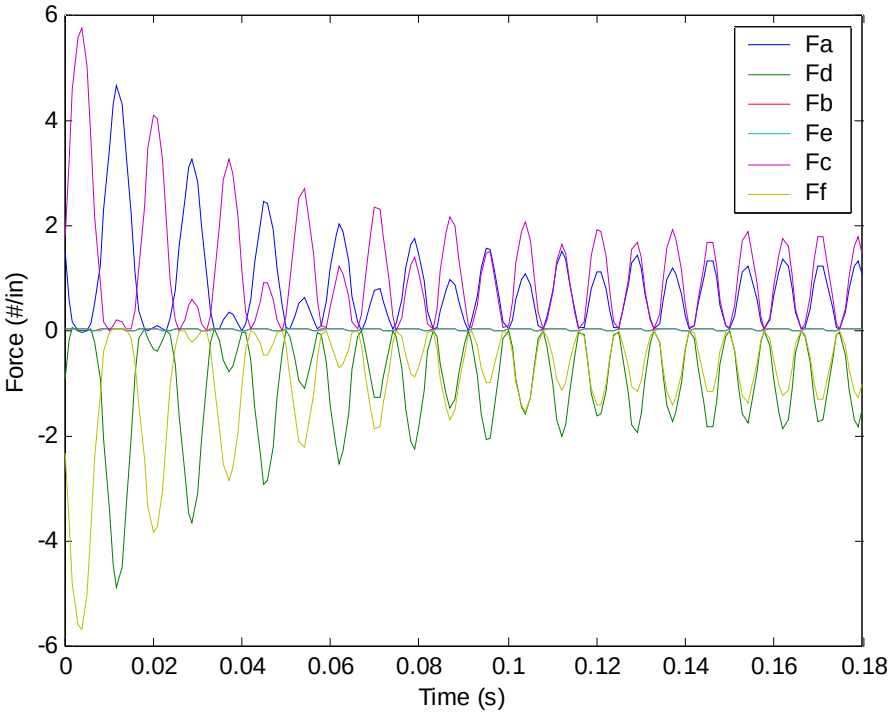

Figure A.7: A to C Phase Fault Conductor Forces

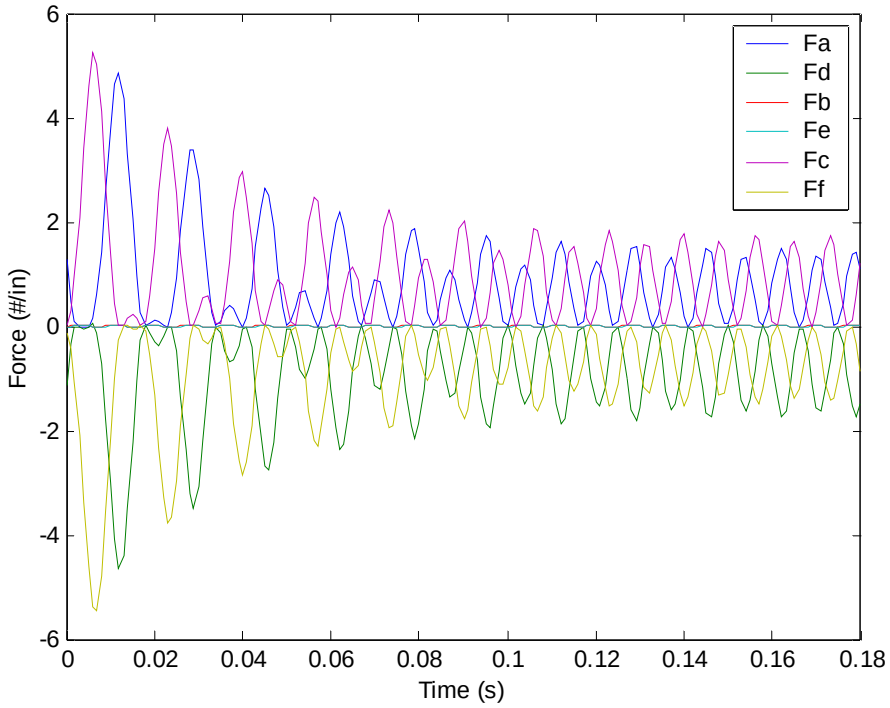

Figure A.8: A to C to Ground Phase Fault Conductor Forces

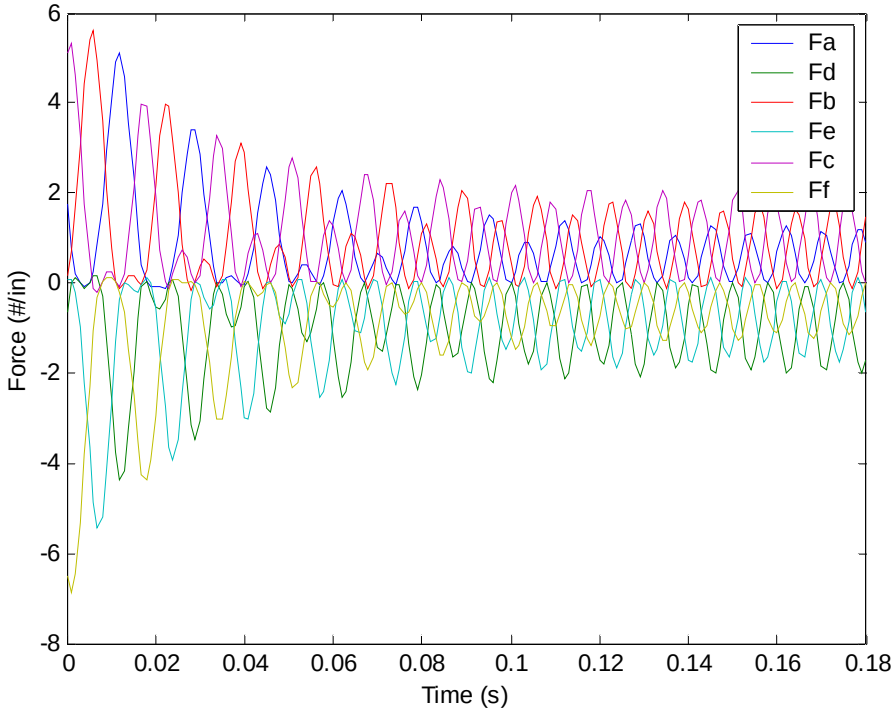

Figure A.9: Three Phase Phase Fault Conductor Forces

The force plots indicate a waveform similar to figure 4.14. The use of bundled conductors shows near symmetry for bundles and thus depicts near equal force distribution between conductor bundles. While there is some notable interaction between faulted conductor phases outside the bundles, the settings can be determined based on the deflection of any bundle involved in the fault. In other words, there are some notable differences on the three phase plot of figure A.5; however, the settings can be designed to detect the largest deflection. The settings chosen should also allow for any deflection differences within bundles due to forces from outside phases at any moment in time.

The forces due to unfaulted phases appear negligible in comparison with the faulted ones. This is due to the ratio of fault to load current and the large separation distances in equation 3.4. The result is negligible deflection due to load currents.

The plots for B phase to ground and C phase to ground forces were not shown because they are the same as figure A.4 with the exception of the bundled conductor generating electromagnetic forces. The same holds true for the B to C phase and B to C phase to ground faults.

The insulators required for the bus span assembly were 230kV voltage class station post insulators. The mechanical specifications [5] for the insulators are contained in table A.2.

Table A.2.NGK 8A-67971A 230kV Insulator Mechanical Specifications

Insulator Description	**Quantity**
Height	80 in
Core Diameter	5 in
Max Cantilever Load	2810 lb
Spring Constant	2631 lb/in
Weight	322 lb
Poisson's Ratio	0.3

The spring constant for the conductor span is determined using equation 4.7. Using fixed ends on the span with 2-1/2" schedule 40 aluminum 6061-T6 conductor, the value of k_{bus} is calculated to be 25508.35 lb/in.

The mass matrix of equation 4.14 is built assuming m_1 is the effective weight of the conductor transmitted to the support fitting. This translates to ½ the weight of the conductor. The full weight of the conductor is m_2. Since the conductor's weight is given as 2.004 lb/ft, the 20 foot span design would create a system mass matrix:

$$\overline{\overline{M}} = \begin{pmatrix} 20.04 & 0 \\ 0 & 40.08 \end{pmatrix}$$

The system stiffness matrix is determined to be:

$$\overline{\overline{K}} = \begin{pmatrix} 28139.35 & -25508.35 \\ -25508.35 & 25508.35 \end{pmatrix}$$

Determination of the natural frequencies for a system is accomplished using equation 4.16. The eigenvalues of $\overline{\overline{M}}^{-1}\overline{\overline{K}}$ are solved using computer software to provide two solutions, ω_1^2 and ω_2^2. The natural frequencies are calculated to be 44.1233 rad/s (7.0260 Hz) and 9.5745 rad/s (1.5246 Hz). Thus, the fundamental frequency is 1.5246 Hz.

Because of the low natural frequencies, the DC component of the fault short circuit forces can be approximated using the system step response. The magnification factor for the 120Hz steady state fault current is calculated using equation 4.5 to be 6% gain for the AC portion. To ensure this is recognized through modeling, a margin will be applied to the minimum pulse width.

The primary relay settings are given in figure A.10. A backup relay for the system should take the form of a vertical line on the overcurrent relay setting plot (figure 1.3).

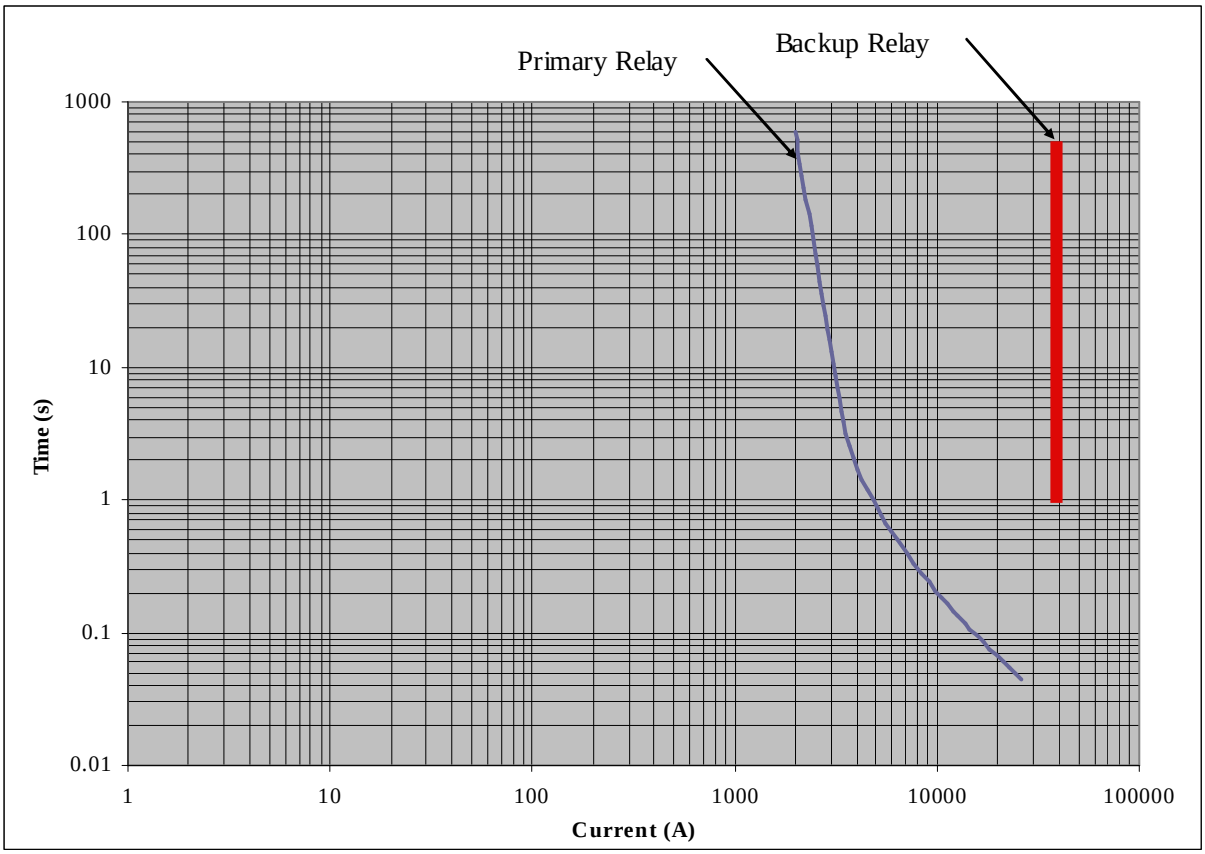

Figure A.10: Primary Overcurrent Relay Settings

The physical response of the bundled conductors to a three phase fault at bus #2 is depicted in figure A.11 at time t=1sec. The response assumes the primary relay has tripped at 0.07 seconds. This is equivalent to a step function to the bus system for duration of 0.07 seconds (including breaker operation with detection according to figure A.10).

The reflecting mirrors for all phases will be 5". This could be adjusted if necessary for lower magnitude faults. Figure A.11 shows the mirror size as ½ L_{mirror} equal to 2 ½".

Figure A.12 shows the pulse width produced representing deflection during operation of the primary relaying. The pulse width is .067 seconds. It is critical, therefore, for the setting of the fault detector to be above this value. Since this reflects a 30kA fault, the pulse width for a

40kA fault (maximum) is also calculated to be .080 seconds. For a margin of protection, the value of 0.1 second pulse width will be considered as the minimum pickup pulse width.

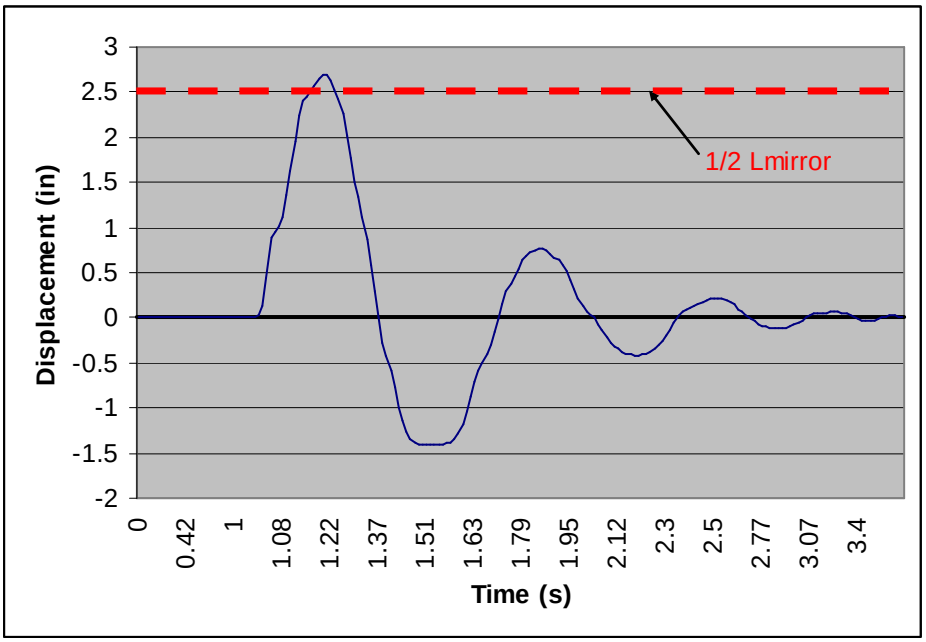

Figure A.11: Conductor Deflection Using Primary Relaying

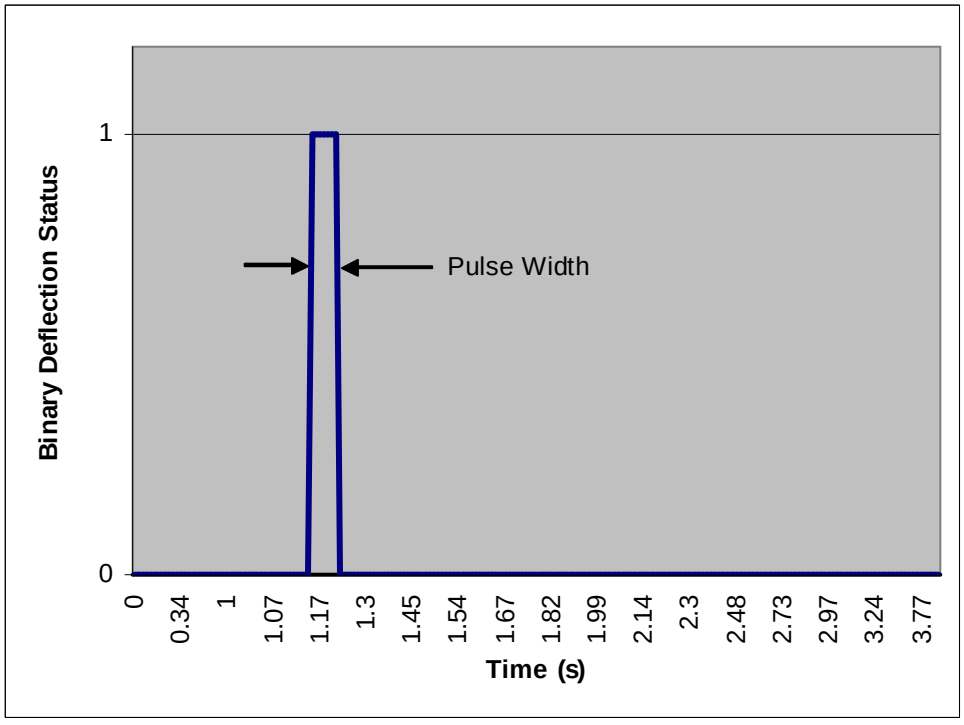

Figure A.12: Pulse Width Using Primary Relaying

The next step in determining the relay settings is calculation of conductor displacement during each type of fault in figures A.4 through A.8. Figures A.13 through A.28 show the displacement for the faulted bundles and the associated pulse widths using a mirror size of 5".

Table A.3 lists the displacement detector's time for each conductor bundle using the fault conditions in figures A.4 through A.9.

Table A.3: Detection Time Table Summary

Fault Type	**AΦ**	**DΦ**	**BΦ**	**EΦ**	**CΦ**	**FΦ**
A Phase to Ground	0.88s	0.88s	-	-	-	-
A to B Phase	0.783s	.903s	.903s	.783s	-	-
A to B Phase to Ground	.808s	.903s	.903s	.808s	-	-
A to C Phase	.808s	.903s	-	-	.903s	.808s
A to C Phase to Ground	.888s	.903s	-	-	.903s	.888s
Three Phase	.805s	.903s	.903s	.903s	.903s	.803s
Min. Bundle Overlap Time	.777s		.783s		.732s	

It can be determined from figures A.13 through A.28 and table A.3 that the minimum detection time for the 30kA fault is a three phase fault on the outer conductor bundles. The time for the mutual displacement is 0.732 seconds assuming the fault is cleared by opening the circuit breaker after 1 second (60 cycles). It can then be concluded that the required delay time for the logic diagram of figure 5.2 should be 0.73 seconds for a 30kA fault or above. If less than a 1 second time is desired, the analysis can be rerun to determine the new setting. Additionally, if the fault current is higher than 30kA, the device will still operate. The time-overcurrent setting curve of the device is represented as the red line of figure A.10.

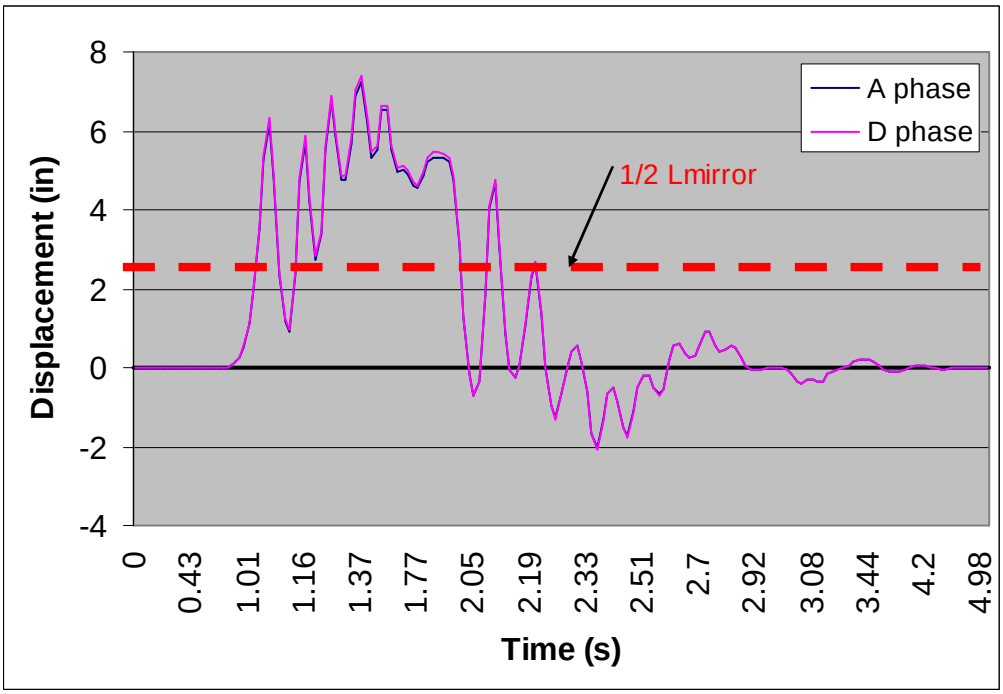

Figure A.13: A Phase to Ground Fault Conductor Displacements

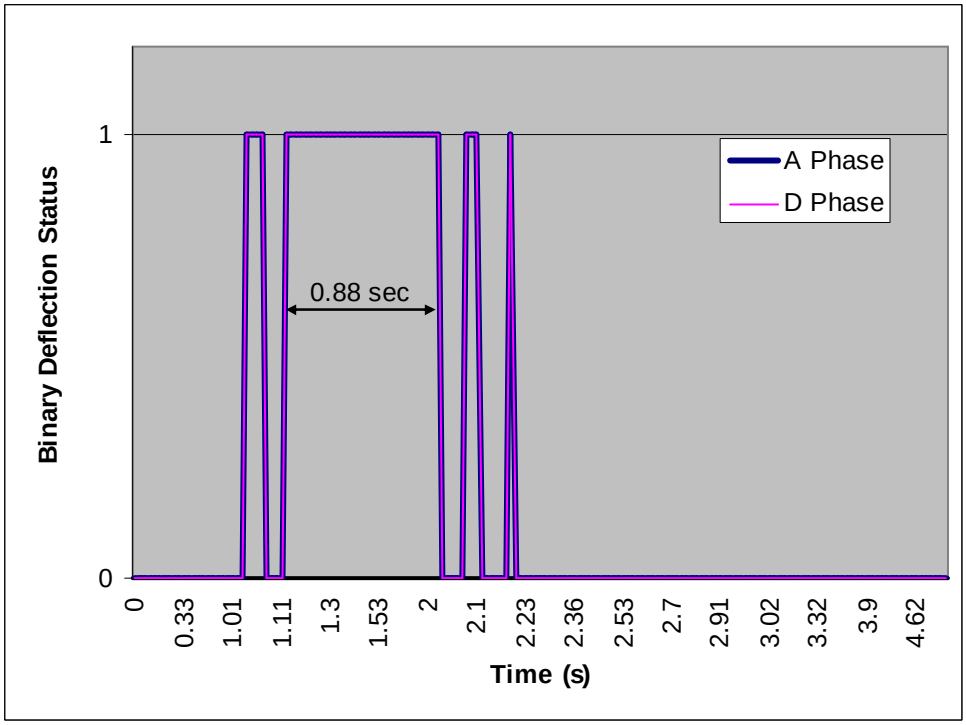

Figure A.14: A Phase to Ground Fault Conductor Deflection Detector Pulses

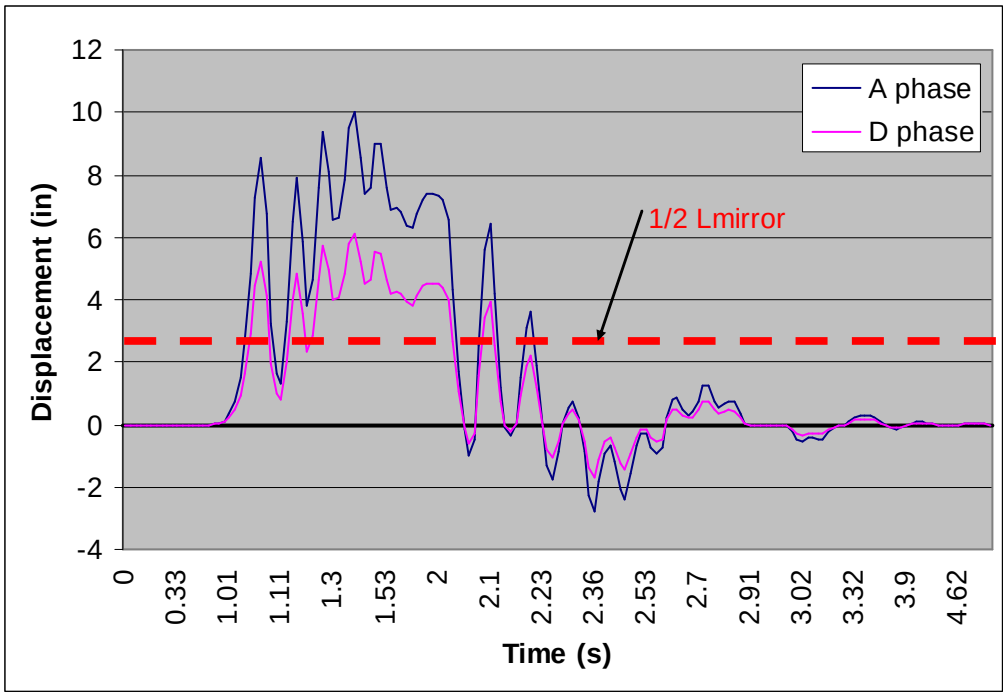

Figure A.15: A to B Phase to Phase Fault Conductor Displacements

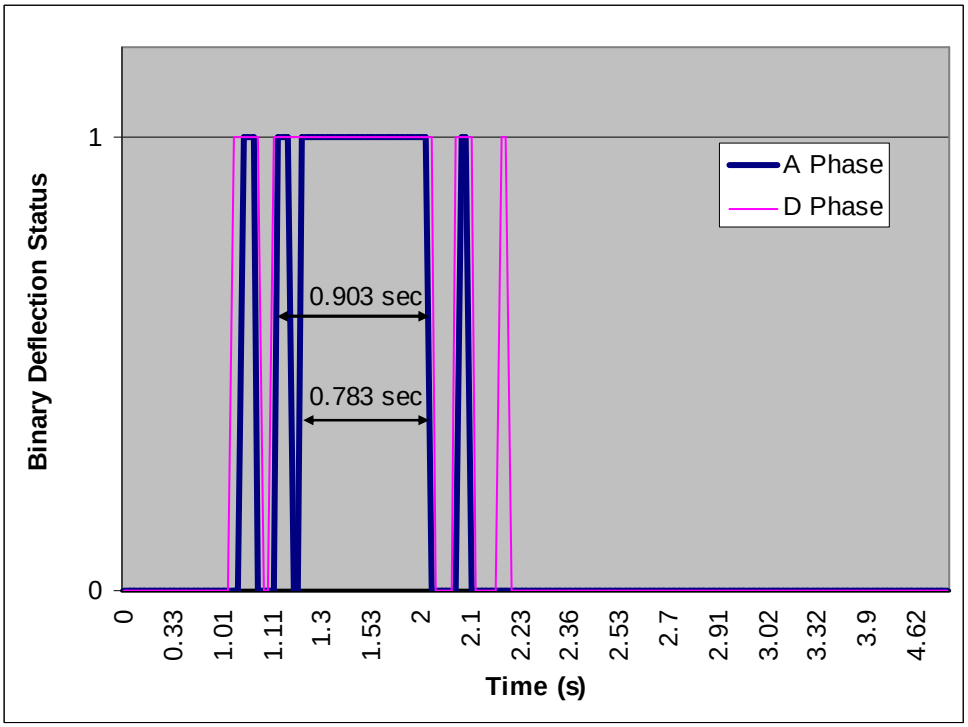

Figure A.16: A to B Phase to Phase Fault Deflection Detector Pulses

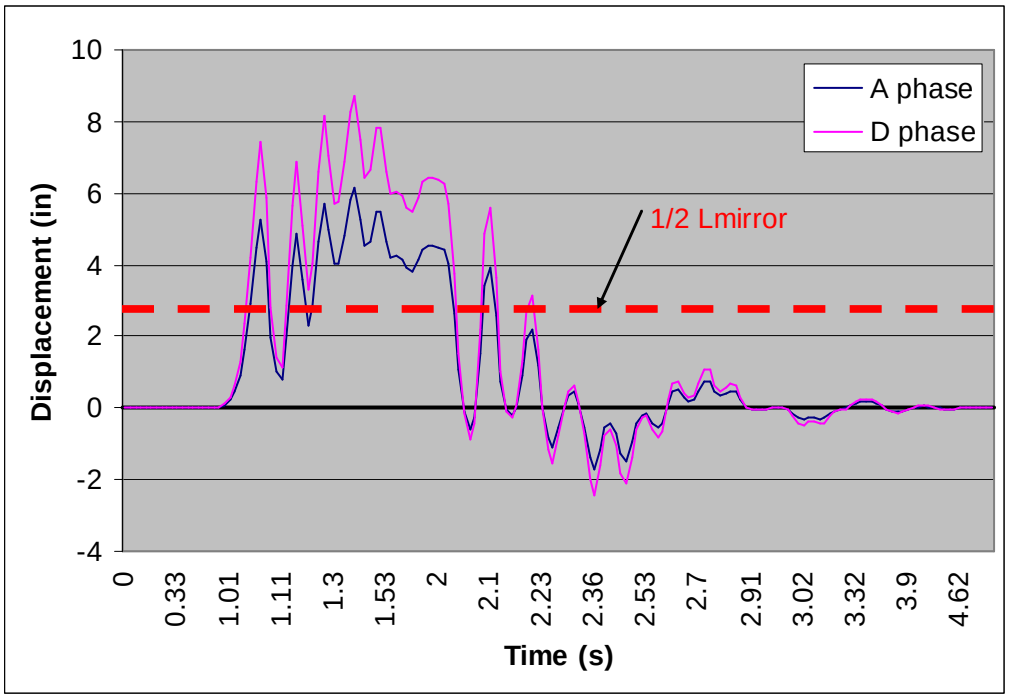

Figure A.17: A to B Phase to Ground Fault Conductor Displacements

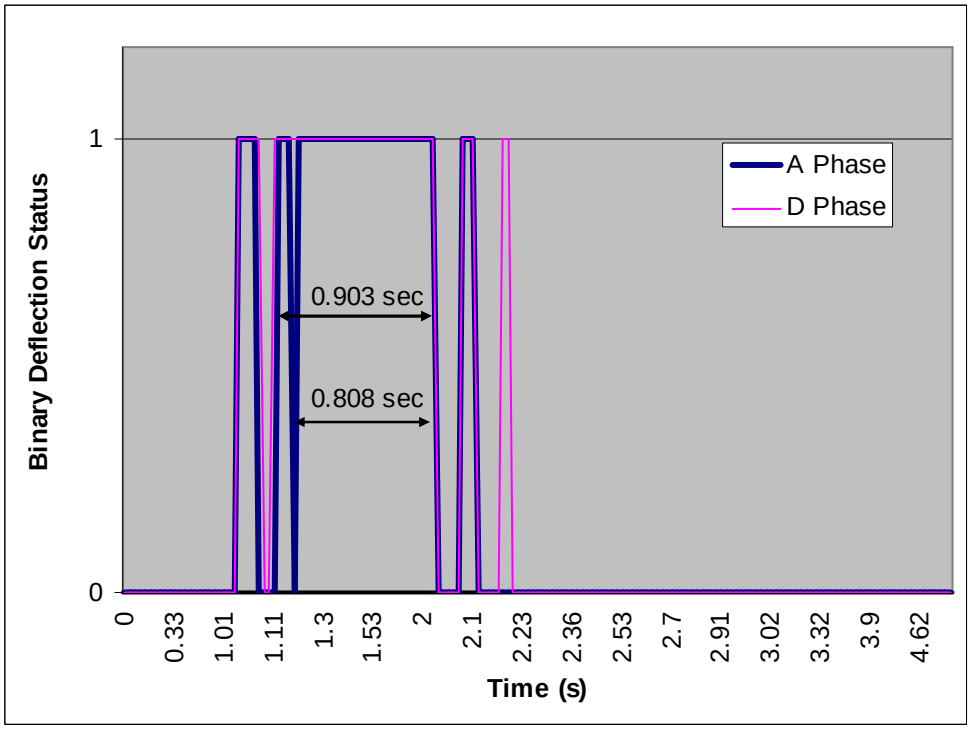

Figure A.18: A to B Phase to Ground Fault Deflection Detector Pulses

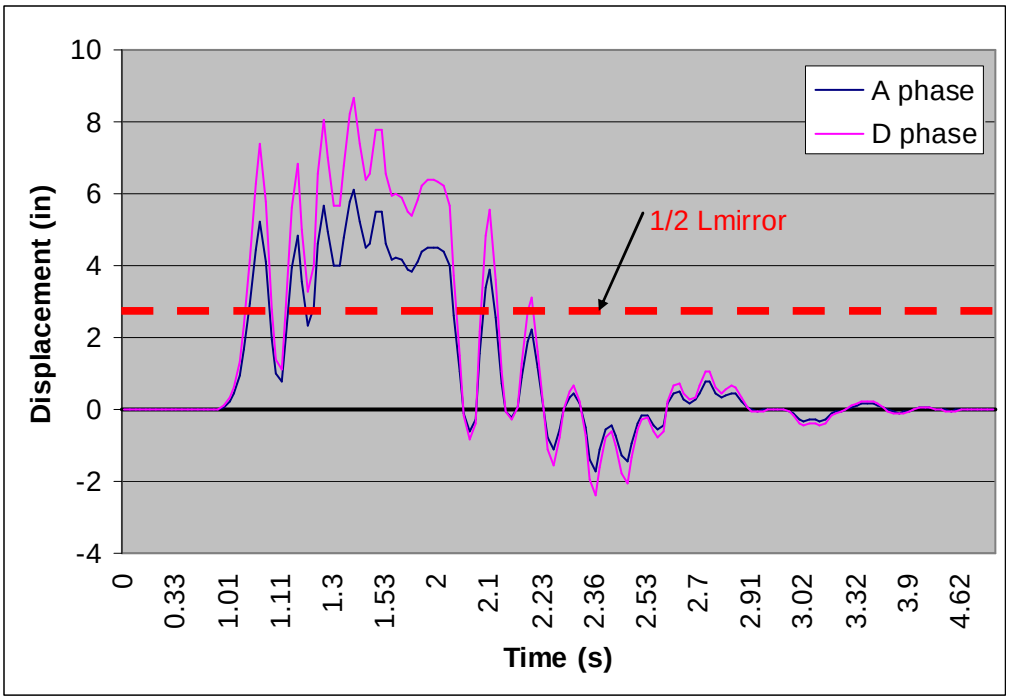

Figure A.19: A to C Phase to Phase Fault Conductor Displacements

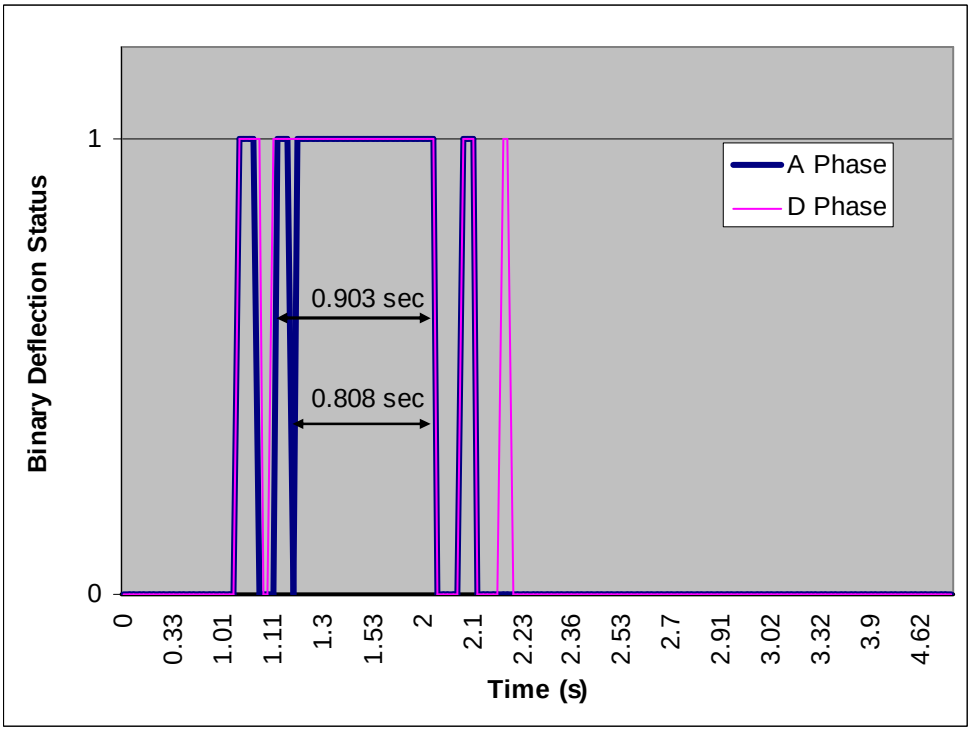

Figure A.20: A to C Phase to Phase Fault Deflection Detector Pulses

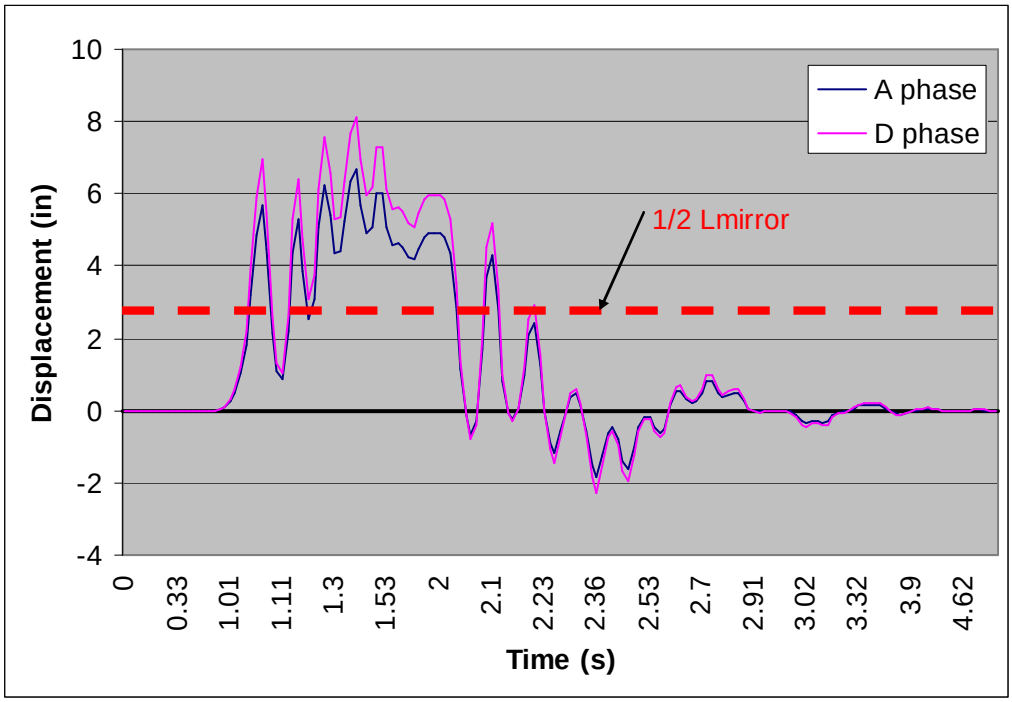

Figure A.21: A to C Phase to Ground Fault Conductor Displacements

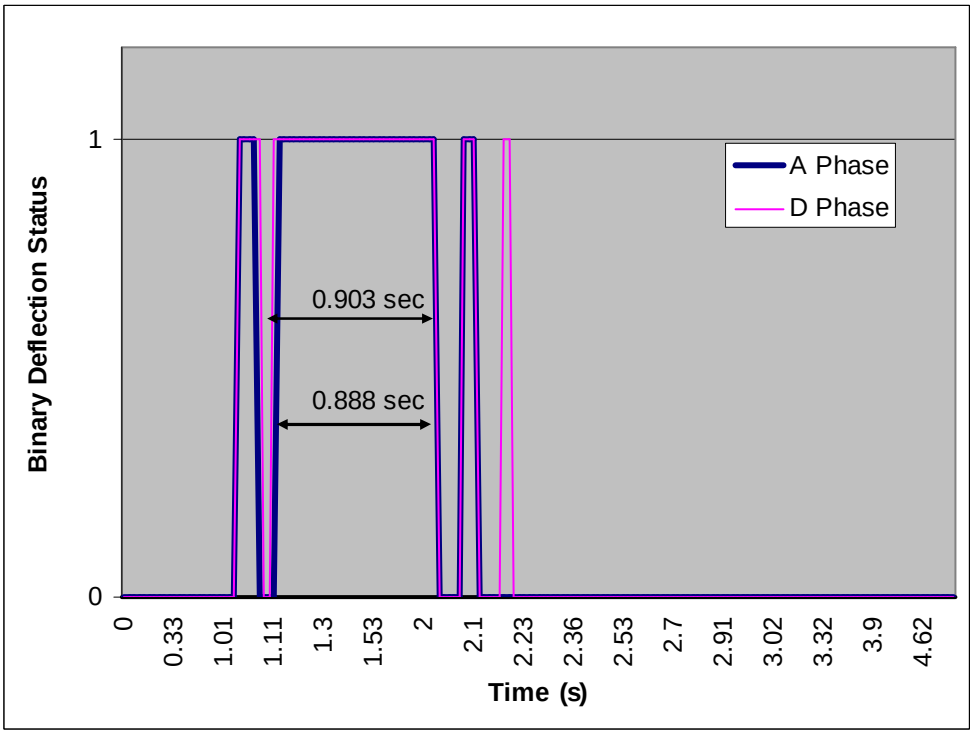

Figure A.22: A to C Phase to Ground Fault Deflection Detector Pulses

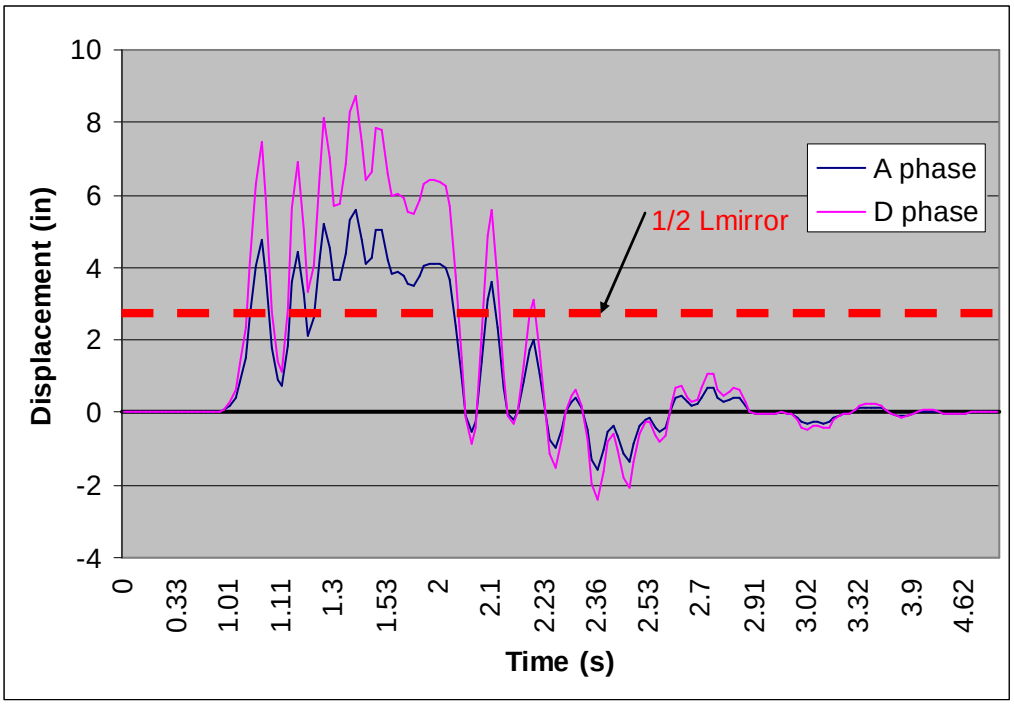

Figure A.23: Three Phase Fault A and D Bundle Conductor Displacements

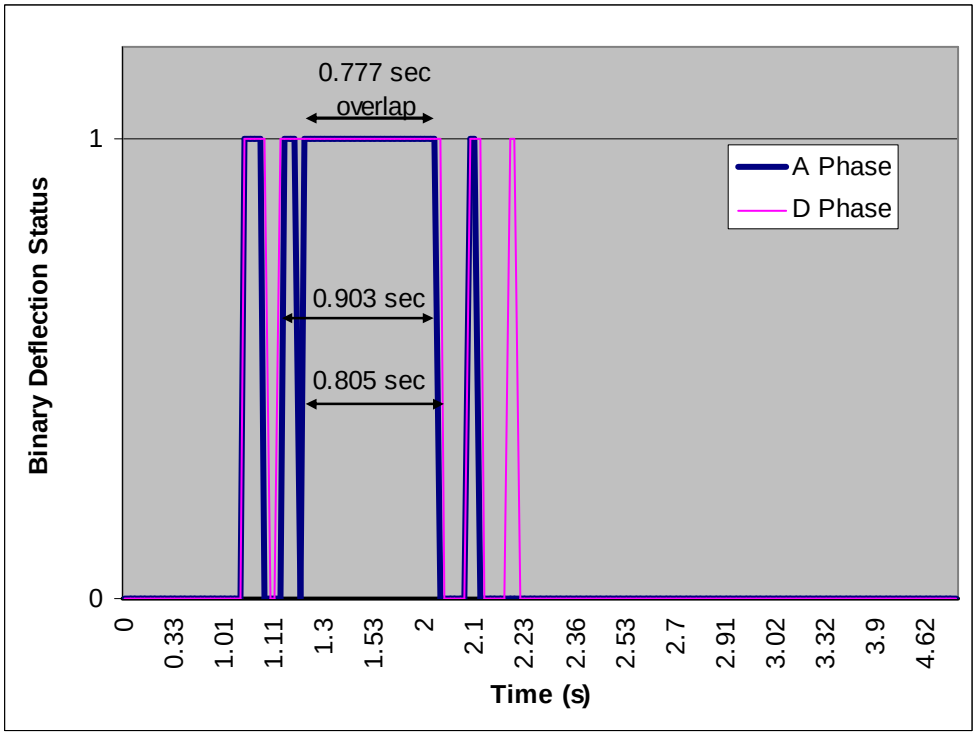

Figure A.24: Three Phase Fault A and D Bundle Deflection Detector Pulses

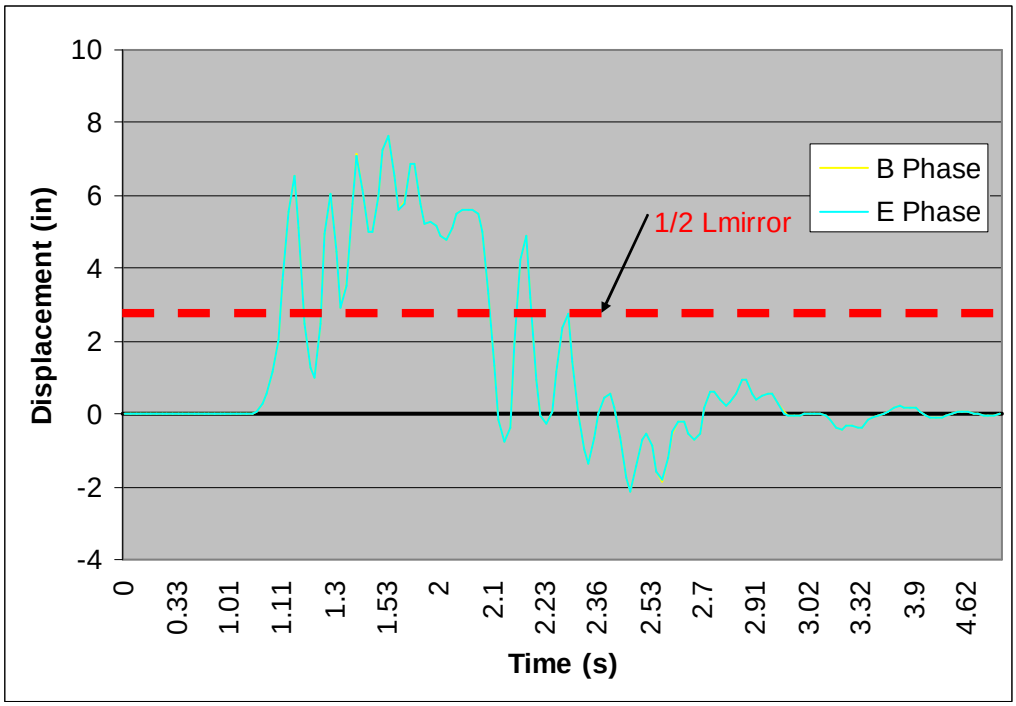

Figure A.25: Three Phase Fault B and E Bundle Conductor Displacements

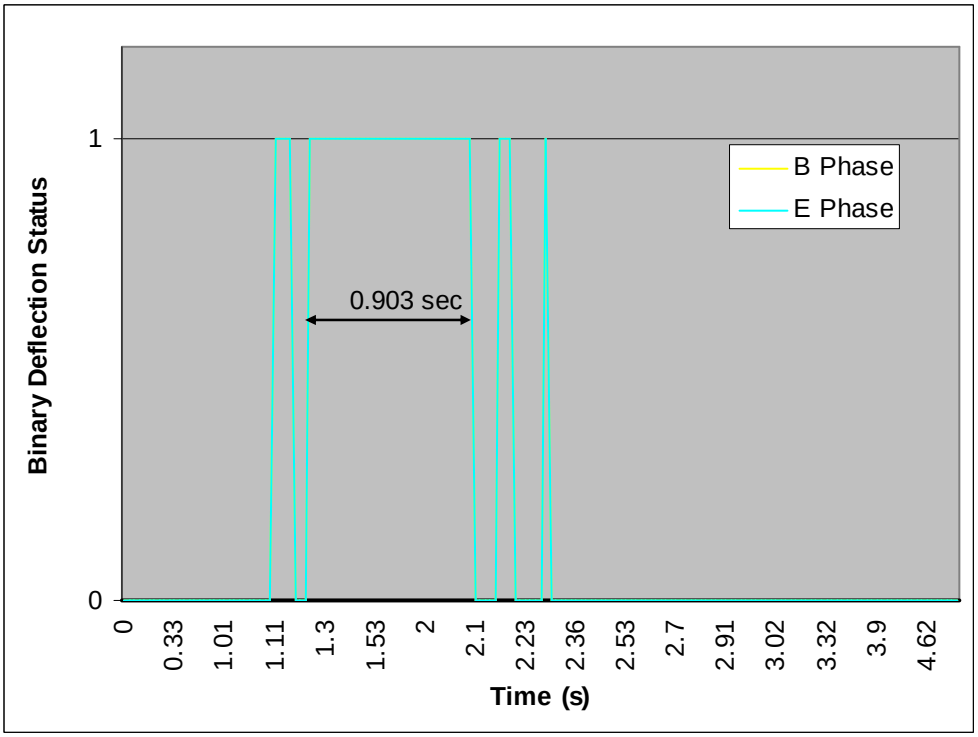

Figure A.26: Three Phase Fault B and E Bundle Deflection Detector Pulses

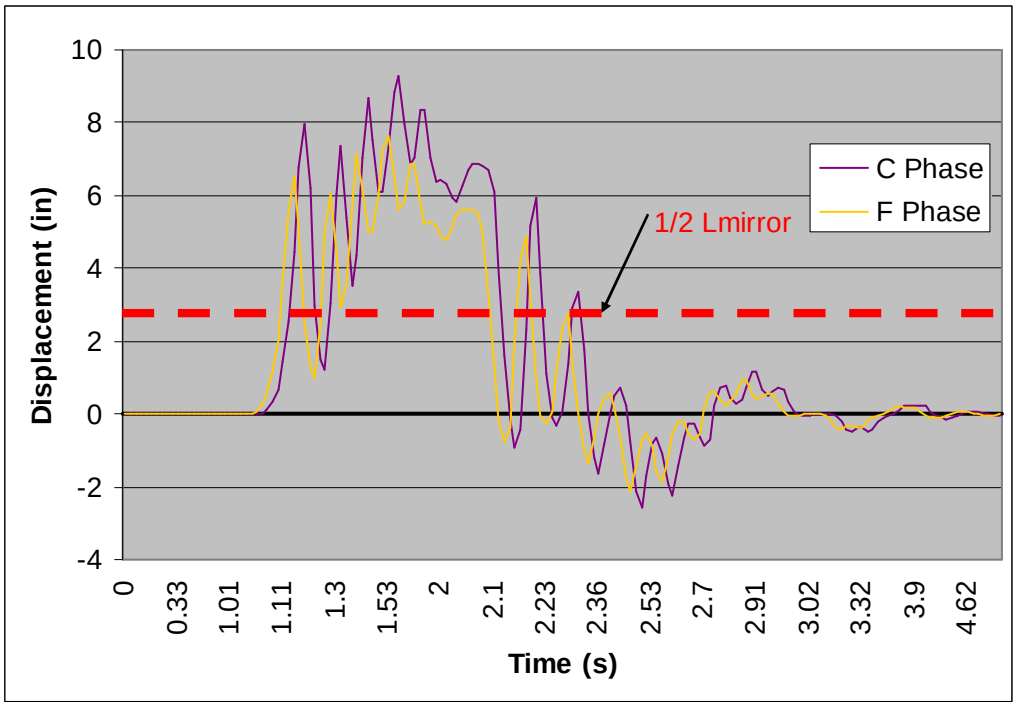

Figure A.27: Three Phase Fault C and F Bundle Conductor Displacements

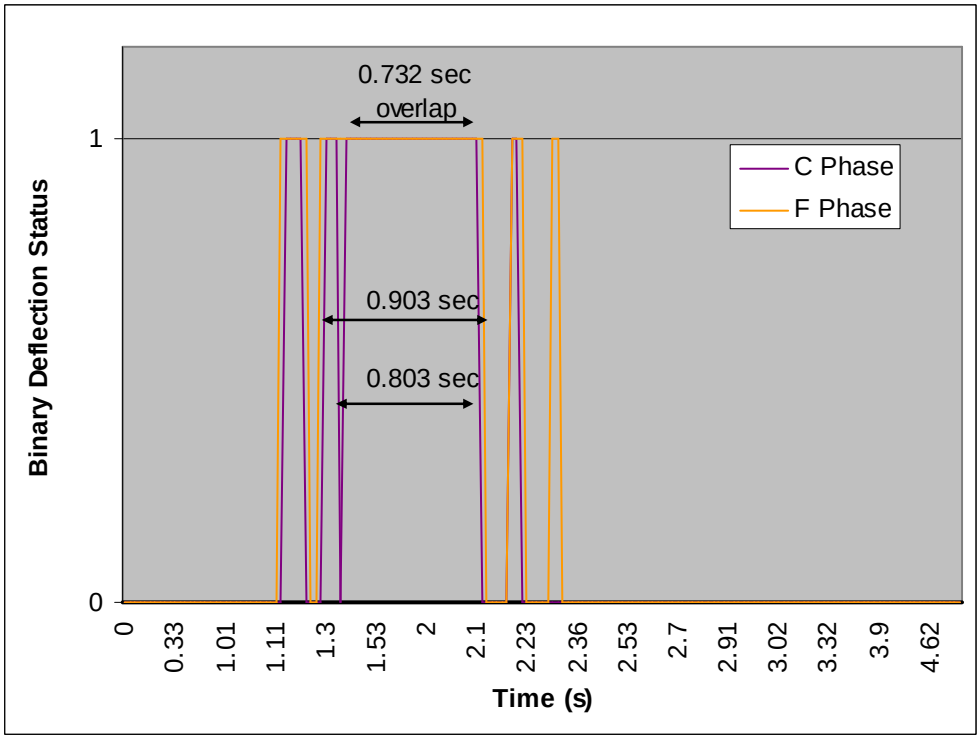

Figure A.28: Three Phase Fault C and F Bundle Deflection Detector Pulses

Appendix B

Bus Dynamic Fault Detector Design Flowchart

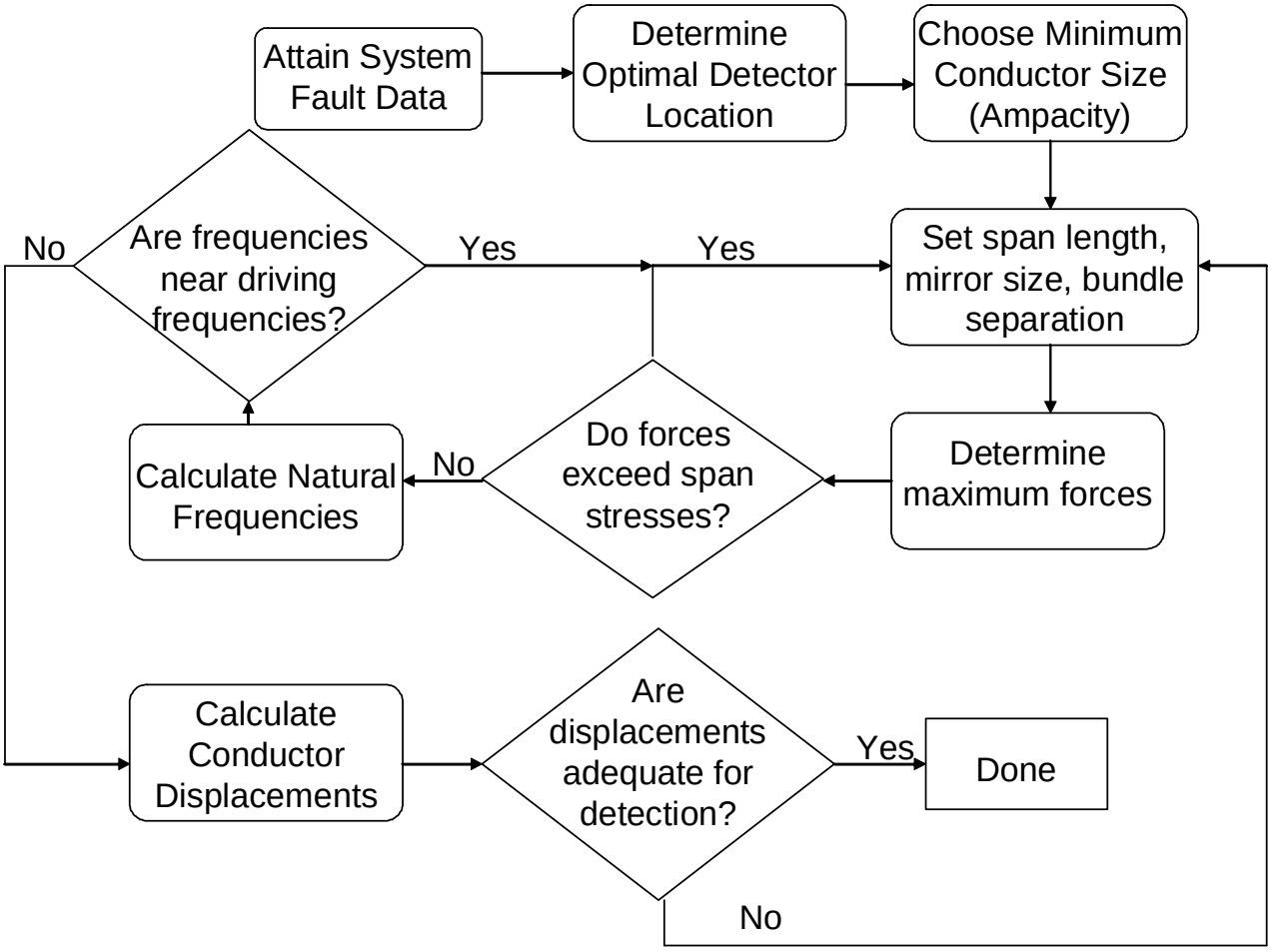

Figure B.1: Design Flowchart

References

[1] Grainger, John J. & Stevenson, William D. Jr, "Power System Analysis," McGraw-Hill, Inc., 1994.

[2] Substations Committee of the IEEE Power Engineering Society, "IEEE Guide for Design of Rigid-Bus Structures," IEEE Std 605-1998, August 1998.

[3] Meliopoulos, A.P. Sakis, "Power System Grounding and Transients: An Introduction," Marcel Dekker, Inc., 1988.

[4] Develle, B.A., "Finite Element Analysis Applied to Substation Busbar Design," Graduate Thesis, University of New Orleans, May 1992.

[5] Bergeron, David Allen, "Improved Static Finite Element Analysis of Substation Busbar Structures," Graduate Thesis, University of New Orleans, December 1995.

[6] Ward, Daniel J, "Overhead Distribution Conductor Motion Due to Short-Circuit Forces", IEEE Transactions on Power Delivery, Vol. 18, No. 4, October, 2003.

[7] Halliday, David; Resnick, Robert; Walker, Jearl, "Fundamentals of Physics, Fourth Edition", John Wiley & Sons, Inc, 1993.

[8] American Institute of Steel Construction, "Manual of Steel Construction", July, 1989

[9] Thomson, William T & Dahleh, Marie Dillon, "Theory of Vibration with Applications, Fifth Edition," Prentice-Hall, Inc., 1998, 1993.

[10] Beer, Ferdinand P. & Johnston, Russell E. Jr, "Vector Mechanics for Engineers: Dynamics, Sixth Edition", The McGraw-Hill Companies, Inc., 1997.

[11] Landry, Michel; Beauchemin, Roger; Venne, Andre, "De-icing EHV Overhead Transmission Lines Using Electromagnetic Forces Generated by Moderate Short-Circuit Currents" IEEE Transactions on Power Delivery, 37C-TP-15, 2000.

[12] Chen, Huaxiong, “System Identification Applications in Substation Busbar Structure Modeling”, Graduate Thesis, University of New Orleans, July 1996.

[13] Stewart, James, “Calculus: Early Transcendentals, Third Edition”, Brooks/Cole Publishing Company, 1995

Vita

Jeff Dicharry was born in New Orleans, LA in 1978. He attended Brother Martin High School and graduated with a Bachelor's Degree in Electrical Engineering from Louisiana State University in December, 2000. He was employed in the substation design group of Entergy Services, Inc. from January, 2001 to November, 2004. He is involved with the rigid bus and cable systems subcommittees of the IEEE substation committee with contributions including conductor ampacity calculations. He is currently employed in the Transmission Operations Planning group of Entergy Services, Inc. and is completing his Master of Science in Electrical Engineering from the University of New Orleans. He hopes to continue working in the power industry and utilize his employment and educational experiences to teach collegiate level engineering courses in the future.